STABLE ORBITS

ABOUT THE MARTIAN MOONS

THESIS

Scott W. Jansson
Captain, USAF

AFIT/GA/ENY/89D-3

DEPARTMENT OF THE AIR FORCE
AIR UNIVERSITY
AIR FORCE INSTITUTE OF TECHNOLOGY

Wright-Patterson Air Force Base, Ohio

AFIT/GA/ENY/89D-3

STABLE ORBITS
ABOUT THE MARTIAN MOONS

THESIS

Presented to the Faculty of the School of Engineering

of the Air Force Institute of Technology

Air University

In Partial Fulfillment of the

Requirements for the Degree of

Master of Science in Astronautical Engineering

Scott W. Jansson, B.S.

Captain, USAF

December 1989

Acknowledgements

I would like to thank my advisor, Dr. William Wiesel for his expert assistance. His enthusiasm and support made this project both interesting and educational.

Table of Contents

List of Figures

Appendix C

Appendix D

List of Tables

Notation

a,b,c	axis lengths of moon
dM	differential element of mass
d	position vector of the satellite with respect to Mars
D	position vector of the moon with respect to Mars
G	universal gravitational constant
H	Hamiltonian
I_{xx}, I_{yy}, I_{zz}	moon mass moments of inertia
I_{xy}, I_{xz}, I_{yz}	moon mass products of inertia
L	Lagrangian
m,M	mass
P_i	generalized momenta
Q_i	generalized coordinates
r	position vector of the satellite with respect to the differential element of moon mass
R	position vector of the satellite with respect to the moon
T	kinetic energy
v	velocity
V	potential energy
x	moon's minimum axis of inertia
y	moon's intermediate axis of inertia
z	moon's maximum axis of inertia

Greek Notation

β	position vector of differential element of moon mass with respect to the center of gravity
w	angular velocity - revolution rate of moon
Ω	angular velocity - rotation rate of moon

Abstract

Orbits about the Martian moons, Phobos and Deimos, were investigated using the Poincare' surface of section technique. Hamilton's canonical equations were derived to describe the dynamics of the modified restricted three-body problem (Mars, moon, artificial satellite). The surface of section technique involved the numerical integration of several test orbits with the same value for the Hamiltonian. Apoapsis and periapsis points of the orbits are plotted in the two-dimensional configuration space. Stable orbits were discovered when the points formed sets of closed curves; chaotic orbits were indicated by the scattering of the points.

I. Introduction

Phobos and Deimos, the Martian moons, are just two of the many natural satellites in the solar system which may be modeled as triaxial ellipsoids. They are in nearly circular orbits about Mars and rotate about their major axes of inertia. The objective of this study is to determine whether or not stable orbits can be found about either one of these moons.

Hamilton's canonical equations will be derived to describe the dynamics of the modified restricted three-body problem (Mars, moon, artificial satellite). These equations will then be numerically integrated using the Haming algorithm to produce test orbits.

In the surface of section method, numerous test orbits are integrated with the same value of the system Hamiltonian. When a spacecraft passes through the closest or furthest approach to the moon (periapsis and apoapsis, respectively), a point is plotted in the orbital plane. If a set of closed curves is formed by the points, the orbit is stable; otherwise, the orbit is unstable.

Plots of the periapsis and apoapsis points for various Hamiltonian values will be presented. Where appropriate, stable orbits will be identified from these plots.

II. Problem Dynamics

The coordinate system used in this investigation is illustrated in Figure 1. Phobos and Deimos may be modeled as triaxial ellipsoids as shown in the figure. Each moon rotates synchronously. That is, the rotation rate (Ω) of the moon about its own axis (z) is equal to the revolution rate (w) of the moon about Mars. Therefore, the moon's minimum axis of inertia, x, remains pointed toward Mars while it rotates about its maximum axis of inertia, z. The intermediate axis of inertia, y, completes the "right-handed" set of orthogonal axes.

Mars and the artificial satellite are modeled as symmetric spheres with their masses concentrated at their centers. The center of mass of Mars is assumed to be fixed in inertial space. The only forces assumed to be acting on the three-body system are the gravitational ones between the bodies; all others are neglected. Additionally, the satellite is assumed to be sufficiently small so as not to affect the motion of the other bodies.

The moon's orbit about Mars is taken to be circular. This assumption is acceptable since the eccentricities of Phobos and Deimos are .015 and .00052, respectively (3:422). The position of the moon with respect to Mars is denoted by **D**. The position of the satellite with respect to the moon is denoted by **R** and with respect to Mars by **d**. Various geometric and kinematic parameters used in this study for

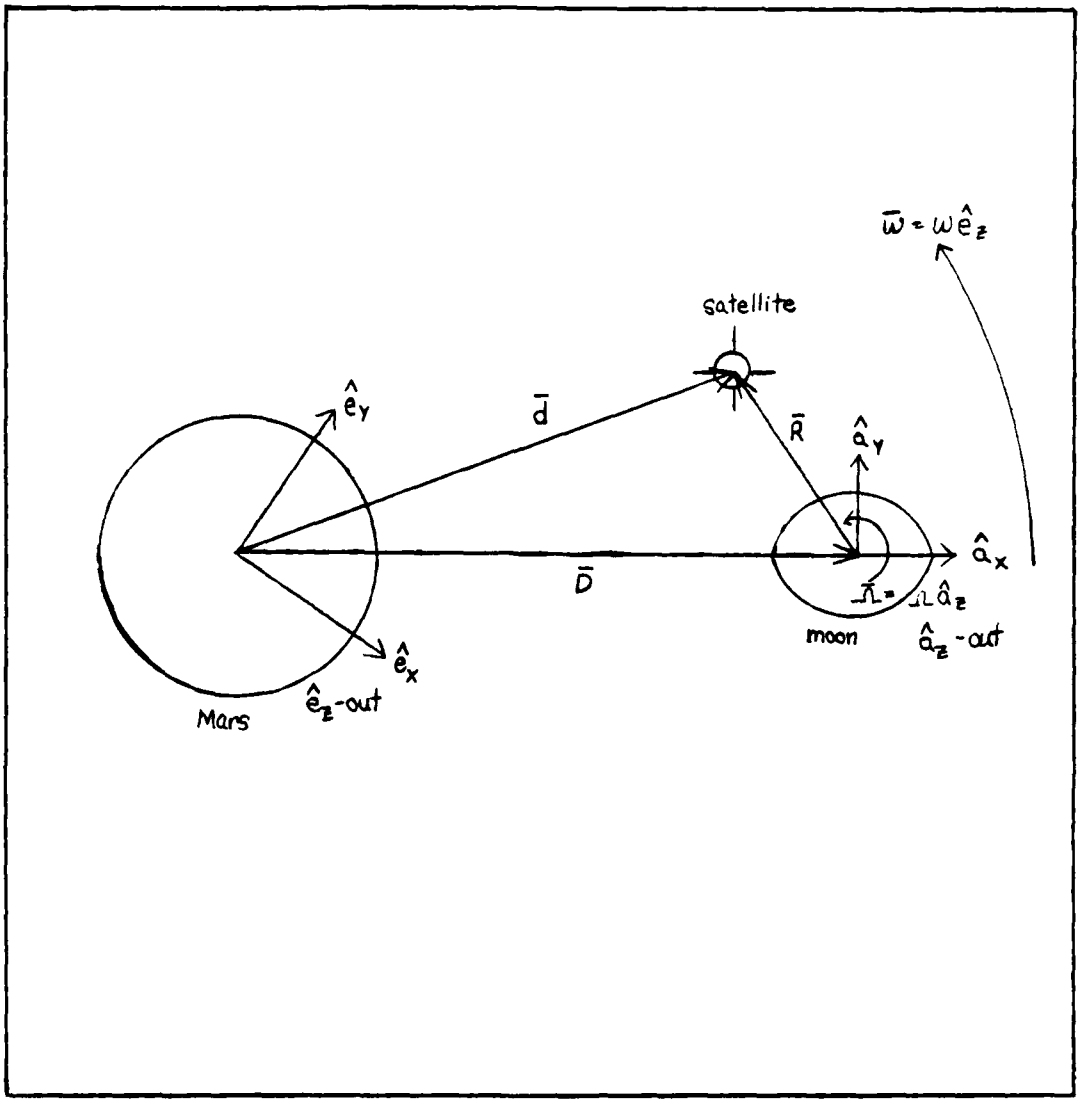

Figure 1. Coordinate System

Mars, Phobos, and Deimos are given in Appendix A.

Equations of Motion

The equations of motion of the satellite will be derived in the form of Hamilton's canonical equations. The Hamiltonian is defined as

$$H = \Sigma P_i \dot{Q}_i - L \tag{1}$$

where Q_i and P_i are the generalized coordinates and generalized momenta, respectively. L is termed the Lagrangian and is given by

$$L = T - V \tag{2}$$

where T and V are the kinetic energy and potential energy, respectively. The first step then, in determining the equations of motion is to find T and V in terms of the generalized coordinates (Q_i's) and generalized velocities ($\dot{Q}_i$'s).

Kinetic Energy. The kinetic energy of the satellite is given by

$$T_{sat} = \frac{1}{2} mv^2 \tag{3}$$

where m is the mass of the satellite and v is the inertial velocity of the satellite. In this study, the inertial reference frame is taken to be at the center of mass of Mars.

Therefore,

$$v^2 = \dot{\mathbf{d}} \cdot \dot{\mathbf{d}} \tag{4}$$

Throughout this investigation, a dot ($\cdot$) over a vector will indicate the time rate of change of the vector with respect to the inertial frame (an inertial derivative). As seen in Figure 1, d may be written as

$$\mathbf{d} = \mathbf{D} + \mathbf{R} \tag{5}$$

Therefore

$$\dot{\mathbf{d}} = \dot{\mathbf{D}} + \dot{\mathbf{R}} \tag{6}$$

$\dot{\mathbf{D}}$ may be expressed as

$$\dot{\mathbf{D}} = \frac{{}^{i}d}{dt}\,\mathbf{D} = \frac{{}^{r}d}{dt}\,\mathbf{D} + \mathbf{w}^{ri} \times \mathbf{D} \tag{7}$$

where the superscripts i and r indicate derivatives taken in the inertial and rotating (moon-fixed) frames, respectively. Because D remains constant in the rotating frame,

$$\frac{{}^{r}d}{dt}\,\mathbf{D} = 0 \tag{8}$$

and Eq (7) simplifies to

$$\dot{\mathbf{D}} = \mathbf{w}^{ri} \times \mathbf{D} \tag{9}$$

but

$$\mathbf{w}^{ri} = \Omega \hat{\mathbf{a}}_z \tag{10}$$

Therefore

$$\dot{D} = (\Omega \hat{a}_z) \times (D\hat{a}_x) = \Omega D \hat{a}_y \tag{11}$$

Now R is defined to be

$$R = X\hat{a}_x + Y\hat{a}_y + Z\hat{a}_z \tag{12}$$

$\dot{R}$ may then be expressed as

$$\dot{R} = \frac{i_d}{dt} R = \frac{r_d}{dt} R + w^{ri} \times R \tag{13}$$

$$= \dot{X}\hat{a}_x + \dot{Y}\hat{a}_y + \dot{Z}\hat{a}_z \tag{14}$$

$$+ (\Omega \hat{a}_z) \times (X\hat{a}_x + Y\hat{a}_y + Z\hat{a}_z)$$

Therefore

$$\dot{R} = (\dot{X} - \Omega Y)\hat{a}_x + (\dot{Y} + \Omega X)\hat{a}_y + \dot{Z}\hat{a}_z \tag{15}$$

Combining Eqs (6), (11), and (15) results in

$$\dot{d} = (\dot{X} - \Omega Y)\hat{a}_x + (\dot{Y} + \Omega X + \Omega D)\hat{a}_y + \dot{Z}\hat{a}_z \tag{16}$$

Combining Eqs (3), (4), and (16) yields

$$T_{sat} = \frac{1}{2} m[(\dot{X} - \Omega Y)^2 + (\dot{Y} + \Omega X + \Omega D)^2 + \dot{Z}^2] \tag{17}$$

Potential Energy. The potential energy of the satellite may be divided into two parts, one due to Mars and one due to the moon.

$$V_{sat} = V_{mars} + V_{moon} \tag{18}$$

Potential Energy Due to Mars. The potential energy of the satellite due to the gravitational attraction of Mars is easily derived. In this study, Mars is assumed to possess spherical symmetry. Therefore, the center of mass of Mars is assumed to coincide with its center of gravity. The potential energy of the satellite due to the gravitational attraction of Mars may, therefore, be written in the simple Newtonian form as

$$V_{mars} = - \frac{GM_{mars}m}{d} \tag{19}$$

where d is

$$d = |\mathbf{d}| = |\mathbf{D} + \mathbf{R}| = [(X + D)^2 + Y^2 + Z^2]^{1/2} \tag{20}$$

Potential Energy Due to Moon. The potential energy of the satellite due to the gravitational attraction of the moon is more difficult to determine since the moon is not spherically symmetric. Its shape is assumed to be a triaxial ellipsoid as shown in Figure 2. The gravitational potential for an arbitrarily shaped body is given in Meirovitch (9:430-436).

The potential energy in an inverse square force field may be written as

$$V_{moon} = - Gm\int \frac{dM_{moon}}{r} \tag{21}$$

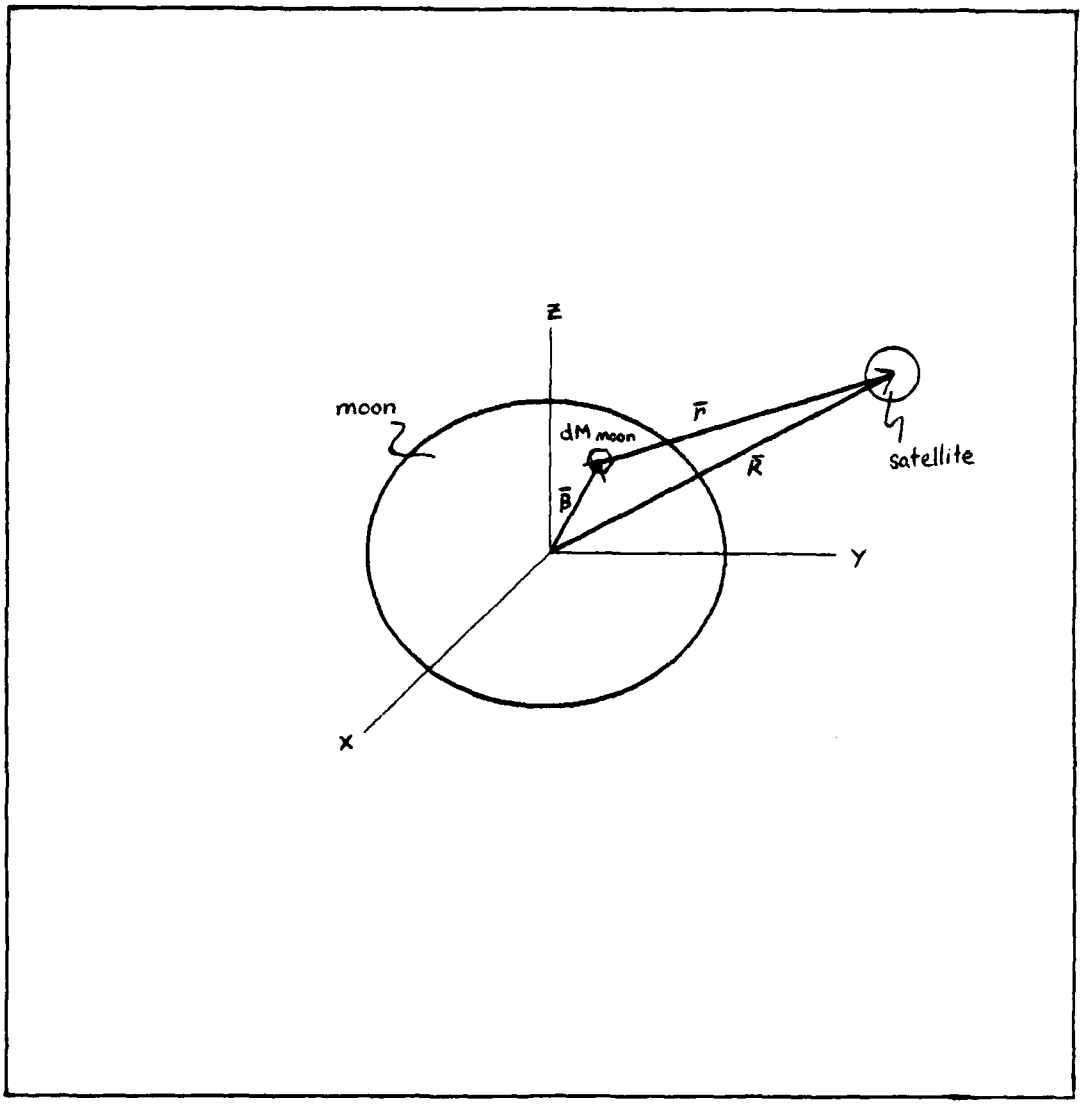

Figure 2. Gravitational Potential Due to Moon

The scalar r is the distance between the satellite center of gravity and a mass differential element of the moon, dM_{moon}. It may be written as

$$r = |r| = |R - \beta| \tag{22}$$

Its inverse may be written as

$$r^{-1} = |R - \beta|^{-1} = [(R - \beta)^2]^{-1/2} \tag{23}$$

$$= (R^2 - 2R\cdot\beta + \beta^2)^{-1/2} \tag{24}$$

$$= [R^2(1 - 2\frac{R\cdot\beta}{R^2} + \frac{\beta^2}{R^2})]^{-1/2} \tag{25}$$

$$= R^{-1}[1 - (2\frac{R\cdot\beta}{R^2} + \frac{\beta^2}{R^2})]^{-1/2} \tag{26}$$

Using a binomial expansion, it can then be written in the form of a power series as

$$r^{-1} = R^{-1}\{1 + \frac{R\cdot\beta}{R^2} - \frac{1}{2}(\frac{\beta}{R})^2 + \frac{3}{8}[2\frac{R\cdot\beta}{R^2} - (\frac{\beta}{R})^2]^2 + \ldots\} \tag{27}$$

$$= R^{-1} + R^{-3}(R\cdot\beta) - \frac{1}{2}R^{-3}\beta^2 + \frac{3}{2}R^{-5}(R\cdot\beta)^2 \tag{28}$$

$$- \frac{3}{2}R^{-5}(R\cdot\beta)\beta^2 + \frac{3}{8}R^{-5}\beta^4 + \ldots$$

From Figure 2, the following vectors are defined

$$R = X\hat{a}_x + Y\hat{a}_y + Z\hat{a}_z \tag{29}$$

$$\beta = a\hat{a}_x + b\hat{a}_y + c\hat{a}_z \tag{30}$$

Therefore

$$R^2 = X^2 + Y^2 + Z^2 \tag{31}$$

$$\beta^2 = a^2 + b^2 + c^2 \tag{32}$$

$$\mathbf{R} \cdot \boldsymbol{\beta} = aX + bY + cZ \tag{33}$$

Combining Eqs (21), (28), and (31)-(33) results in

$$V_{moon} = - GmR^{-1}\int dM_{moon} - GmR^{-3}\int (aX + bY + cZ)dM_{moon} \tag{34}$$

$$+ \frac{1}{2}GmR^{-3}\int (a^2 + b^2 + c^2)dM_{moon}$$

$$- \frac{3}{2}GmR^{-5}\int (aX + bY + cZ)^2 dM_{moon}$$

The higher order terms resulting from the binomial expansion have been dropped since their effect is negligible.

Eq (34) may now be broken down into smaller parts.

$$- GmR^{-1}\int dM_{moon} = - GmR^{-1}M_{moon} \tag{35}$$

Because the origin is taken to be at the center of mass,

$$- GmR^{-3}\int (aX + bY + cZ)dM_{moon} = 0 \tag{36}$$

Combining the third and fourth terms of Eq (34) results in

$$- \frac{1}{2}GmR^{-3}\int [3R^{-2}(aX + bY + cZ)^2 - (a^2 + b^2 + c^2)]dM_{moon} \tag{37}$$

$$= - \frac{1}{2}GmR^{-3}\int [3R^{-2}(a^2X^2 + b^2Y^2 + c^2Z^2) \tag{38}$$

$$+ 6(abXY + acXZ + bcYZ) - (a^2 + b^2 + c^2)]dM_{moon}$$

$$= -\frac{1}{2}GmR^{-3}[(3R^{-2}X^2 - 1)\int a^2 dM_{moon} \tag{39}$$

$$+ (3R^{-2}Y^2 - 1)\int b^2 dM_{moon} + (3R^{-2}Z^2 - 1)\int c^2 dM_{moon}$$

$$+ 6(XY\int abdM_{moon} + XZ\int acdM_{moon} + YX\int bcdM_{moon})]$$

But

$$\int a^2 dM_{moon} = \frac{1}{2}\int[(a^2 + b^2) + (a^2 + c^2) - (b^2 + c^2)]dM_{moon} \tag{40}$$

$$= \frac{1}{2}(I_{zz} + I_{yy} - I_{xx}) \tag{41}$$

$$\int b^2 dM_{moon} = \frac{1}{2}\int[(a^2 + b^2) + (b^2 + c^2) - (a^2 + c^2)]dM_{moon} \tag{42}$$

$$= \frac{1}{2}(I_{zz} + I_{xx} - I_{yy}) \tag{43}$$

$$\int c^2 dM_{moon} = \frac{1}{2}\int[(a^2 + c^2) + (b^2 + c^2) - (a^2 + b^2)]dM_{moon} \tag{44}$$

$$= \frac{1}{2}(I_{yy} + I_{xx} - I_{zz}) \tag{45}$$

$$\int abdM_{moon} = I_{xy} \tag{46}$$

$$\int acdM_{moon} = I_{xz} \tag{47}$$

$$\int bcdM_{moon} = I_{yz} \tag{48}$$

I_{xx}, I_{yy}, and I_{zz} are the mass moments of inertia. I_{xy} I_{xz}, and I_{yz} are the mass products of inertia. Using principal axes, the mass products of inertia for the triaxial ellipsoid are

$$I_{xy} = I_{xz} = I_{yz} = 0 \tag{49}$$

The mass moments of inertia are calculated using the following equations (8:542)

$$I_{xx} = \frac{1}{5}M_{moon}(b^2 + c^2)$$

$$I_{yy} = \frac{1}{5}M_{moon}(a^2 + c^2)$$

$$I_{zz} = \frac{1}{5}M_{moon}(a^2 + b^2)$$

where a, b, and c are the axis lengths of the moon.

The potential energy due to the moon may now be written

$$V_{moon} = - GmM_{moon}R^{-1} \tag{50}$$
$$- \frac{1}{4}GmR^{-3}[(3R^{-2}X^2 - 1)(I_{yy} + I_{zz} - I_{xx})$$
$$+ (3R^{-2}Y^2 - 1)(I_{xx} + I_{zz} - I_{yy})$$
$$+ (3R^{-2}Z^2 - 1)(I_{xx} + I_{yy} - I_{zz})]$$

$$V_{moon} = - GmM_{moon}R^{-1} + \frac{1}{4}GmR^{-3}(I_{xx} + I_{yy} + I_{zz}) \tag{51}$$
$$- \frac{3}{4}GmR^{-5}[X^2(I_{yy} + I_{zz} - I_{xx})$$
$$+ Y^2(I_{xx} + I_{zz} - I_{yy}) + Z^2(I_{xx} + I_{yy} - I_{zz})]$$

Lagrangian. The next step in determining the equations of motion is to find the Lagrangian. Combining Eqs (2), (17), (19), (20) and (51) the Lagrangian becomes

$$L = T - V = \frac{1}{2}m[(\dot{X} - \Omega Y)^2 + (\dot{Y} + \Omega X + \Omega D)^2 + \dot{Z}^2] \qquad (52)$$

$$+ GM_{mars}md^{-1}$$

$$+ GM_{moon}mR^{-1} - \frac{1}{4}GmR^{-3}(I_{xx} + I_{yy} + I_{zz})$$

$$+ \frac{3}{4}GmR^{-5}[X^2(I_{yy} + I_{zz} - I_{xx})$$

$$+ Y^2(I_{xx} + I_{zz} - I_{yy}) + Z^2(I_{xx} + I_{yy} - I_{zz})]$$

Dividing out the mass of the satellite, m, the Lagrangian may be written on a per unit mass basis as

$$L = \frac{1}{2}[(\dot{X} - \Omega Y)^2 + (\dot{Y} + \Omega X + \Omega D)^2 + \dot{Z}^2] \qquad (53)$$

$$+ GM_{mars}d^{-1}$$

$$+ GM_{moon}R^{-1} - \frac{1}{4}GR^{-3}(I_{xx} + I_{yy} + I_{zz})$$

$$+ \frac{3}{4}GR^{-5}[X^2(I_{yy} + I_{zz} - I_{xx})$$

$$+ Y^2(I_{xx} + I_{zz} - I_{yy}) + Z^2(I_{xx} + I_{yy} - I_{zz})]$$

Generalized Momenta. Next, the generalized momenta, P_i, are derived

$$P_X = \frac{\partial L}{\partial \dot{X}} = \dot{X} - \Omega Y \qquad (54)$$

$$P_Y = \frac{\partial L}{\partial \dot{Y}} = \dot{Y} + \Omega X + \Omega D \qquad (55)$$

$$P_Z = \frac{\partial L}{\partial \dot{Z}} = \dot{Z} \tag{56}$$

Generalized Velocities. Before the Hamiltonian can be defined, the generalized velocities, $\dot{Q}_i$'s, must first be eliminated from the Lagrangian. Rearranging Eqs (54)-(56) results in

$$\dot{X} = P_X + \Omega Y \tag{57}$$

$$\dot{Y} = P_Y - \Omega X - \Omega D \tag{58}$$

$$\dot{Z} = P_Z \tag{59}$$

Substituting Eqs (54)-(56) into the Lagrangian (Eq (53)) provides

$$\begin{aligned} L = {} & \frac{1}{2}(P_X^2 + P_Y^2 + P_Z^2) \\ & + GM_{mars}d^{-1} \\ & + GM_{moon}R^{-1} - \frac{1}{4}GR^{-3}(I_{xx} + I_{yy} + I_{zz}) \\ & + \frac{3}{4}GR^{-5}[X^2(I_{yy} + I_{zz} - I_{xx}) \\ & + Y^2(I_{xx} + I_{zz} - I_{yy}) + Z^2(I_{xx} + I_{yy} - I_{zz})] \end{aligned} \tag{60}$$

Hamiltonian. With the Lagrangian in the correct form, the Hamiltonian may be written as follows

$$\begin{aligned} H = \Sigma P_i \dot{Q}_i - L = {} & P_X(P_X + \Omega Y) + P_Y(P_Y - \Omega X - \Omega D) + P_Z^2 \\ & - \frac{1}{2}(P_X^2 + P_Y^2 + P_Z^2) \end{aligned} \tag{61}$$

$$- GM_{mars}d^{-1}$$

$$- GM_{moon}R^{-1} + \frac{1}{4}GR^{-3}(I_{xx} + I_{yy} + I_{zz})$$

$$- \frac{3}{4}GR^{-5}[X^2(I_{yy} + I_{zz} - I_{xx})$$

$$+ Y^2(I_{xx} + I_{zz} - I_{yy}) + Z^2(I_{xx} + I_{yy} - I_{zz})]$$

$$H = \frac{1}{2}(P_X^2 + P_Y^2 + P_Z^2) + P_X\Omega Y - P_Y\Omega(X + D) \quad (62)$$

$$- GM_{mars}d^{-1}$$

$$- GM_{moon}R^{-1} + \frac{1}{4}GR^{-3}(I_{xx} + I_{yy} + I_{zz})$$

$$- \frac{3}{4}GR^{-5}[X^2(I_{yy} + I_{zz} - I_{xx})$$

$$+ Y^2(I_{xx} + I_{zz} - I_{yy}) + Z^2(I_{xx} + I_{yy} - I_{zz})]$$

Hamilton's Equations. The equations of motion may now be written in canonical form. It is advantageous to use this form because the resulting first order differential equations can be numerically integrated more readily. In addition, since the Hamiltonian contains only the generalized coordinates and momenta, and not their time derivatives, first integrals of motion are easier to determine.

$$\dot{Q}_i = \frac{\partial H}{\partial P_i} \quad (63)$$

$$\dot{X} = \frac{\partial H}{\partial P_X} = P_X + \Omega Y \quad (64)$$

$$\dot{Y} = \frac{\partial H}{\partial P_Y} = P_Y - \Omega(X + D) \quad (65)$$

$$\dot{Z} = \frac{\partial H}{\partial P_Z} = P_Z \tag{66}$$

$$\dot{P}_i = -\frac{\partial H}{\partial Q_i} \tag{67}$$

$$\dot{P}_X = -\frac{\partial H}{\partial X} = \Omega P_Y - GM_{mars}d^{-3}(X + D) - GM_{moon}R^{-3}X \tag{68}$$

$$+ \frac{3}{4}GR^{-5}X(3I_{yy} + 3I_{zz} - I_{xx})$$

$$- \frac{15}{4}GR^{-7}X[X^2(I_{yy} + I_{zz} - I_{xx})$$

$$+ Y^2(I_{xx} + I_{zz} - I_{yy}) + Z^2(I_{xx} + I_{yy} - I_{zz})]$$

$$\dot{P}_Y = -\frac{\partial H}{\partial Y} = -\Omega P_X - GM_{mars}d^{-3}Y - GM_{moon}R^{-3}Y \tag{70}$$

$$+ \frac{3}{4}GR^{-5}Y(3I_{xx} + 3I_{zz} - I_{yy})$$

$$- \frac{15}{4}GR^{-7}Y[X^2(I_{yy} + I_{zz} - I_{xx})$$

$$+ Y^2(I_{xx} + I_{zz} - I_{yy}) + Z^2(I_{xx} + I_{yy} -$$

$$\dot{P}_Z = -\frac{\partial H}{\partial Z} = -GM_{mars}d^{-3}Z - GM_{moon}R^{-3}Z \tag{70}$$

$$+ \frac{3}{4}GR^{-5}Z(3I_{xx} + 3I_{yy} - I_{zz})$$

$$- \frac{15}{4}GR^{-7}Z[X^2(I_{yy} + I_{zz} - I_{xx})$$

$$+ Y^2(I_{xx} + I_{zz} - I_{yy}) + Z^2(I_{xx} + I_{yy} - I_{zz})]$$

These equations of motion are also listed in Appendix B for convenience.

X-Axis Symmetry

The equations of motion may be transformed using the following relationships

$$X \longrightarrow X$$

$$Y \longrightarrow -Y$$

$$t \longrightarrow -t$$

When this transformation is made, the equations of motion do not change in the rotating coordinate system. Therefore, for every orbit, there is a second orbit which is a reflection of the first orbit about the XZ plane. The second orbit, however, is traversed in the opposite direction from the first due to -t. This symmetry becomes very useful in the surface of section technique and effectively doubles the number of data points obtained for a given trajectory.

III. Surface of Section Technique

Poincaré's surface of section method is used to discover stable orbits around the Martian moons. In this technique, the dynamics of the three-body problem are restricted to the planar case and the one known integral of motion is determined. A surface of section is then introduced into the problem in order to determine if further integrals of motion exist. If a second integral of motion exists, stable orbits may be discovered.

Restricted Three-Body Problem

In what is commonly referred to as the Restricted Three-body Problem, only the gravitational forces between the bodies are considered. Perturbations due to other forces such as the gravitational attraction of other bodies, atmospheric drag, a non-spherical body, etc. are assumed to be very small and are ignored. The equations previously derived describe the motion of a satellite in a Modified Restricted Three-body Problem. Gravity terms due to the non-spherical moon are also included.

The artificial satellite in the restricted three-body problem is constrained to motion in the plane formed by the moon revolving around the planet. Because of this planar restriction, Eqs (66) and (70) can be ignored and Z can be set equal to 0 in the remaining equations (Eqs (64), (65), (68), and (69)). These equations of motion describe a

system with two degrees of freedom and four dimensions in the phase space.

Integrals of Motion

When four initial conditions are defined, a solution of the system may be represented in the four-dimensional phase space. If an integral of motion exists, solutions of the system may be represented in a three-dimensional subspace for particular values of the constant integral of motion (13:127).

In this problem, the Lagrangian (Eq 60) does not depend explicitly on time. Therefore

$$\frac{\partial L}{\partial t} = 0 \tag{71}$$

An integral of motion, known as Jacobi's integral may then be determined from the following (9:83)

$$\Sigma \frac{\partial L}{\partial \dot{Q}_i} \dot{Q}_i - L = \text{constant} \tag{72}$$

In this case, the Jacobi integral turns out to be equal to the system Hamiltonian (Eq 62). This was to be expected since the Hamiltonian does not depend explicitly on time.

In this problem, the artificial satellite is constrained to move on a three-dimensional manifold within the four-dimensional phase space because of the existence of the Jacobi Integral (7:6). The Hamiltonian provides a one-dimensional parametrization of the manifolds on which the

satellite motion takes place.

If another independent integral of motion exists, the satellite is further constrained to move on a two-dimensional manifold embedded in the three-dimensional one defined by the Hamiltonian (7:6). The surface of section technique is used to determine the existence of such independent integrals of motion.

Surface

In the surface of section method, a surface is introduced into the phase space according to some given relationship. If a second integral of motion exists, the intersection of the two-dimensional manifold on which the satellite is constrained to move and the introduced surface will generally be one-dimensional (7:6). If a second integral of motion does not exist, the intersection of the surface and the satellite orbit will not be one-dimensional. Instead, the intersection will be scattered over a larger subset of the surface.

In this study, the surface of section is defined by the following condition

$$\mathbf{R} \cdot \mathbf{V} = 0 \tag{73}$$

or for the planar case under consideration

$$X\dot{X} + Y\dot{Y} = 0 \tag{74}$$

This condition occurs at the satellite orbit's apoapsis and

periapsis points. These are the points where the satellite is farthest from and nearest to the moon. Points along the orbit of the satellite where this condition occurs are plotted in the two-dimensional configuration space.

Other criteria for the surface of section are possible; however, $\mathbf{R} \cdot \mathbf{V} = 0$ is used because it indicates, by inspection, whether or not an orbit will collide with the moon. If any of the surface of section points lie beneath its surface, the trajectory will obviously collide with the moon.

Stability of Orbits

If the surface of section points plotted in the configuration space form closed contours, a stable orbit is present for that particular value of the Hamiltonian. A periodic orbit will pass through the centers of the closed curves.

If the surface of section points form closed curves that intersect one another, unstable orbits may be located which pass through the intersection points. The intersection of the curves is often referred to as a saddle point (an unstable equilibrium point).

IV. Solution Method

Satellite trajectories are determined through numerical integration with a FORTRAN computer program. The computer program allows for significant interaction between the operator and computer.

The initial X and Y coordinates for the trajectory and the Hamiltonian value are the primary inputs along with the integration step size and the total integration time. A data file with the X and Y coordinates for all of the surface of section points is the main output.

The output data files for several trajectories, each having the same Hamiltonian value, are then plotted with a two-dimensional graphics package. From these plots, the discovery of orbits, both stable and unstable, may be made.

Initial Conditions

Prior to the integration of the equations of motion, initial conditions for the states X, Y, P_X, and P_Y must be determined. The initial values of X, Y, and the Hamiltonian, H, are chosen. In addition, the starting point of all trajectories is chosen so the surface of section condition of Eqs (73) and (74) is met. Given these conditions, the initial values for P_X and P_Y may be calculated by first obtaining a quadratic expression for $\dot{Y}$.

To obtain a quadratic expression for $\dot{Y}$, the following equations are utilized

$$P_X = \frac{\partial L}{\partial \dot{X}} = \dot{X} - \Omega Y \tag{54}$$

$$P_Y = \frac{\partial L}{\partial \dot{Y}} = \dot{Y} + \Omega X + \Omega D \tag{55}$$

$$H = \frac{1}{2}(P_X^2 + P_Y^2 + P_Z^2) + P_X \Omega Y - P_Y \Omega (X + D) \tag{62}$$

$$- GM_{mars} d^{-1}$$

$$- GM_{moon} R^{-1} + \frac{1}{4} G R^{-3} (I_{xx} + I_{yy} + I_{zz})$$

$$- \frac{3}{4} G R^{-5} [X^2 (I_{yy} + I_{zz} - I_{xx})$$

$$+ Y^2 (I_{xx} + I_{zz} - I_{yy}) + Z^2 (I_{xx} + I_{yy} - I_{zz})]$$

$$\dot{X}\dot{X} + Y\dot{Y} = 0 \tag{74}$$

Substituting Eqs (54) and (55) into Eq (62), and combining all of the potential energy terms into one quantity (V), results in the following expression for the Hamiltonian

$$H = \frac{1}{2}(\dot{X}^2 + \dot{Y}^2 - \Omega^2 X^2 - \Omega^2 Y^2 - \Omega^2 D^2) \tag{75}$$

$$-2\Omega Y\dot{X} - \Omega^2 DX + V$$

Solving Eq (74) for $\dot{X}$ provides

$$\dot{X} = -\frac{Y}{X}\dot{Y} \tag{76}$$

Substituting Eq (76) into Eq (75) yields the following quadratic expression for $\dot{Y}$

$$(X^2 + Y^2 + 4\Omega Y^2)\dot{Y}^2 + (4\Omega XY^2)\dot{Y} \tag{77}$$

$$+ (2X^2)[-\frac{1}{2}(\Omega^2X^2 + \Omega^2Y^2 + \Omega^2D^2) - \Omega^2DX + V - H]Y = 0$$

Solving the above expression for $\dot{Y}$ results, of course, in two different values. Either value may be chosen. In many instances, choosing one value will result in a prograde trajectory, while choosing the other value will result in a retrograde trajectory.

$\dot{X}$ may be calculated from Eq (76). The required initial values for the generalized momenta, P_X and P_Y, may then be determined from Eqs (54) and (55).

Trajectory Integration

Haming's Ordinary Differential Equations Integrator is used to integrate the equations of motion (Eqs (64), (65), (68), and (69)). It is a fourth order predictor-corrector algorithm. It extrapolates the last four values of the state vector to obtain a predicted next value (the prediction step) (16:120). It then evaluates the equations of motion at the predicted value and corrects the extrapolated point using a higher order polynomial (the correction step) (16:120). The Haming method is numerically very stable and provides high accuracy.

Surface of Section Points

After each integration step, the value of **R•V** is calculated. The current value is compared to the last value and

if the sign of the value has changed, the surface of section condition (Eq 73) has been met.

In order to obtain very precise values for the surface of section points, the last four values of the integration time, the X and Y coordinates, and the **R•V** calculation are maintained. When a check of the **R•V** value indicates the orbit has passed through a surface of section point, the Newton interpolation polynomial (1:112) is used with the last four integration states to obtain a very precise determination of the coordinates of the surface of section point. **R•V** is a function of X and Y, however. Therefore, inverse interpolation is used to determine the X and Y coordinates for which **R•V** = 0 (1:119).

As discussed earlier, there is trajectory symmetry about the X-axis. Therefore, in addition to the surface of section point determined from the trajectory being integrated (X,Y), the reflection of that point about the X-axis (X,-Y) is also obtained.

Orbit Checks

Several checks are made during the integration of the trajectories. The location of the satellite relative to the moon is continuously checked.

If the satellite travels too far away from the moon an escape trajectory is assumed. In many cases, the satellite escapes into a Martian orbit. If, on the other hand, the

satellite passes too closely to the center of the moon, the singularity at that point causes the integration to "blow up." Whenever either one of these conditions occurs, integration of the trajectory is halted.

Even though trajectories which pass through (or very close to) the center of the moon become numerically unstable, other trajectories continue right through collisions with the moon without difficulty. These trajectories are allowed to continue, since they may provide useful results in the surface of section technique. In any event, a check of the trajectory will determine that a "collision" has occurred in these cases and make that fact known.

Dynamics Verification and Computer Program Checks

In order to verify that the equations of motion were correctly derived and that the computer program was performing as intended, various checks were made.

Two-Body Problem. One verification check involved reducing the dynamics of the problem to a simple two-body problem. In this case, the gravitational attraction of Mars (GM_{mars}), the system rotation (Ω), the moon's moments of inertia (I_{xx}, I_{yy}, and I_{zz}), and the distance to the origin of the coordinate system (D) were all set to 0. The satellite was then given circular speed relative to the moon for its initial altitude. The orbit integrated was indeed circular and did return to the original starting point. When the moments of inertia were included, the orbit became

slightly elliptical and contracted as expected.

In another case, the gravitational attraction of the moon (GM_{moon}) and the initial velocity of the satellite were set to 0. The starting point of the trajectory was chosen very near to the moon. The satellite remained relatively stationary in the rotating coordinate system, indicating it was indeed in the expected circular orbit of mars.

Conservation of the Hamiltonian. Another check involves the Hamiltonian. As discussed previously, the Hamiltonian is a constant integral of motion. It should remain invariant over the entire trajectory. H, therefore, is periodically checked throughout the trajectory integration to insure it is conserved to several decimal places.

V. Results and Discussion

Stable orbits were discovered about each of the Martian moons. The discussion of results will be presented separately for Phobos and Deimos. However, the nature of the orbits about each of the moons is quite similar, as might be expected.

Phobos

Figure 3 is a typical surface of section plot for Phobos. Each of the test trajectories was initiated along the negative X-axis (between the moon and Mars). Several stable trajectories (3-9) were integrated for each chosen Hamiltonian value. They were evenly spaced out over the "*region of stability*". *In this region*, all of the test trajectories remain in orbit around Phobos for the entire integration time. They demonstrate, at the very least, practical stability. The trajectories initiated beyond this region were unstable. Their surface of section points were scattered in the configuration space.

In Figure 3, eight stable test trajectories were integrated for the Hamiltonian value, H = -6.8528. Separate curves for each of them are readily identifiable in the figure.

Trajectories which were initiated outside the stable region, closer to the moon, proceeded to the moon's center. As expected, unstable trajectories closer to the moon

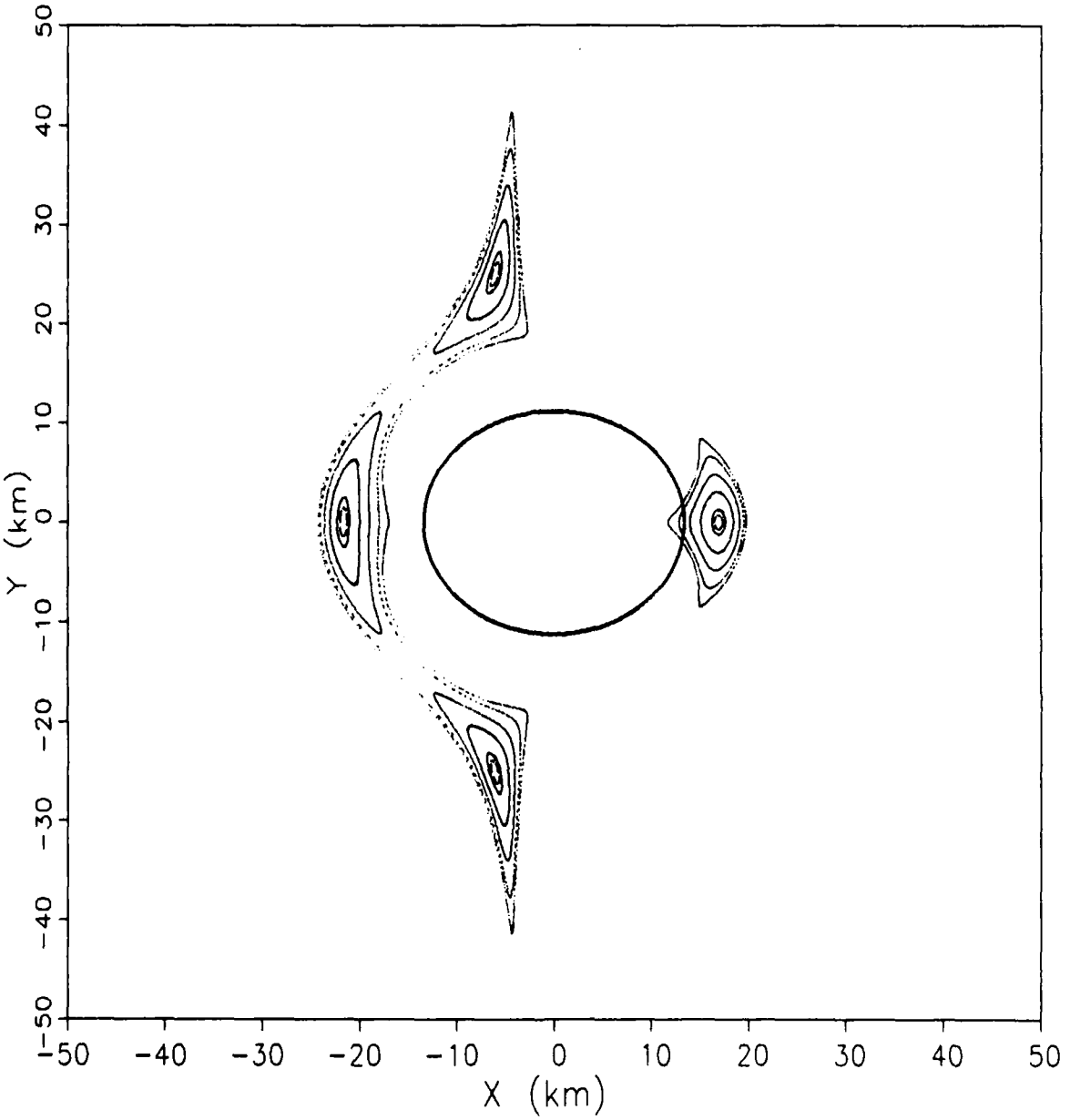

Figure 3. Phobos Surface of Section, H = -6.8528

reached the center in far fewer orbits than those further away from the moon. Trajectories that were initiated outside the stable region, further from the moon, escaped the moon's influence. They normally entered a Mars orbit similar to the orbit of the moon itself. These characteristics were similar to those of previous thesis efforts.

All of the trajectories were integrated for 5,000,000 seconds (57.9 days). This integration time provided thousands of surface of section points; enough so the size and shape of the curves formed were easily recognizable. The integration step size normally used was 200 seconds. Under these conditions, the run time on a main frame computer was several minutes. In a few instances, a smaller step size (50-100 seconds) was required to prevent numerical integration problems; usually for trajectories close to the center of the moon. Even with the large step size, the location of the surface of section points was accurately calculated with the inverse interpolation method discussed earlier.

Typical Orbits. For the typical orbit, four points meeting the surface of section criteria ($R \cdot V = 0$) were determined each time a trajectory encircled the moon. For the retrograde trajectories represented, the points appeared successively in a counter-clockwise manner. The four regions where the points were determined are easily identifiable in Figure 3. The curves formed for each trajectory are closed and thus indicate stable orbits. However, most of

the orbits rotate or precess about the moon and are not simple, closed periodic orbits. The four surface of section points rotate regularly within their "own region" for each successive encirclement of the moon.

The centers of the closed curves represent the surface of section points for a stable, closed periodic orbit. Figure 4 shows the simple periodic orbit associated with the surface of section of Figure 3. In order to demonstrate that the surface of section points for the closed periodic orbit do in fact coincide with the centers of the closed curves, the orbit has been superimposed with the surface of section plot. The orbit's eccentricity is .221 and its period is 13,900 seconds (3.86 hours). A satellite placed in this orbit would encircle the moon approximately twice during the orbital period of Phobos about Mars.

The surface of section technique was used to discover many stable orbits about Phobos. The orbit altitudes vary from just above the moon's surface to several hundred kilometers away. The surface of section plot associated with each of the orbits is contained in Appendix C. They are each identified with their particular Hamiltonian value, H.

Table I provides a summary of the characteristics of each of the stable, closed periodic orbits. The period of the first orbit listed is approximately half that of Phobos's orbit about Mars. The period of all of the other orbits is approximately equal to Phobos's orbit period

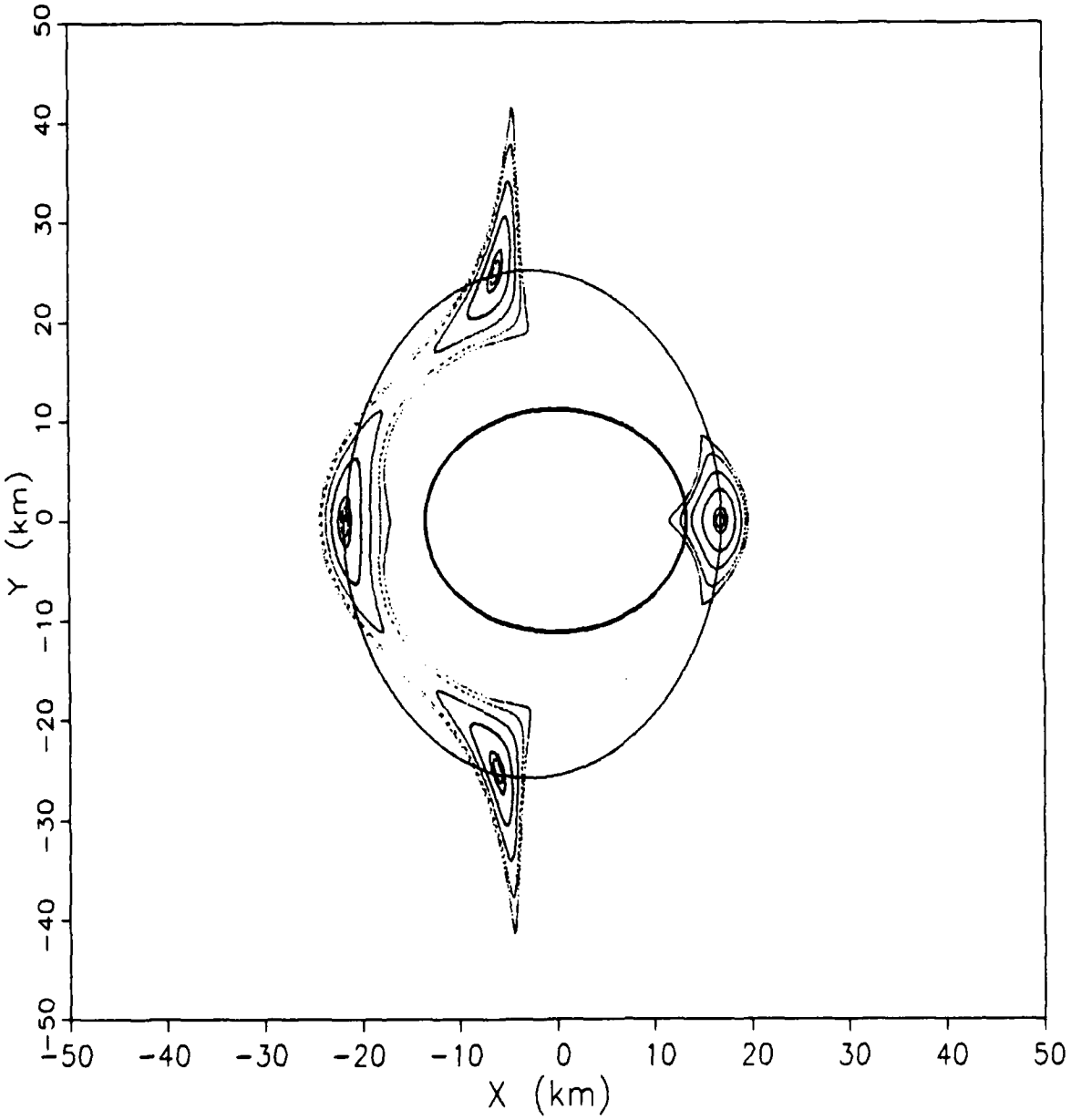

Figure 4. Stable Orbit About Phobos, H = -6.8528

Table I. Characteristics of the Stable Orbits About Phobos

H	I.C.'s	R_p	R_a	a	b	e	P
-6.8528	-22,0	17	26	22	21	.221	13,900
-6.8527	-68,0	61	126	93	87	.352	26,600
-6.8526	-93,0	86	178	132	123	.350	27,200
-6.8525	-112,0	105	217	161	151	.346	27,400
-6.8524	-129,0	121	251	186	174	.348	27,400
-6.8523	-143,0	136	279	208	195	.344	27,500
-6.8522	-156,0	150	307	228	214	.344	27,500
-6.8521	-169,0	161	331	246	231	.346	27,400
-6.8520	-179,0	173	356	265	249	.345	27,600
-6.85	-332,0	325	657	491	462	.338	27,600
-6.84	-708,0	695	1410	1052	990	.340	27,500

H - Hamiltonian, km^2/sec^2
I.C.'s - initial conditions, km
R_p - pericenter distance, km
R_a - apocenter distance, km
a - semi-major axis, km
b - semi-minor axis, km
e - eccentricity
P - period, sec

(Phobos rotates beneath each orbit in the rotating coordinate system). The eccentricities of the orbits are all about .34 - .35 with the exception of the first orbit which is slightly less eccentric (.221). The table also indicates the altitudes of the orbits increase at a lower and lower rate as the value of H increases.

The initial velocities of the orbits range from 11.4 m/s for the lowest orbit (H = -6.8528) to 327 m/s for the highest orbit (H = -6.84).

Variation of the Semi-Major Axis. Figures 3 and 4 demonstrate an interesting and unexpected phenomenon. For each orbit in a normal Keplerian ellipse, only two points will meet the surface of section criteria ($R \cdot V = 0$) used in this investigation. These two points, apoapsis and periapsis, are found at the ends of the major axis. For the closed orbit of Figures 3 and 4, however, four points meeting the surface of section criteria were discovered. This orbit does not represent a simple rotating Keplerian ellipse as expected.

The semi-major axis is not constant as the satellite orbits the moon. Instead, it varies with a period equal to half that of the satellite's orbital period. It can be seen from Figure 4 that a second, longer apoapsis distance is achieved during the first quarter of the orbit period. However, after half of the orbit period, the major axis has shifted back to its original position and the expected

periapsis point is achieved.

During the second half of the orbit, the major axis shifts again. The resulting apoapsis is symmetric about the X-axis with respect to the larger apoapsis which occurred during the first half of the orbit period. By the time the satellite has completed one orbit, the major axis has shifted back to its original position again. This perturbation occurs in all of the orbits discovered around Phobos.

This phenomenon was discovered by Tycho Brahe in the orbit of the Earth's moon (11:289). Brahe found that the semi-major axis of the Moon's orbit executed small oscillations. This perturbation, termed "the variation," has a period of half a synodic month. It results from the fact that there is less pull on the Moon in the radial direction of the Earth at new and full moon (the force potential is a maxima) than at the quarters (the force potential is a minima) (2:287). The curvature of the Moons's orbit, therefore, is least at new and full moon and greatest at the quarters, so that the orbit is elongated, with its longer axis perpendicular to the direction of the Sun (2:287).

The results obtained in this study demonstrate the same perturbation phenomenon. In this case, Mars is the third body that causes the effect. As in the case of the Moon's orbit, the satellite's major axis in this study is elongated in a direction perpendicular to the third body.

Collision Orbits. As discussed earlier, the surface of

section criteria provides a clear indication of orbit trajectories that will impact the moon. Figure 5 clearly indicates all of the trajectories integrated are collision orbits. All of the periapsis points, and in some cases even the apoapsis points, lie below the surface of the moon. The stable, closed periodic orbit indicated does in fact lie partially below the moon's surface as seen in Figure 6.

Orbit Resonance. Nonlinear systems often exhibit resonances at any rational multiple of the forcing frequency (16:140). In the case at hand, resonances occur when the period of the satellite is a rational multiple of the moon's orbit period. Resonant orbits usually produce several "islands" associated with a stable periodic orbit. These "chains of islands" were first described by Hénon and Heiles (5:76).

Figures 7 and 8 provide an excellent indication of orbit resonance. Figure 7 shows the entire surface of section plot for H = -6.8527. Figure 8 is a magnification of the same surface of section plot for the region closest to Mars.

As expected, a stable, closed periodic orbit is located by the center of the four concentric closed curves of Figure 8. Figures 9 and 10 show the simple closed orbit superimposed on the surface of section plot.

Seven separate closed curves or "loops" are also clearly evident in Figure 8 in the region between the outermost

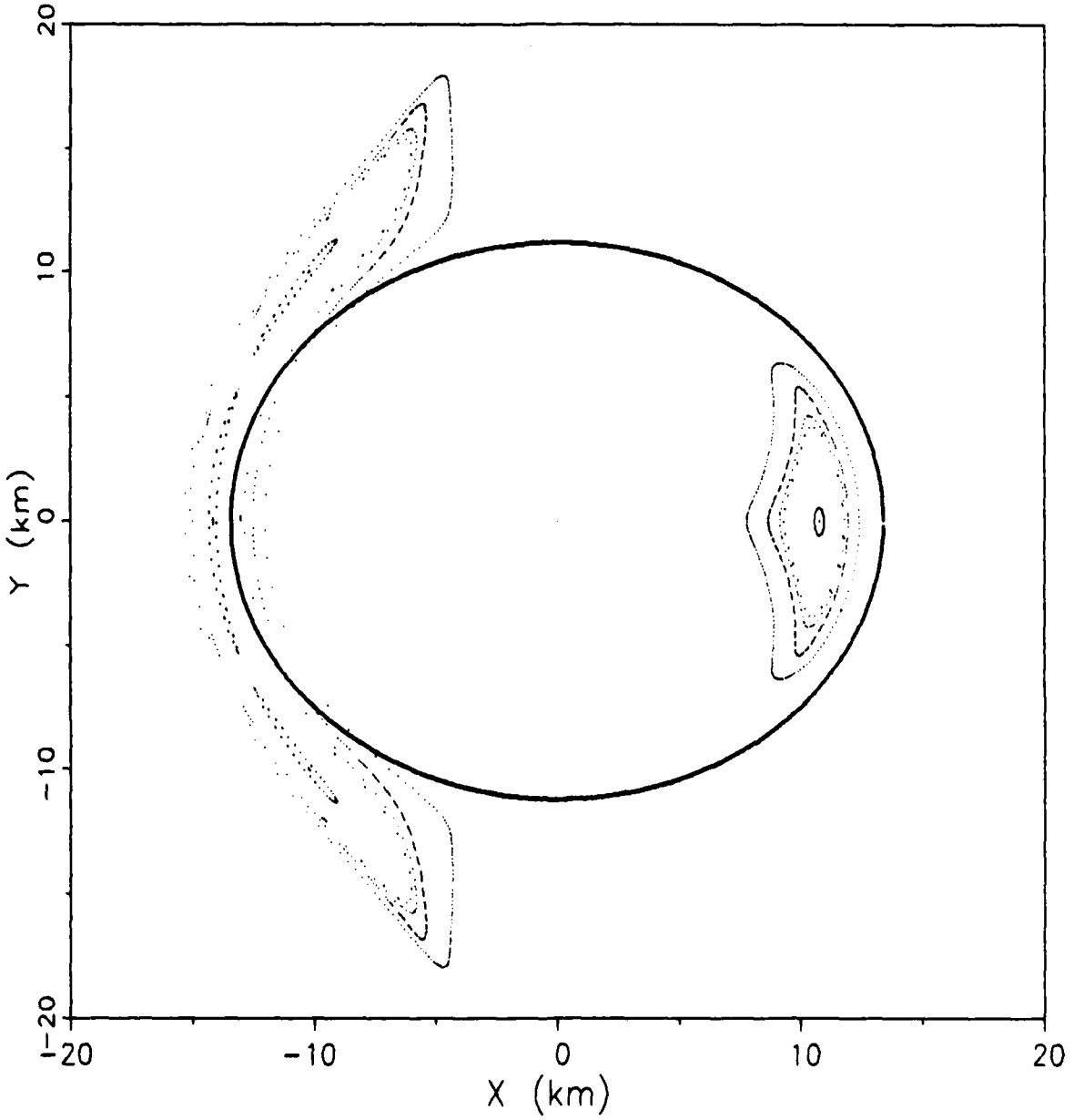

Figure 5. Phobos Surface of Section, H = -6.852813

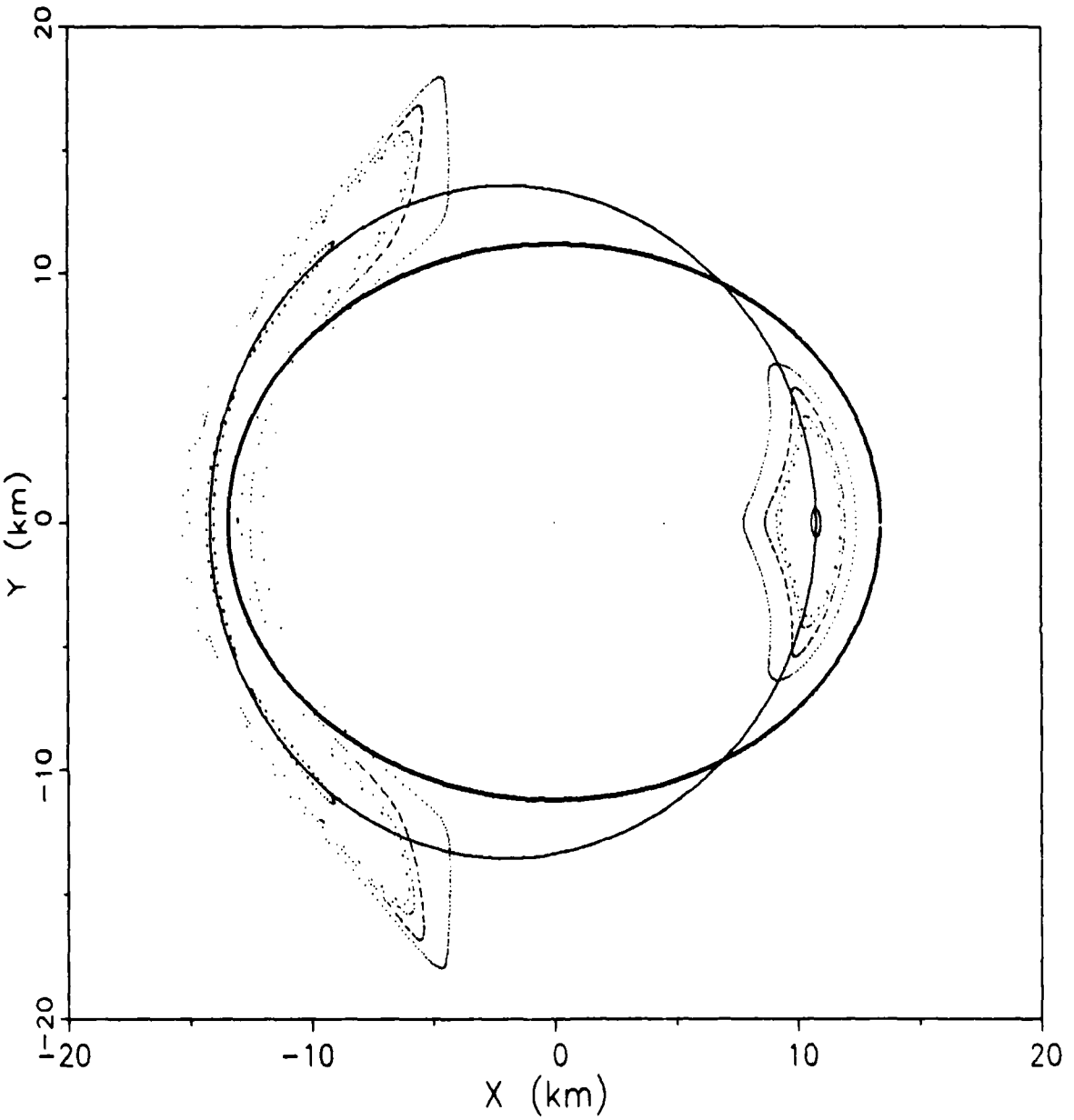

Figure 6. Phobos Collision Orbit, H -6.852813

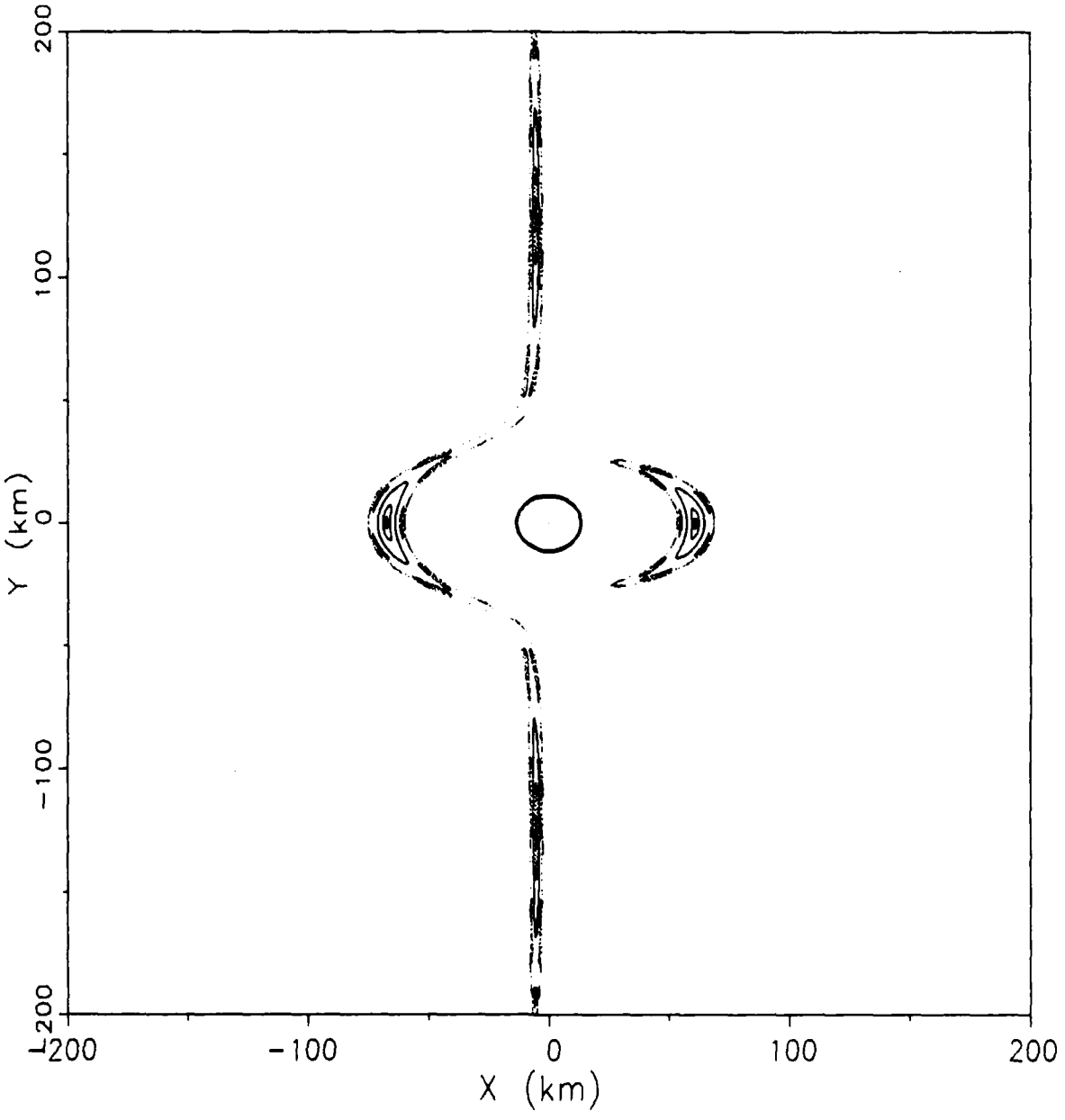

Figure 7. Phobos Surface of Section, H = -6.8527

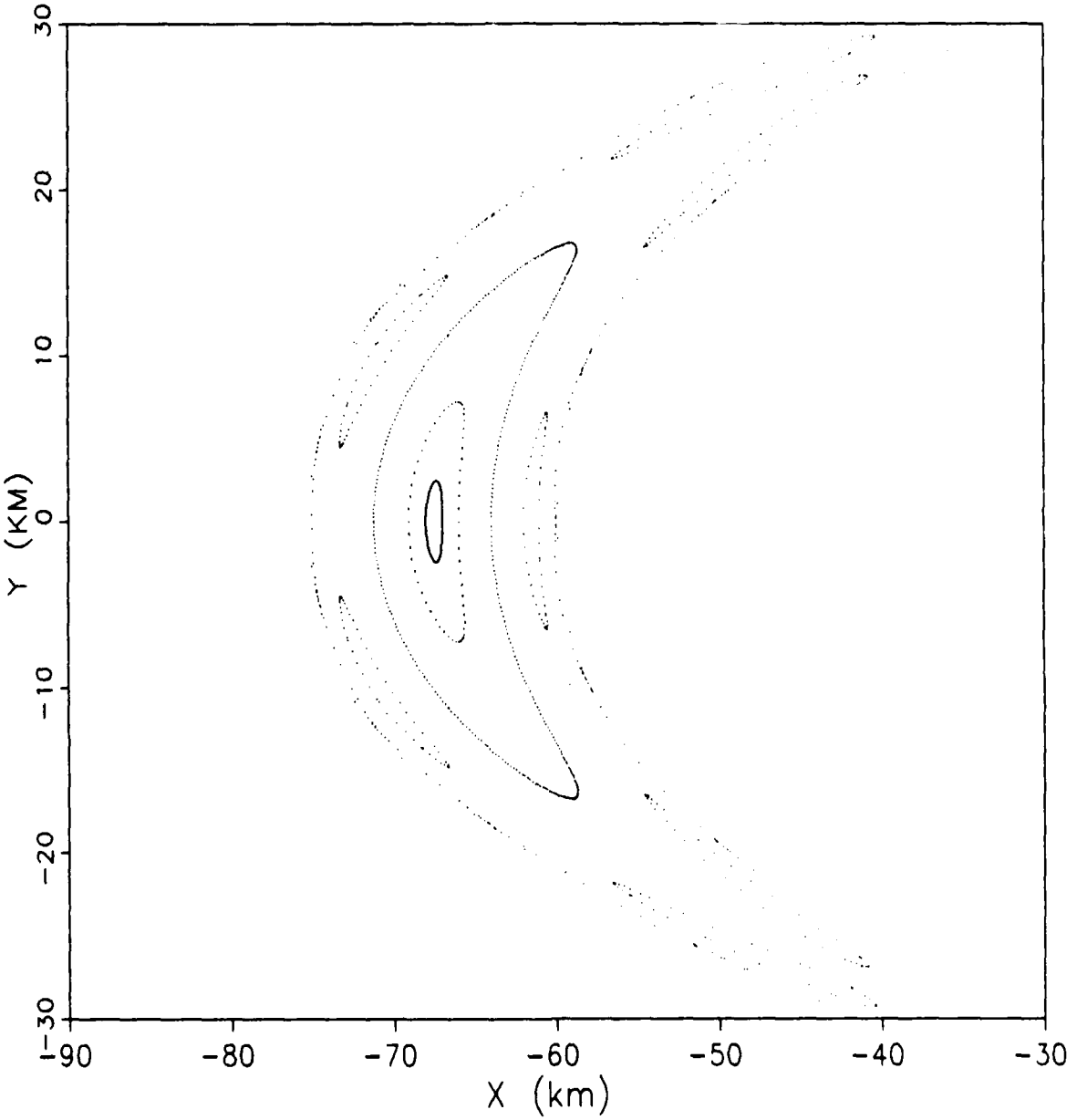

Figure 8. Phobos Surface of Section, H = -6.8527

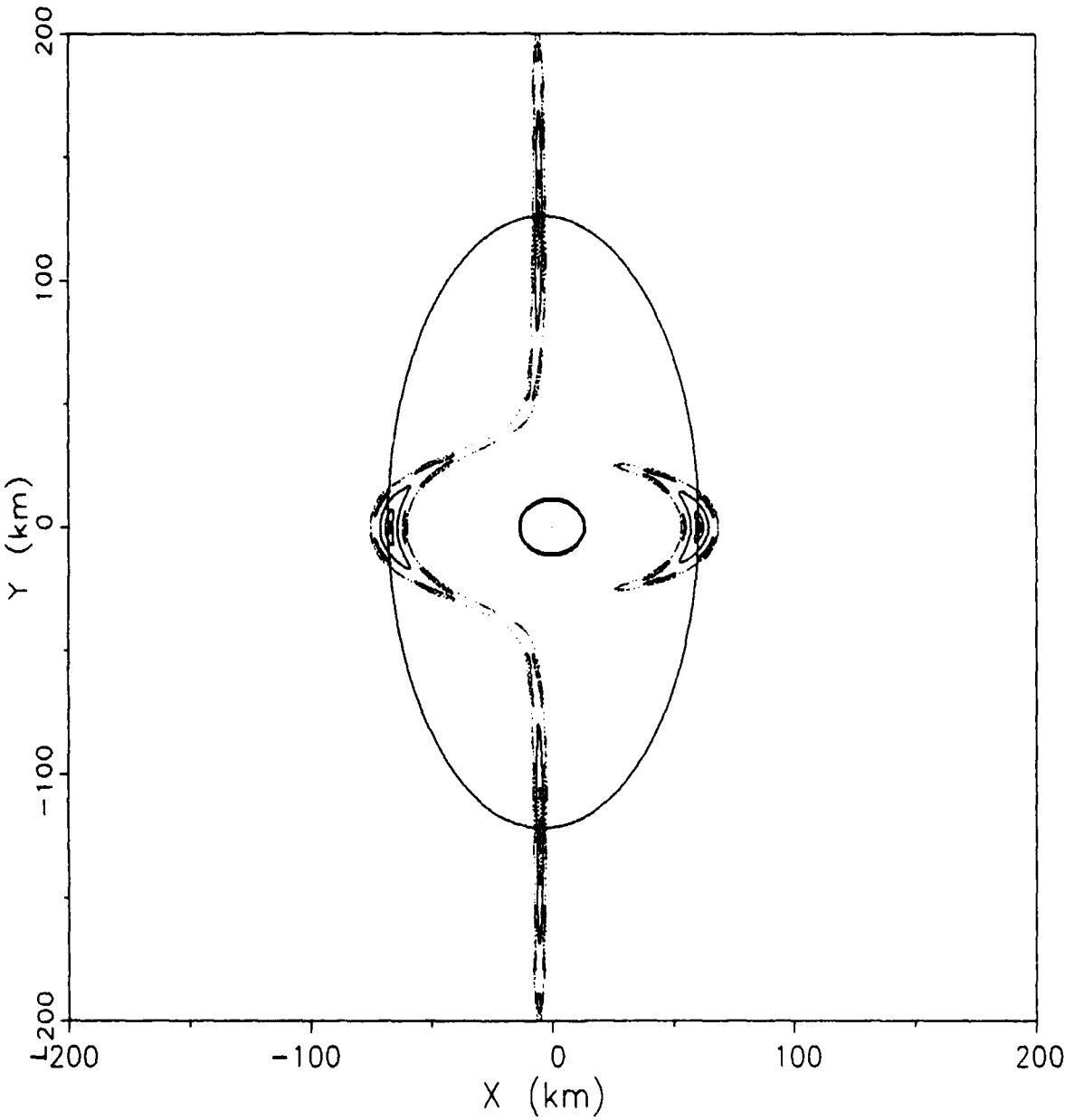

Figure 9. Stable Orbit About Phobos, H = -6.8527

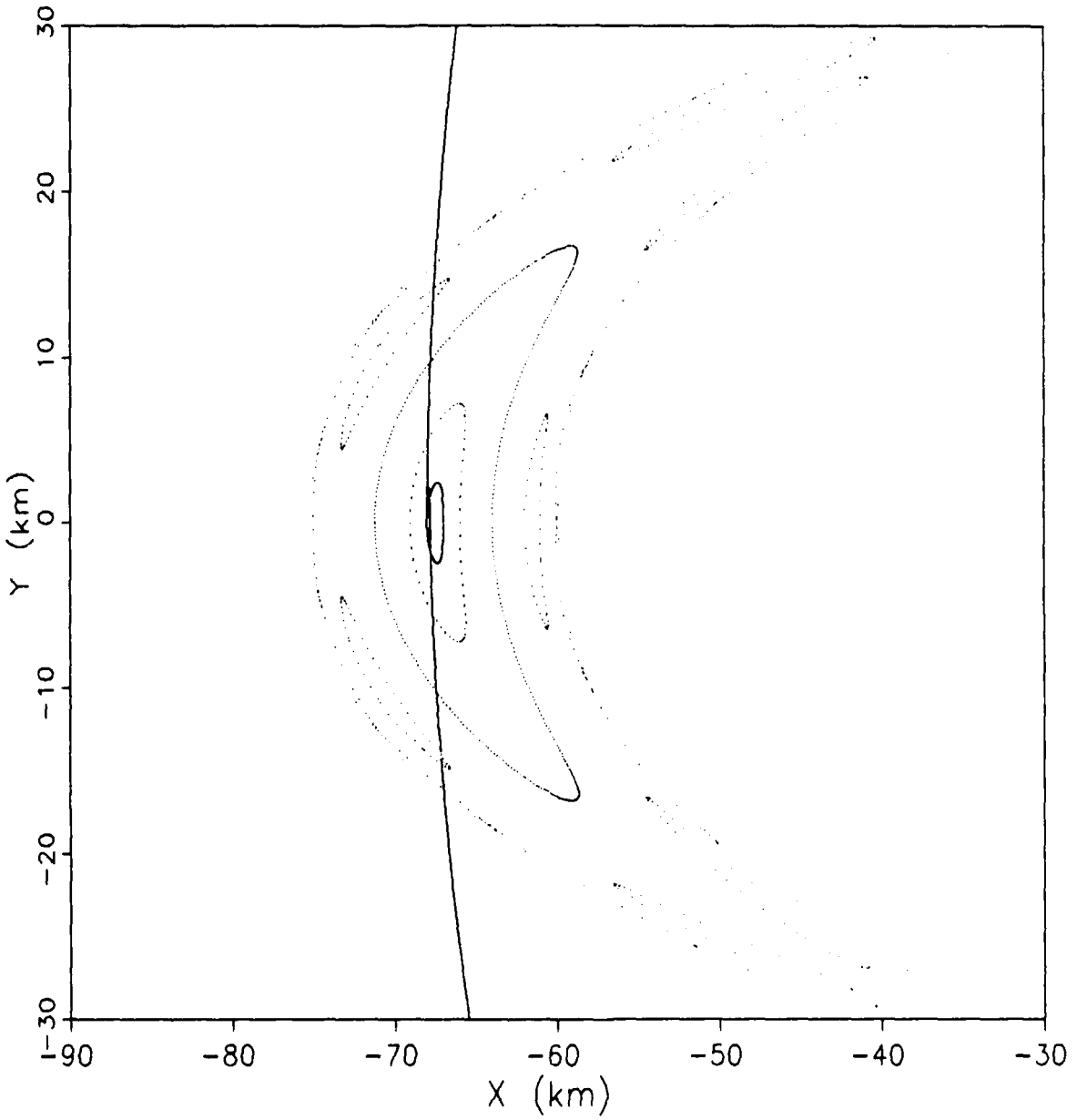

Figure 10. Stable Orbit About Phobos, H -6.8527

closed curve and the inner closed curves. These seven loops are the chain of islands associated with a single periodic orbit. Seven islands exist in each of the four portions of the surface of section plot. The orbit trajectory associated with this resonance travels through a different one of the seven islands for each encirclement of the moon. After seven encirclements, the trajectory comes back to the original island and this periodic behavior continues. Figures 11 and 12 show the periodic orbit superimposed on the surface of section plot. The period of this resonant orbit is approximately seven times greater than the period of the simple, closed periodic orbit. It is also seven times greater than the orbit period of Phobos.

Several other resonant orbits are indicated by the surface of section plots. Figures 28 and 32 also indicate the presence of stable periodic orbits with a resonance implied by seven islands. Figures 34, 38, 42, 44, and 46 indicate even greater resonances. Figures 34-36 represent an especially interesting case of higher order resonance.

Orbit Evolution. As the Hamiltonian is increased, orbits are found further and further from the moon. Trajectories "on the edge" of the stable regions in the surface of section plots become more and more elliptical and their periapsis points move closer and closer toward the moon. The orbits become less and less stable with respect to Phobos and are essentially orbits of Mars instead, which are

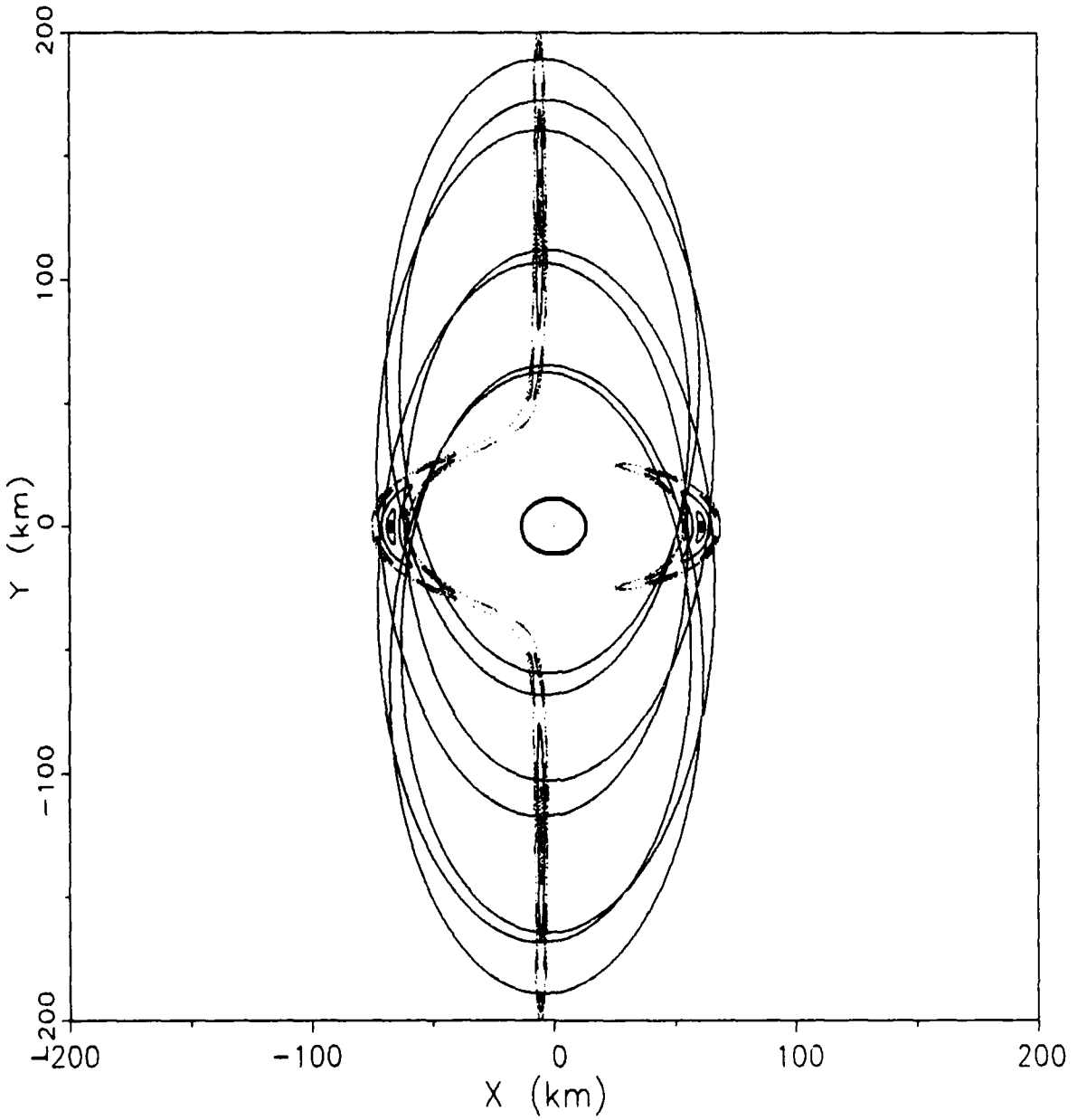

Figure 11. Stable Orbit About Phobos, $H = -6.8527$

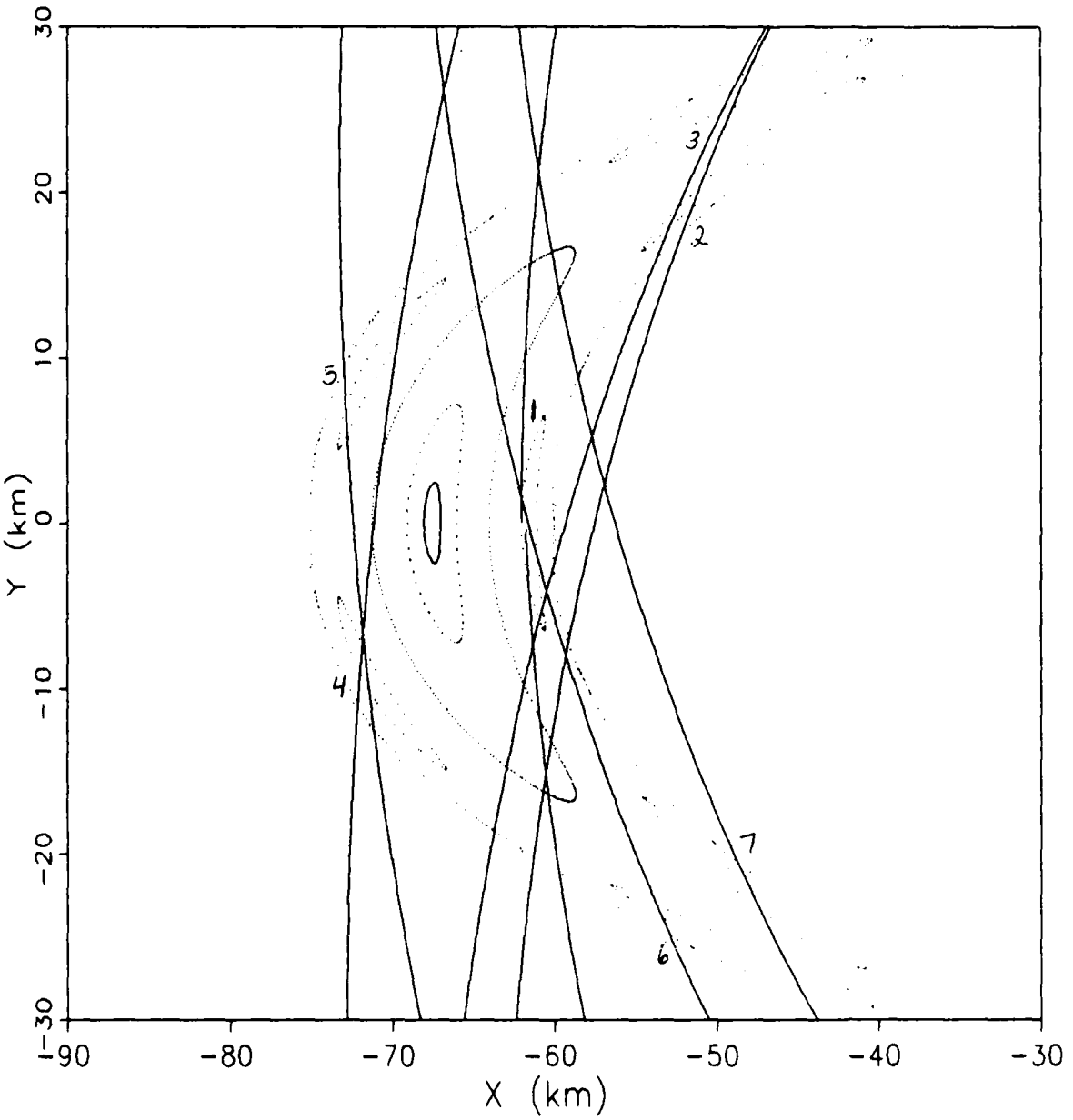

Figure 12. Stable Orbit About Phobos, H = -6.8527

perturbated by Phobos.

It is also interesting to note that closed periodic orbits are much more difficult to find further from the moon. The closed curves associated with these orbits become very narrow and elongated. The initial conditions for these orbits must, therefore, be determined very precisely, making them much less navigable.

The characteristics associated with the evolution of the surface of section plots can be observed in Figures 13 and 14. The upper and lower branches of the surface of section plot in Figure 13 clearly demonstrate that the trajectories are almost in orbit about Mars. The surface of section points on these branches are formed as the moon rotates beneath the very elliptical trajectories. Figure 14 implies that the initial conditions for the stable, closed periodic orbit indicated must be determined very accurately; otherwise, a satellite could be many kilometers from its starting point after completing only one orbit of the moon.

Orbit Direction. The surface of section plots provide no indication of the direction of the orbits. This information must be determined from other a priori knowledge. All of the stable orbits discovered in this investigation were retrograde (counter-clockwise).

Several attempts were made to discover prograde (clockwise) orbits. However, the test trajectories quickly escaped the influence of the moon or quickly collided with the

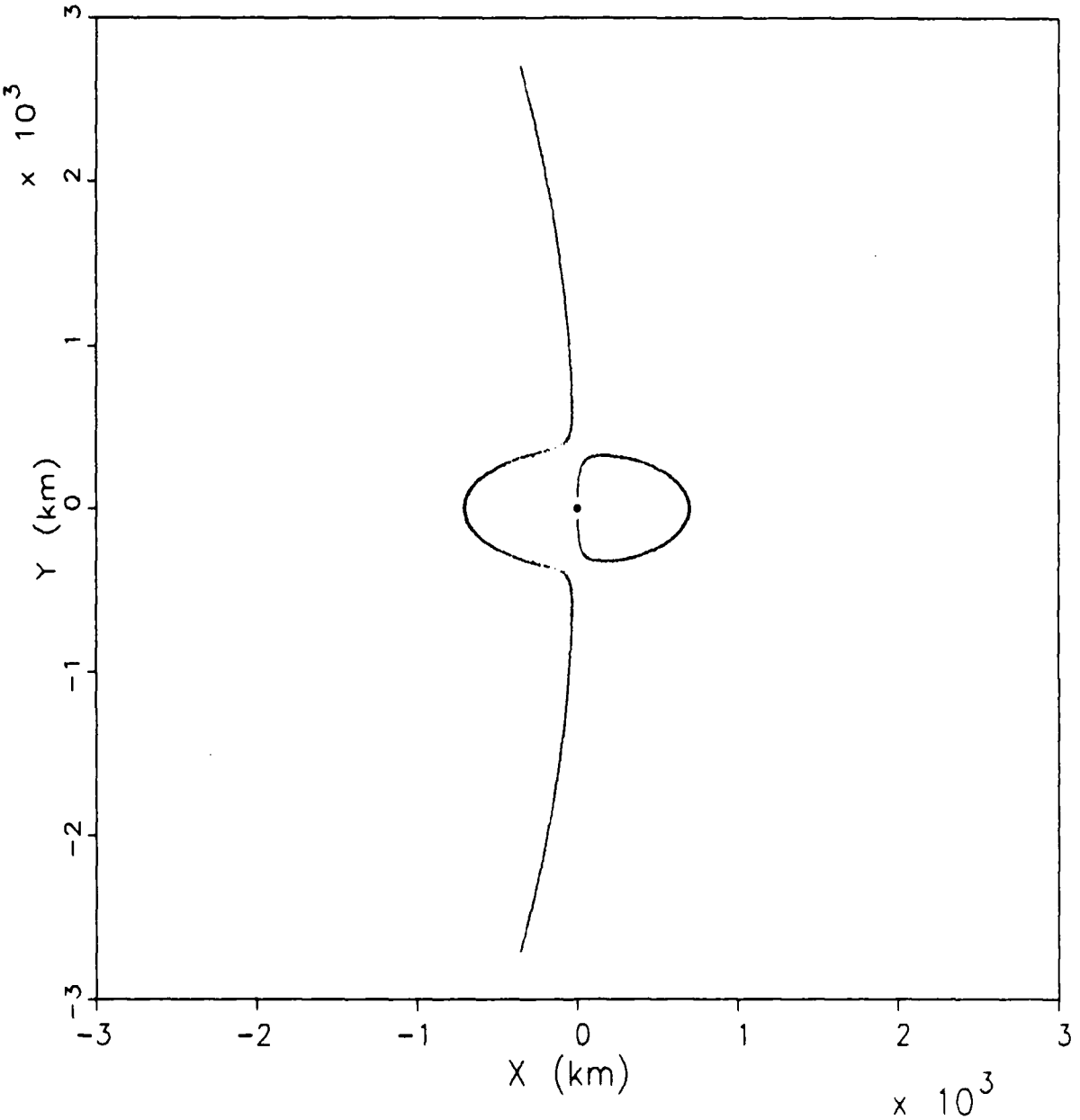

Figure 13. Phobos Surface of Section, H = -6.84

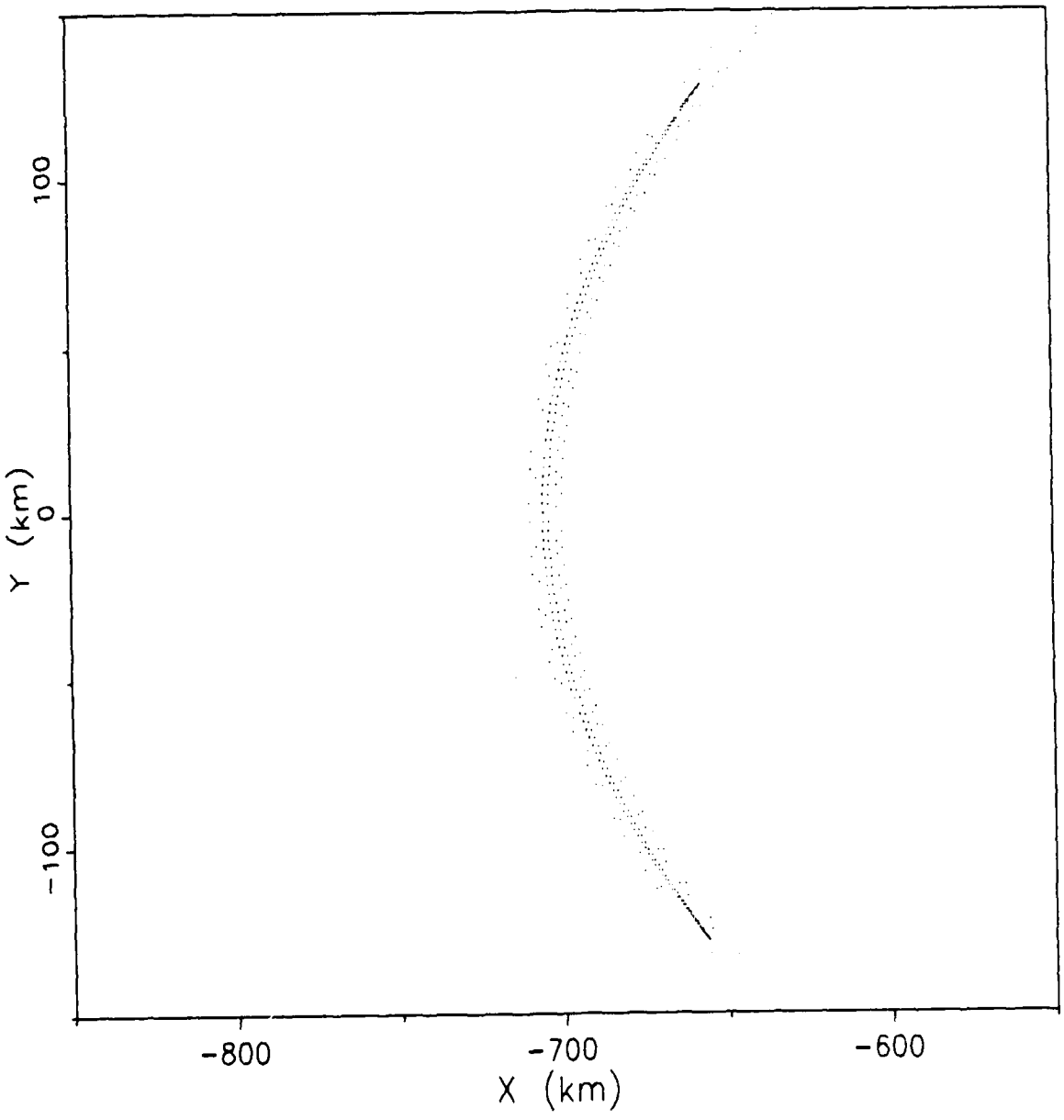

Figure 14. Phobos Surface of Section, H = -6.84

moon. Few, if any, useful surface of section points could be determined.

Jefferies discovered in his work that stable retrograde orbits appear for much smaller values of the Hamiltonian than stable prograde orbits (7:16). The Martian moons may be too small to support any prograde orbits. The value of H for which stable prograde orbits might otherwise appear, may be greater than that required for escape trajectories.

Deimos

In the same manner as the Phobos analysis, several evenly-spaced test trajectories were initiated along the X-axis. All of the trajectories were integrated for 10,000,000 seconds (116 days). Because the orbit periods were generally greater than those of the Phobos orbits, a longer integration time was used. The longer integration time was required so the sufficient number of surface of section points needed to indicate the shape and size of any closed curves could be obtained.

Table II provides a summary of the characteristics of each of the stable, closed periodic orbits discovered about Deimos. The orbit period of the first orbit listed is approximately one-fourth of Deimos's orbit about Mars. As expected, the orbit periods increase as the orbit altitude is increased.

The eccentricities of the orbits are approximately .33 - .35 with the exception of the closer orbits which are more

Table II. Characteristics of the Stable Orbits About Deimos

H	I.C.'s	R_p	R_a	a	b	e	P
-2.738592	-10,0	10	11	11	11	.036	18,800
-2.738591	-13,0	13	15	14	14	.063	25,800
-2.738590	-18,0	16	20	18	18	.115	35,400
-2.738589	-23,0	23	33	28	27	.190	53,600
-2.738588	-31,0	31	49	40	50	.232	72,100
-2.738487	-41,0	38	68	53	50	.309	83,200
-2.738586	-48,0	44	84	64	61	.309	90,800
-2.738585	-56,0	48	103	76	71	.358	93,000
-2.73858	-75,0	75	156	116	108	.352	106,000
-2.73857	-109,0	108	216	162	153	.332	108,000
-2.73856	-135,0	132	267	199	188	.340	108,000
-2.73855	-156,0	153	310	231	217	.339	108,000
-2.7385	-233,0	232	464	348	328	.334	109,000
-2.7384	-340,0	336	679	507	478	.338	109,000
-2.7383	-418,0	417	839	628	592	.335	109,000

H - Hamiltonian, km^2/sec^2
I.C.'s - initial conditions, km
R_p - pericenter distance, km
R_a - apocenter distance, km
a - semi-major axis, km
b - semi-minor axis, km
e - eccentricity
P - period, sec

circular in nature. Table II also indicates, once again, that the altitudes of the orbits increase at a lower and lower rate as the value of the Hamiltonian increases.

The initial velocities of the orbits range from 4.15 m/s for the lowest orbit (H = -2.738592) to 43.8 m/s for the highest orbit (H = -2.7383).

All of the orbits discovered were retrograde. Attempts to discover stable prograde orbits were unsuccessful as in the Phobos case. With the exception of the low altitude orbits, the evolution of the surface of section plots was similar to that seen for Phobos.

Variations in the semi-major axis that are quite similar to those of the Phobos orbits were discovered. However, no resonant orbits were discovered. This may result from the fact that Deimos is further away from Mars than Phobos, thereby limiting the resonances associated with the third body effects. At low altitudes, orbits representing simple, rotating Keplerian ellipses were discovered. None were discovered in the Phobos analysis.

Rotating Ellipses. The surface of section plots for low altitude orbits about Deimos are quite different than those of the other orbits. The nearly circular closed curves encompassing the entire moon in the surface of section plot of Figure 15 indicate the presence of rotating orbits. Figure 16 is the isolated surface of section formed by only one trajectory. In this case, the orbit is a Keple-

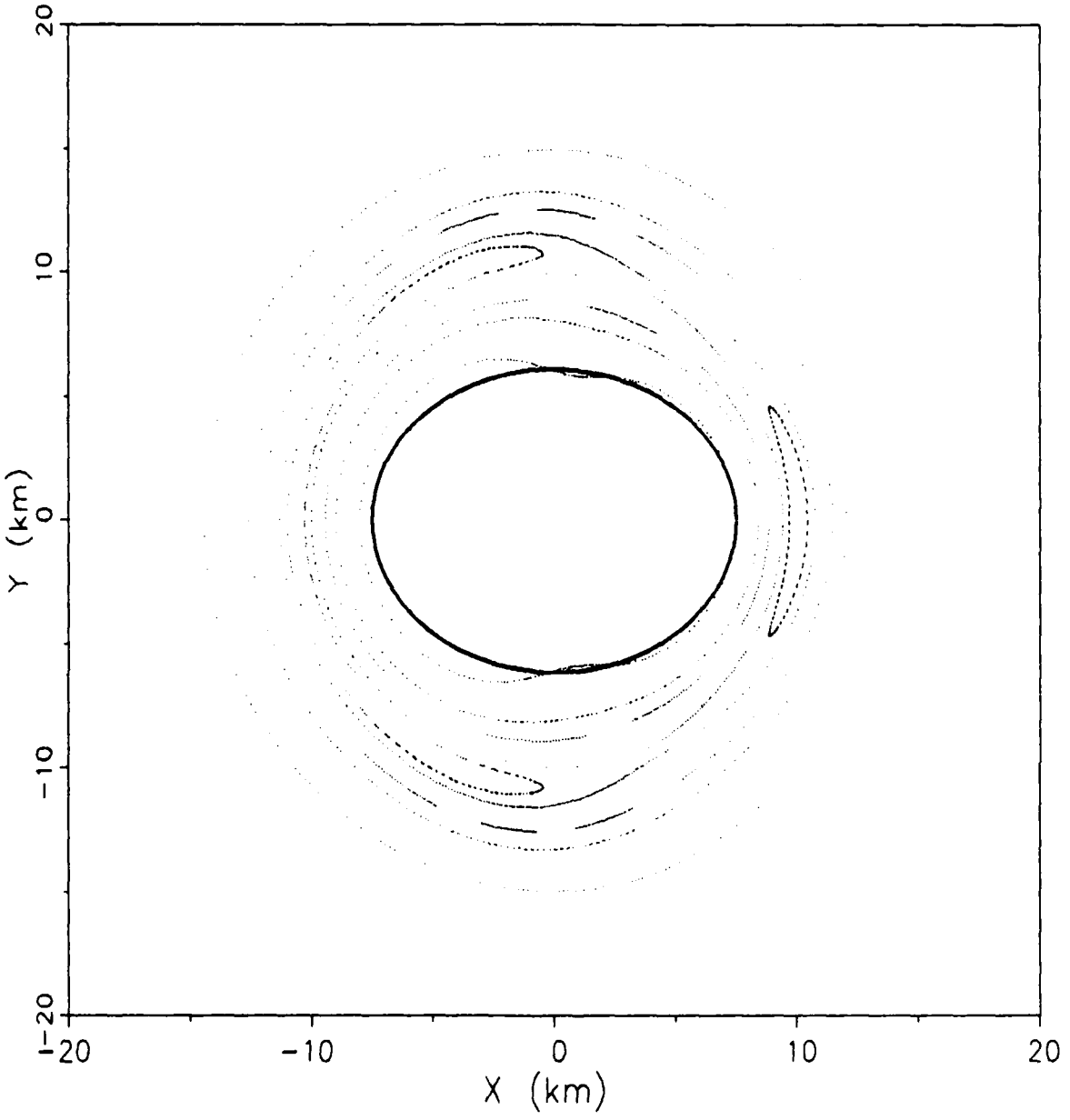

Figure 15. Deimos Surface of Section, H = -2.738592

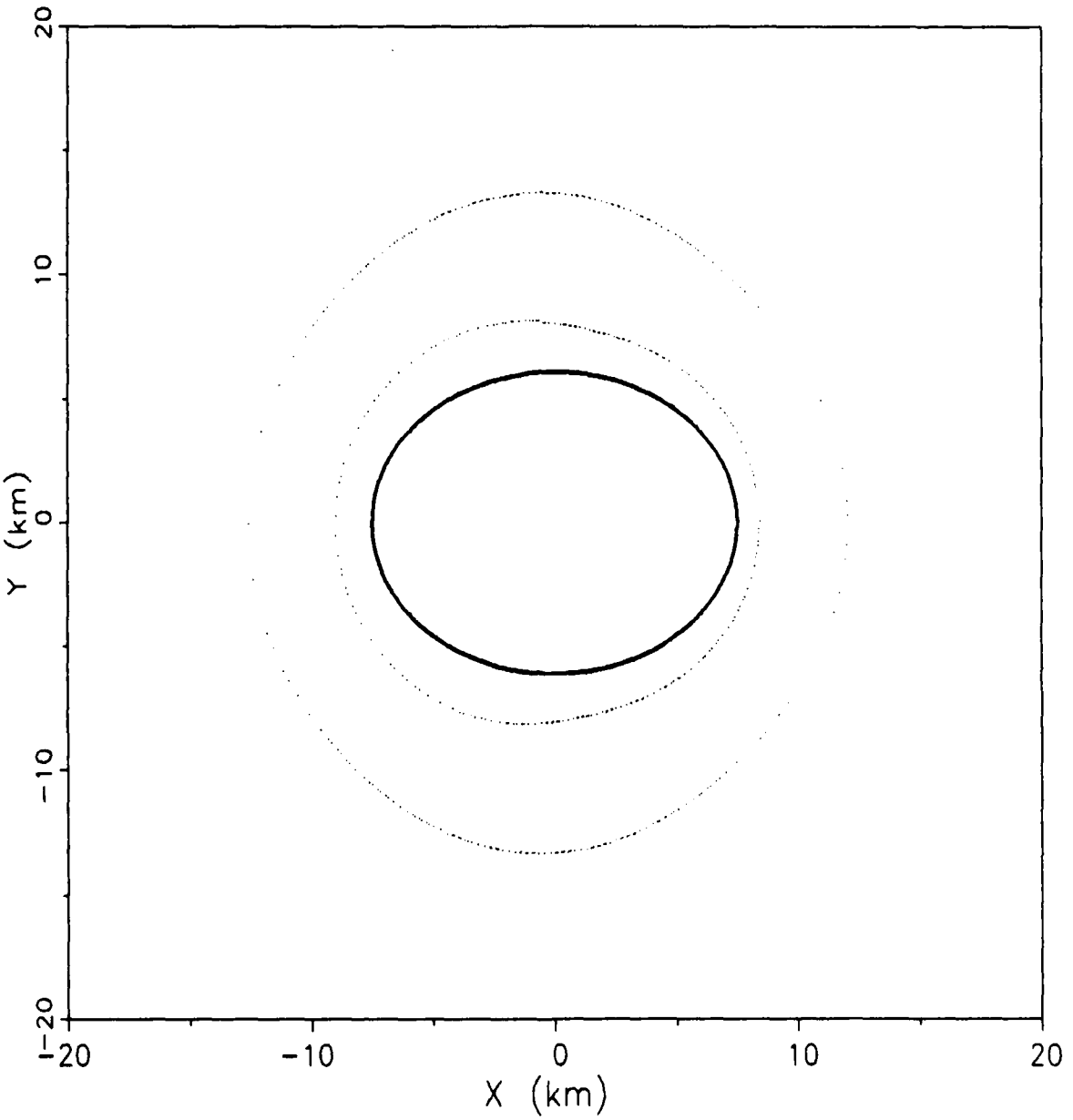

Figure 16. Deimos Surface of Section, H = -2.738592

rian ellipse that rotates about the moon. The periapses and apoapses occur at roughly the same altitude for each encirclement of the moon. Therefore, the curves traced out by these points, as the orbit rotates about the moon, are nearly circular. Figure 17 demonstrates this behavior. The orbit superimposed on the surface of section of Figure 16 was integrated for 100,000 seconds.

Figure 15 also indicates the emerging presence of islands associated with the semi-major axis perturbation effect discussed earlier. The surface of section for this case is isolated in Figure 18. The stable, closed periodic orbit associated with this surface of section is displayed in Figure 19. With the exception of the narrow region just discussed, an infinite number of stable, rotating, periodic, elliptical orbits may be discovered within the stable region associated with the closed curves of the surface of section plot.

The discovery of rotating ellipses around Deimos and not around Phobos is most likely due to the fact that Deimos is much further away from Mars. As long as the orbits are very close to Deimos, the moon's gravitational field greatly dominates the possible perturbation effects caused by the very distant planet.

Collision Orbits. Trajectories that collide with Deimos are indicated by Figure 20. One such trajectory is shown in Figure 21. All of the periapsis points of this

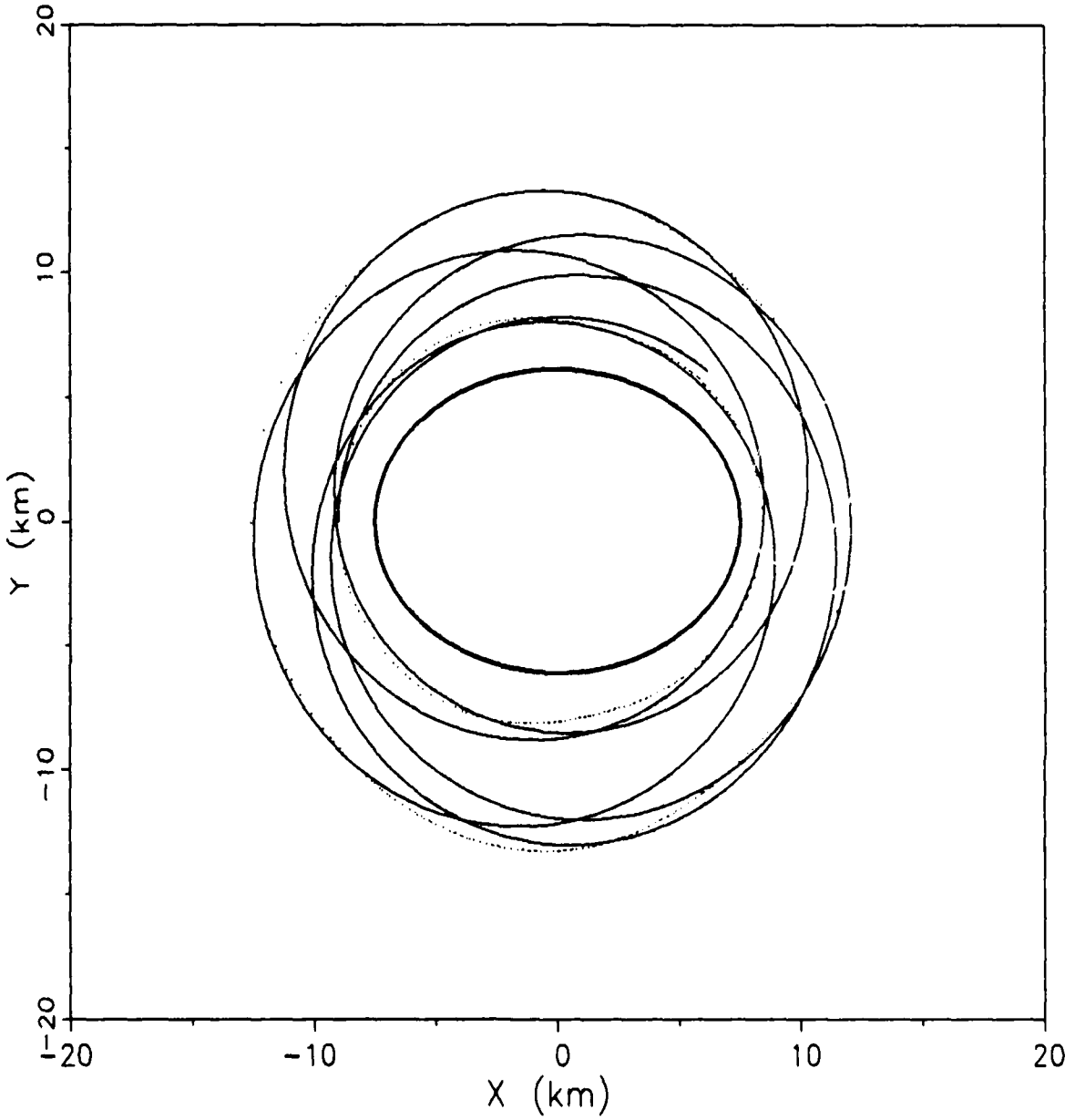

Figure 17. Stable Orbit About Deimos, H = -2.738592

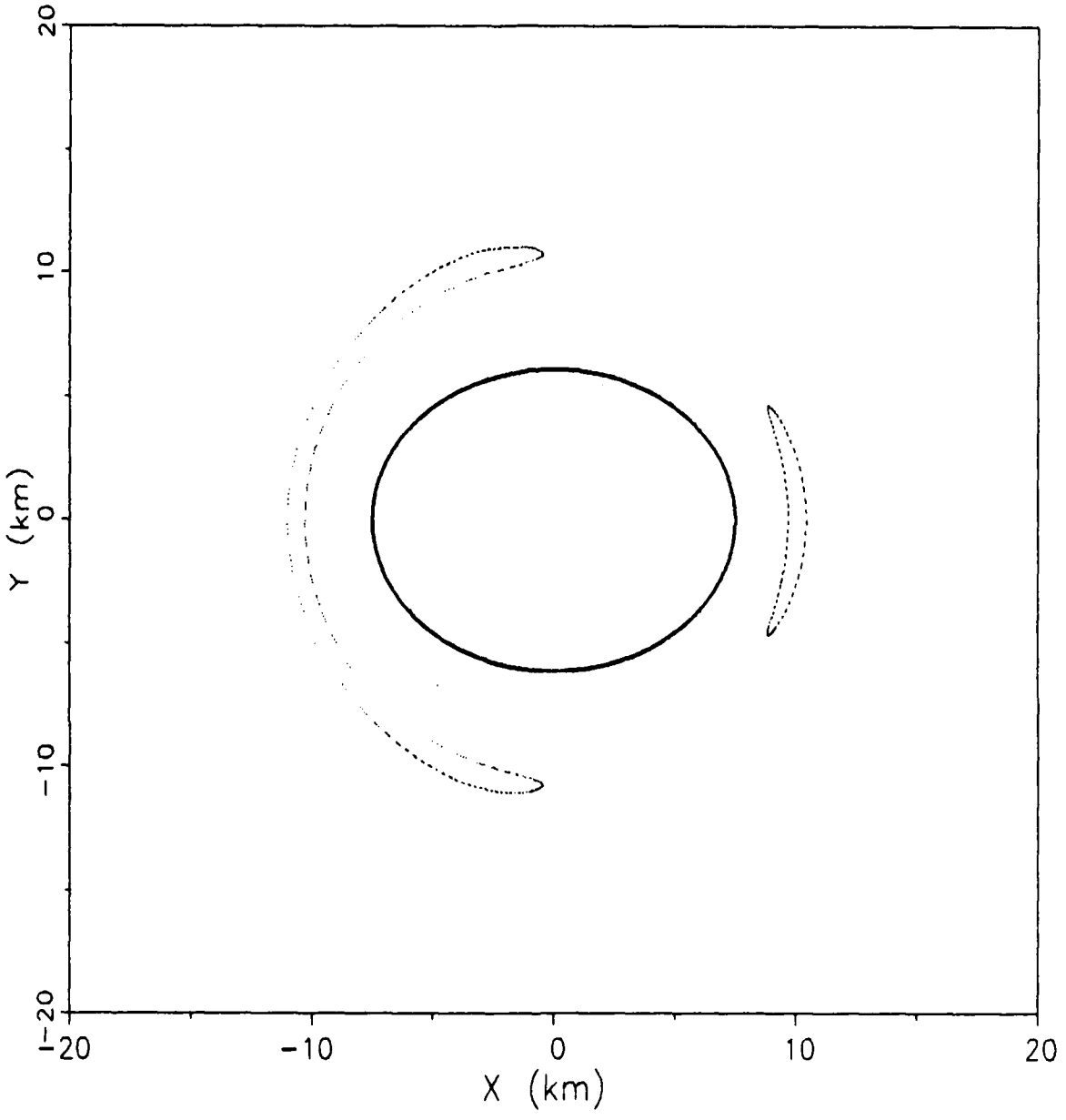

Figure 18. Deimos Surface of Section, H = -2.738592

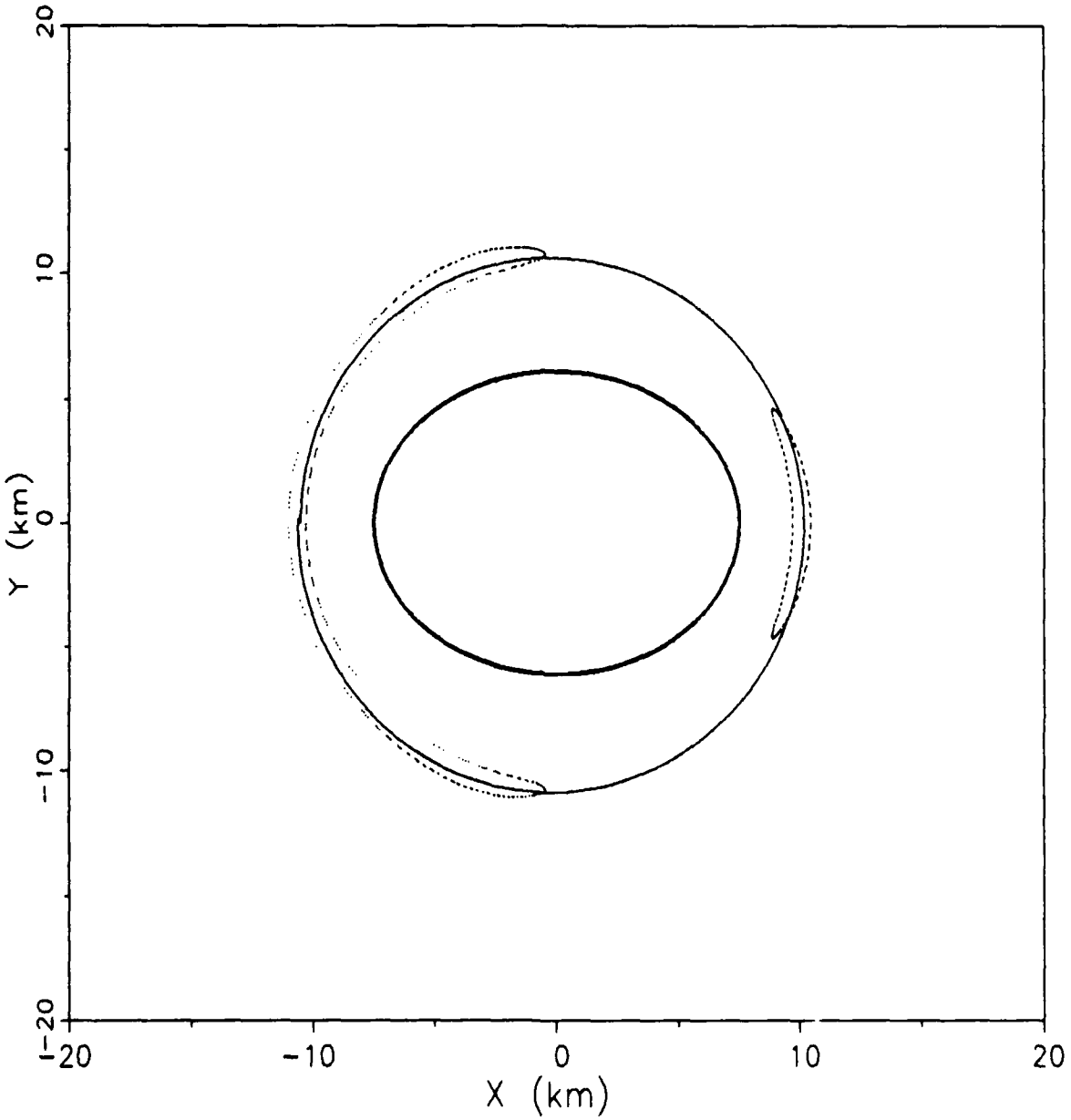

Figure 19. Stable Orbit about Deimos, H = -2.738592

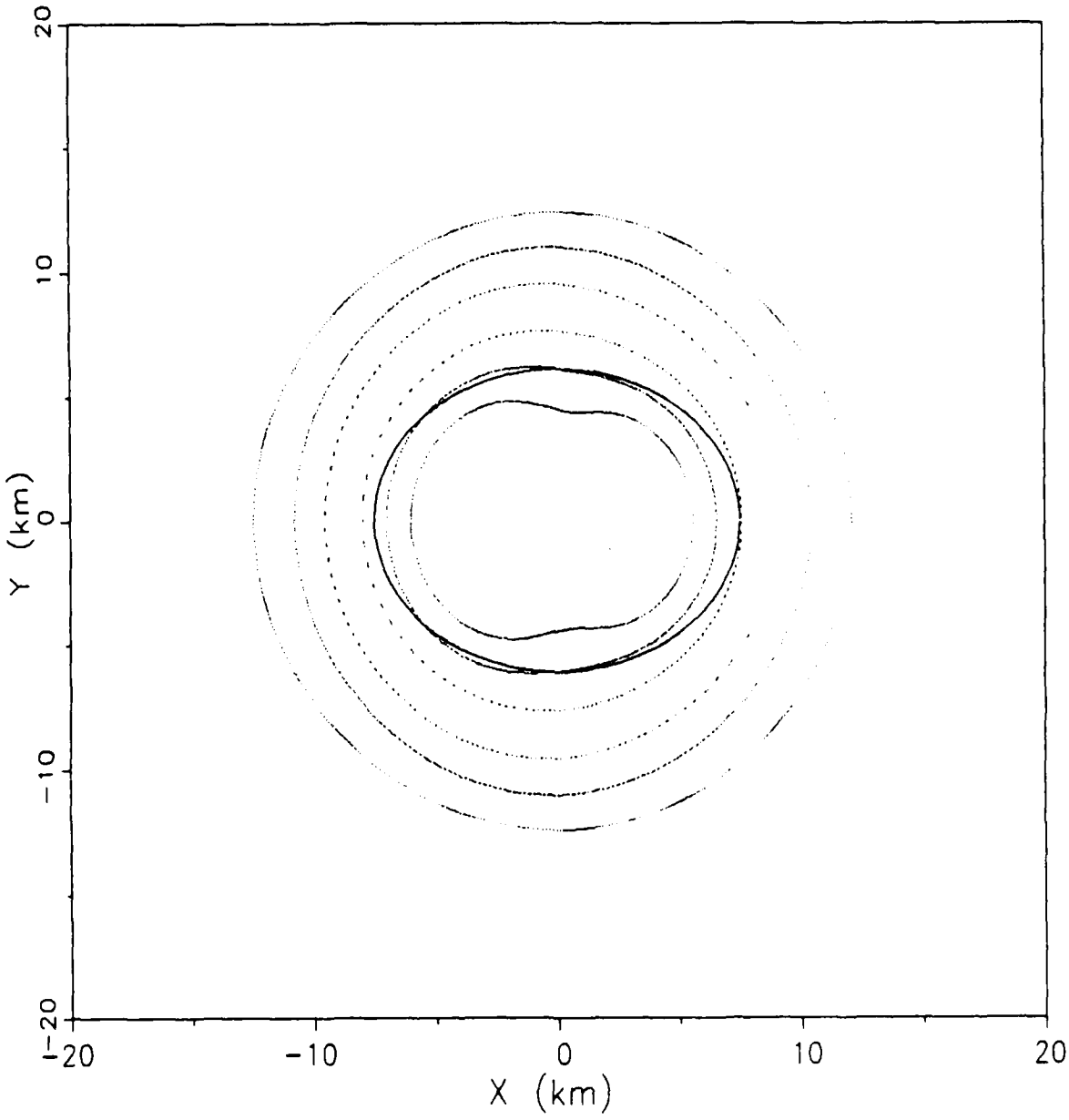

Figure 20. Deimos Surface of Section, H = -2.738593

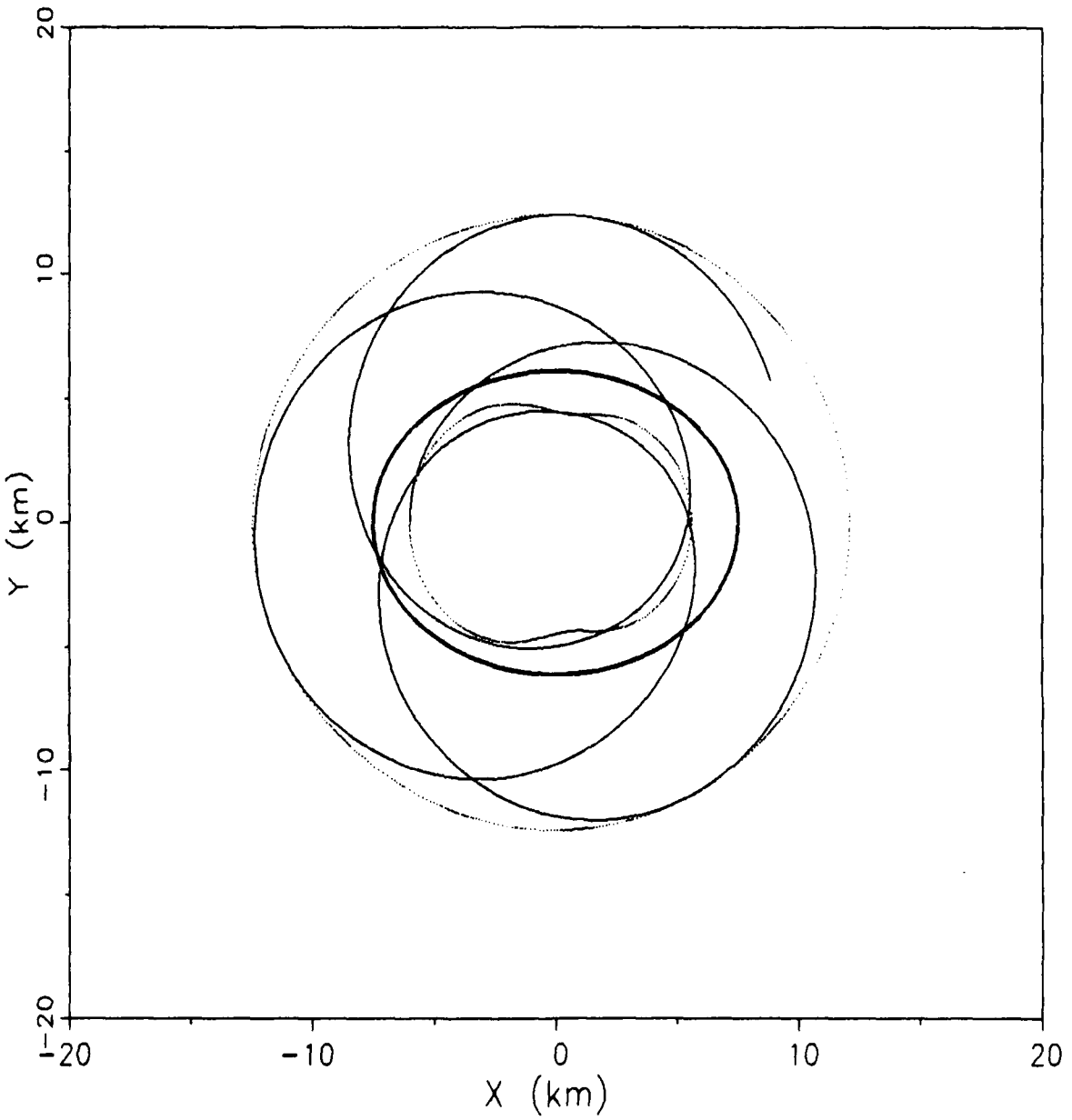

Figure 21. Deimos Collision Orbit, H = -2.738593

rotating orbit are below the moon's surface.

Orbit Evolution. The evolution of orbits about Deimos as the Hamiltonian and altitude increase is very interesting. The orbits discovered just above the surface of Deimos are all rotating ellipses (see Figure 20). However, as the altitude of the orbits increase, variation in the semi-major axis begins to appear (see Figure 15). The areas of the surface of section plots indicating rotating ellipses decrease (see Figure 22) and then begin to disappear completely. In the surface of section of Figure 23, the surface of section points for the unstable trajectory initiated just beyond the stable region were included to indicate the transition to non-rotating orbits with varying semi-major axes. The scattered points from the unstable trajectory indicate the presence of a disappearing rotating ellipse. When H is further increased, only non-rotating orbits are indicated from the surface of section (see Figure 24). The islands first appear to be very isolated. However, as the Hamiltonian (and orbit altitude) is increased, these regions become elongated and begin to approach one another (see Figure 25). At this point, the surface of section plots become quite similar to those created for Phobos.

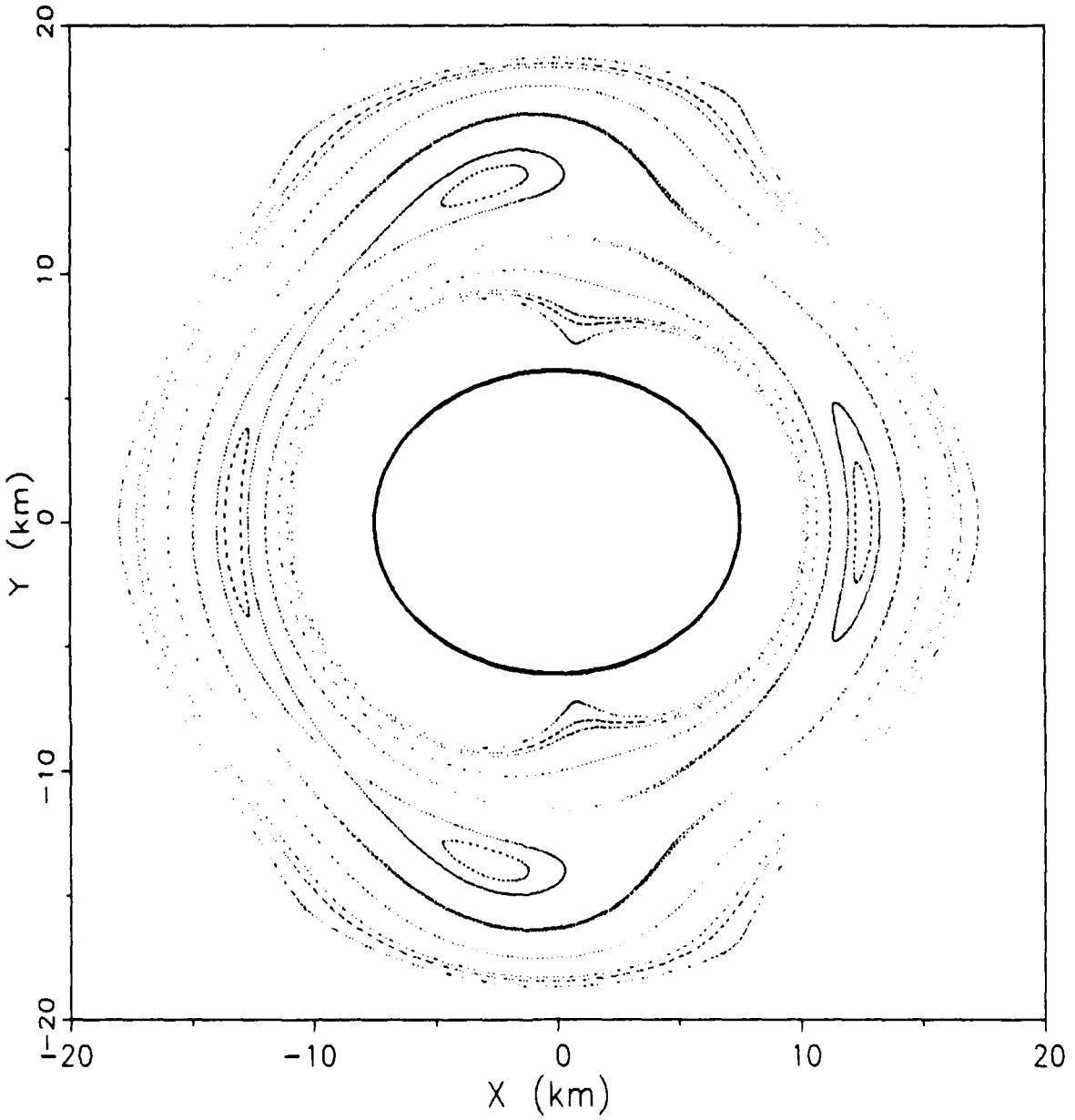

Figure 22. Deimos Surface of Section, H = -2.738591

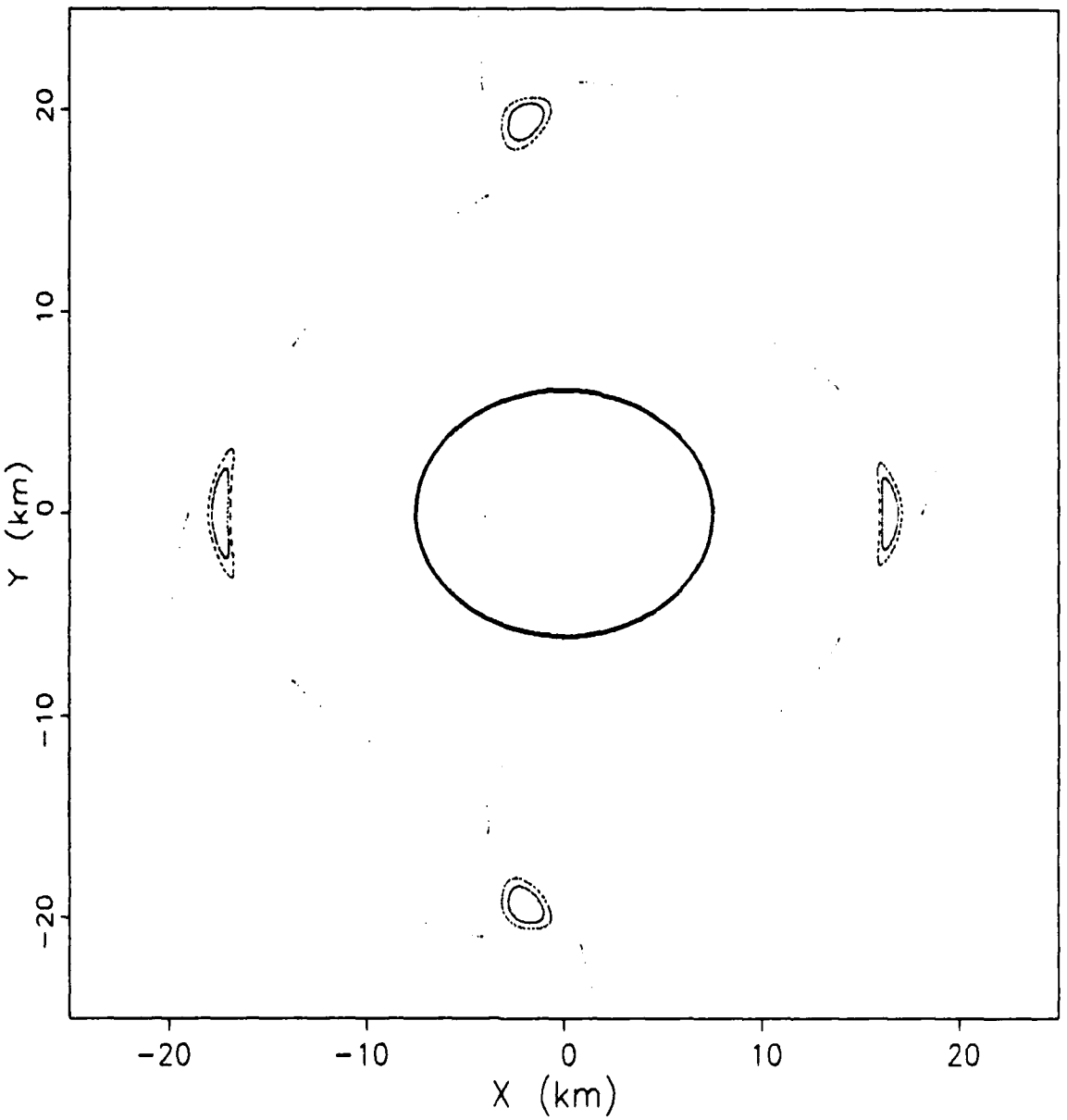

Figure 23. Deimos Surface of Section, H = -2.73859

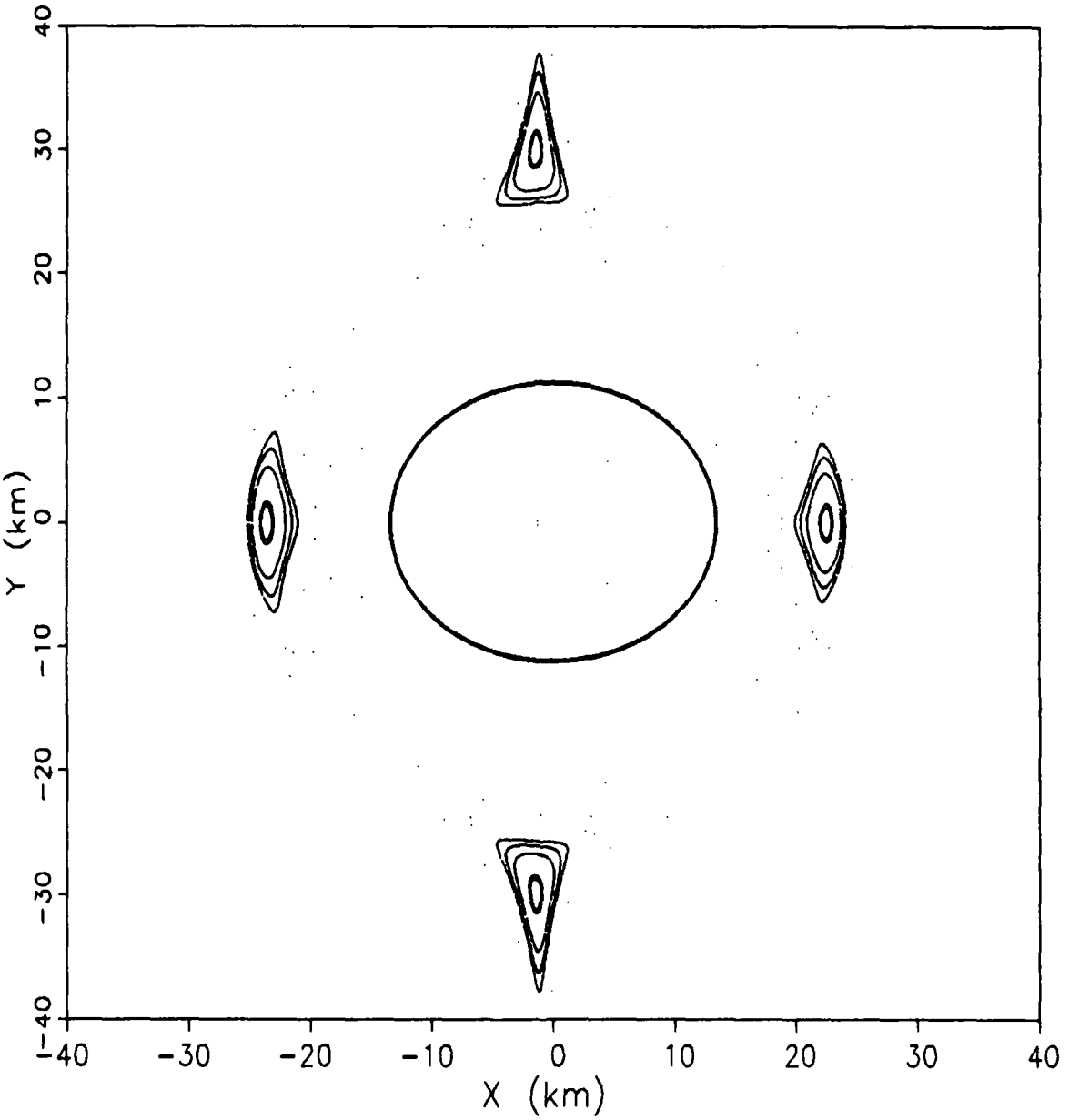

Figure 24. Deimos Surface of Section, H = -2.738589

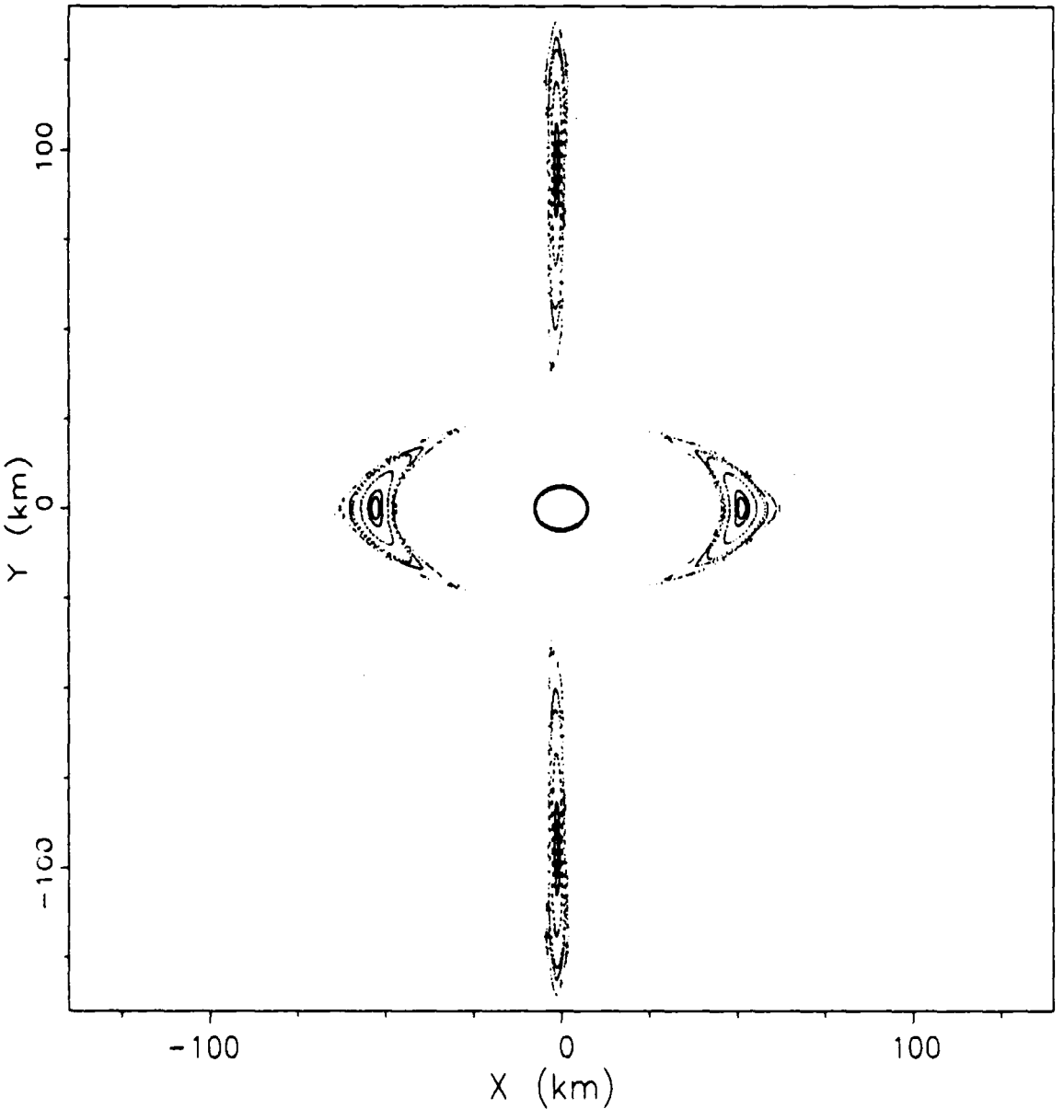

Figure 25. Deimos Surface of Section, H = -2.738585

VI. Conclusions and Recommendations

The surface of section technique was successfully used to determine several stable periodic orbits about both Phobos and Deimos. Most of the orbits displayed a variation in the semi-major axis. Only the orbits very close to Deimos were determined to be simple rotating ellipses.

Closed periodic orbits are much more difficult to discover further away from the moon. In addition, the initial conditions associated with these orbits must be determined much more precisely than those for the low-altitude orbits. The gravitational attraction of Mars dominates for the high-altitude orbits. Therefore, the use of orbits in close proximity to the moons is recommended over the distant orbits. Long term stability may be achieved as long as the orbit velocity can be maintained to within a few meters per second.

These orbits could prove useful as parking orbits for any future manned or unmanned missions to Mars. Because of the low gravity of Phobos and Deimos, the landing of a vehicle on their surfaces from a low altitude orbit would require little expenditure of fuel. The potential extraction of water from the moons makes them attractive targets for exploration.

A possible extension of this research would involve the expansion of the dynamics model to include lesser order effects such as the nonspherical characteristics of Mars

and/or the effects associated with other bodies, especially the sun.

Appendix A: Problem Parameters

Moons:	Phobos	Deimos
Axis Lengths (km) (14:251)		
	x = 13.4	x = 7.5
	y = 11.2	y = 6.1
	z = 9.2	z = 5.2
Density (g/cm^3) (4:1)		
	$\mu = 2.2$	$\mu = 1.7$
Moments of Inertia ($kg \cdot km^2$)		
	$I_{xx} = 42.016 \cdot M_{moon}$	$I_{xx} = 12.850 \cdot M_{moon}$
	$I_{yy} = 52.840 \cdot M_{moon}$	$I_{yy} = 16.658 \cdot M_{moon}$
	$I_{zz} = 61.000 \cdot M_{moon}$	$I_{zz} = 18.692 \cdot M_{moon}$
Orbital Radius (km) (3:423)		
	D = 9,378	D = 23,459
Rotation Rate (rad/sec) (3:423)		
	$\Omega = 2.28 \times 10^{-4}$	$\Omega = 5.76 \times 10^{-5}$
Gravitational Attraction (km^3/sec) (3:423)		
	$GM_{moon} = 6.6 \times 10^{-4}$	$GM_{moon} = 8.8 \times 10^{-5}$

Mars:

Gravitational Attraction (km^3/sec): (10:6-3) $GM_{mars} = 42828.32$

Appendix B: Equations of Motion

$$\dot{X} = P_X + \Omega Y \tag{64}$$

$$\dot{Y} = P_Y - \Omega(X + D) \tag{65}$$

$$\dot{Z} = P_Z \tag{66}$$

$$\begin{aligned}\dot{P}_X = {} & \Omega P_Y - GM_{mars}d^{-3}(X + D) - GM_{moon}R^{-3}X \\ & + \frac{3}{4}GR^{-5}X(3I_{yy} + 3I_{zz} - I_{xx}) \\ & - \frac{15}{4}GR^{-7}X[X^2(I_{yy} + I_{zz} - I_{xx}) \\ & + Y^2(I_{xx} + I_{zz} - I_{yy}) + Z^2(I_{xx} + I_{yy} - I_{zz})]\end{aligned} \tag{68}$$

$$\begin{aligned}\dot{P}_Y = {} & - \Omega P_X - GM_{mars}d^{-3}Y - GM_{moon}R^{-3}Y \\ & + \frac{3}{4}GR^{-5}Y(3I_{xx} + 3I_{zz} - I_{yy}) \\ & - \frac{15}{4}GR^{-7}Y[X^2(I_{yy} + I_{zz} - I_{xx}) \\ & + Y^2(I_{xx} + I_{zz} - I_{yy}) + Z^2(I_{xx} + I_{yy} - I_{zz})]\end{aligned} \tag{69}$$

$$\begin{aligned}\dot{P}_Z = {} & - GM_{mars}d^{-3}Z - GM_{moon}R^{-3}Z \\ & + \frac{3}{4}GR^{-5}Z(3I_{xx} + 3I_{yy} - I_{zz}) \\ & - \frac{15}{4}GR^{-7}Z[X^2(I_{yy} + I_{zz} - I_{xx}) \\ & + Y^2(I_{xx} + I_{zz} - I_{yy}) + Z^2(I_{xx} + I_{yy} - I_{zz})]\end{aligned} \tag{70}$$

Appendix C: Phobos Surface of Section Plots

Figure Page

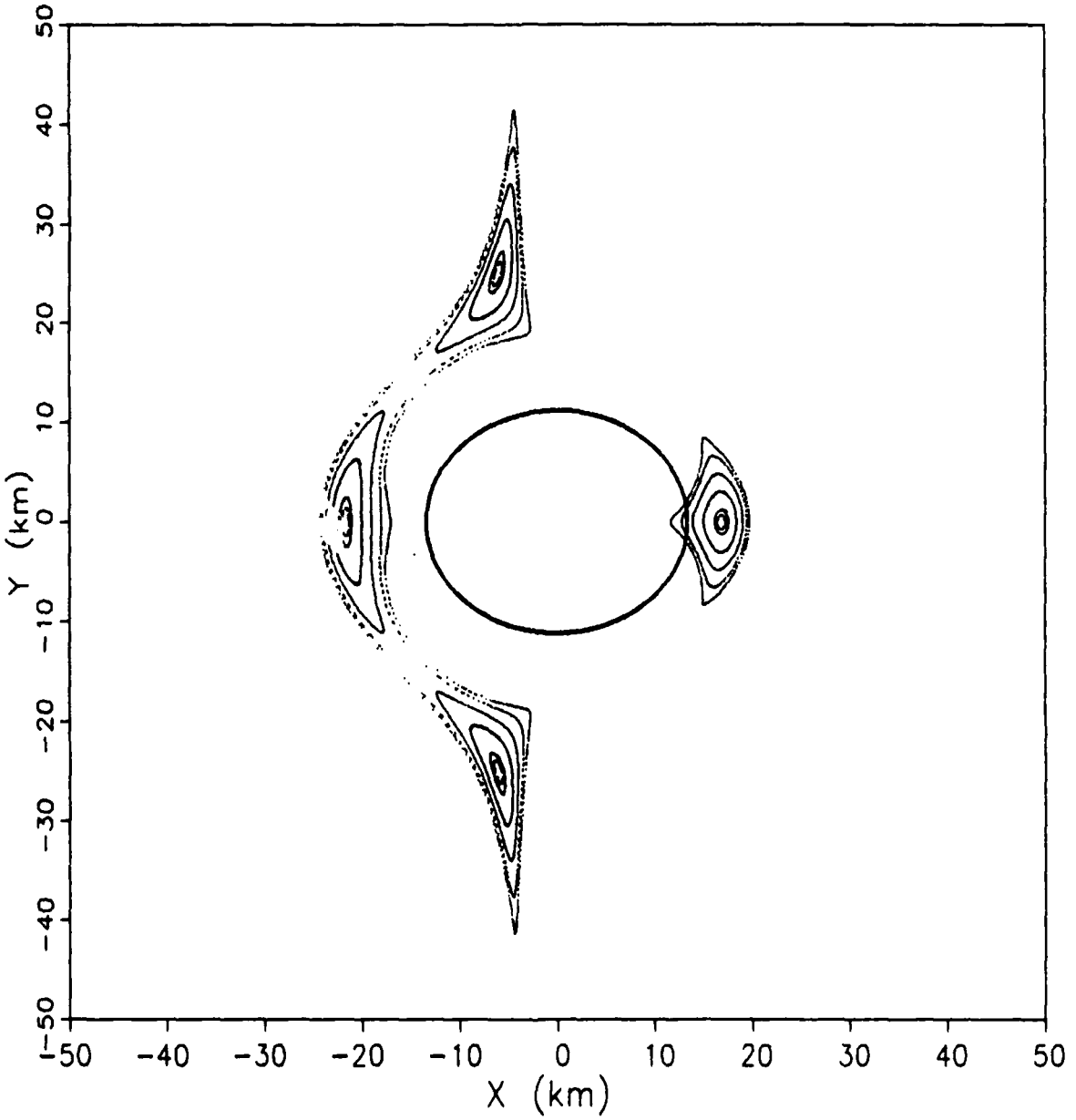

Figure 26. Phobos Surface of Section, H = -6.8528

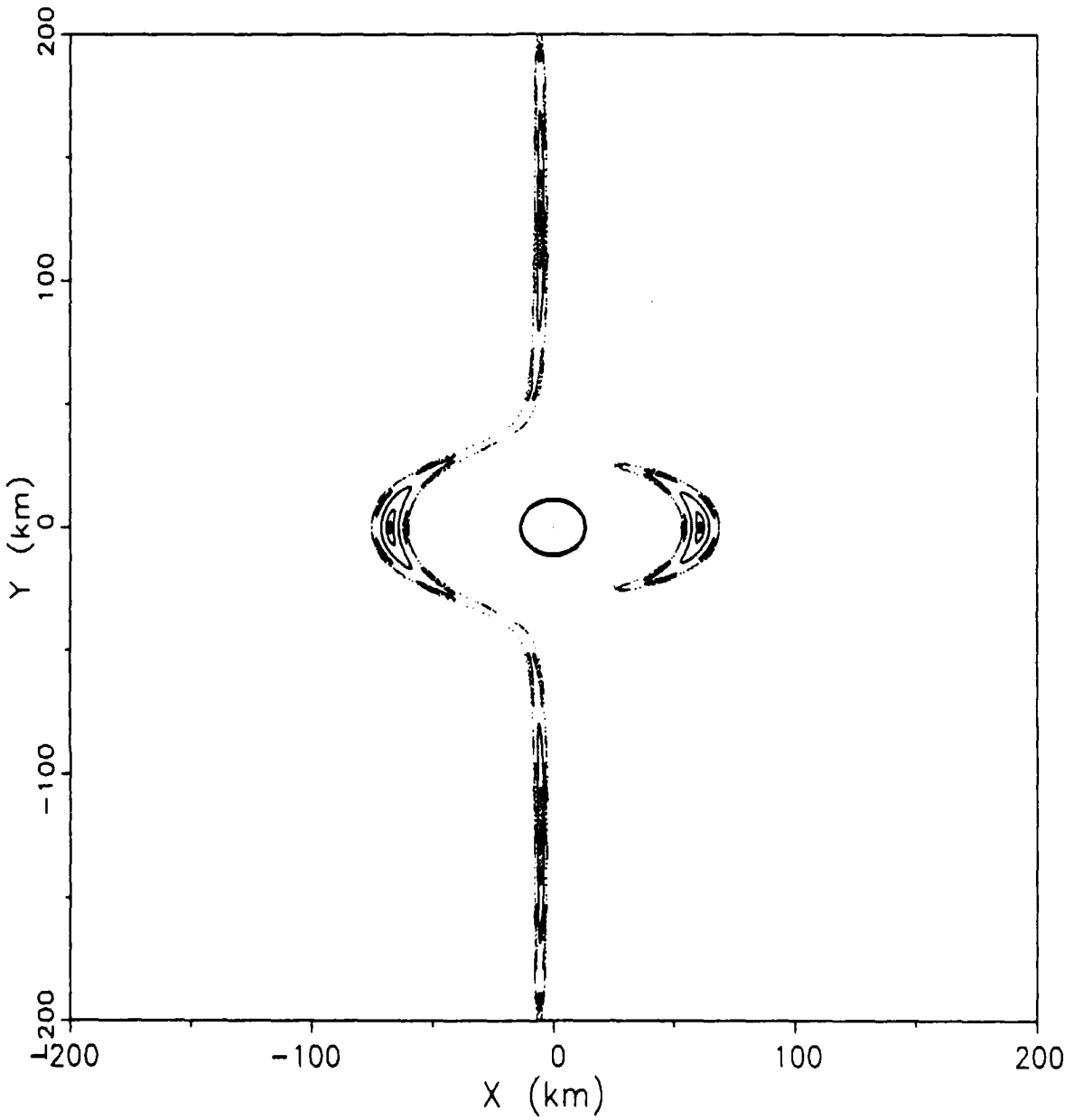

Figure 27. Phobos Surface of Section, H = -6.8527

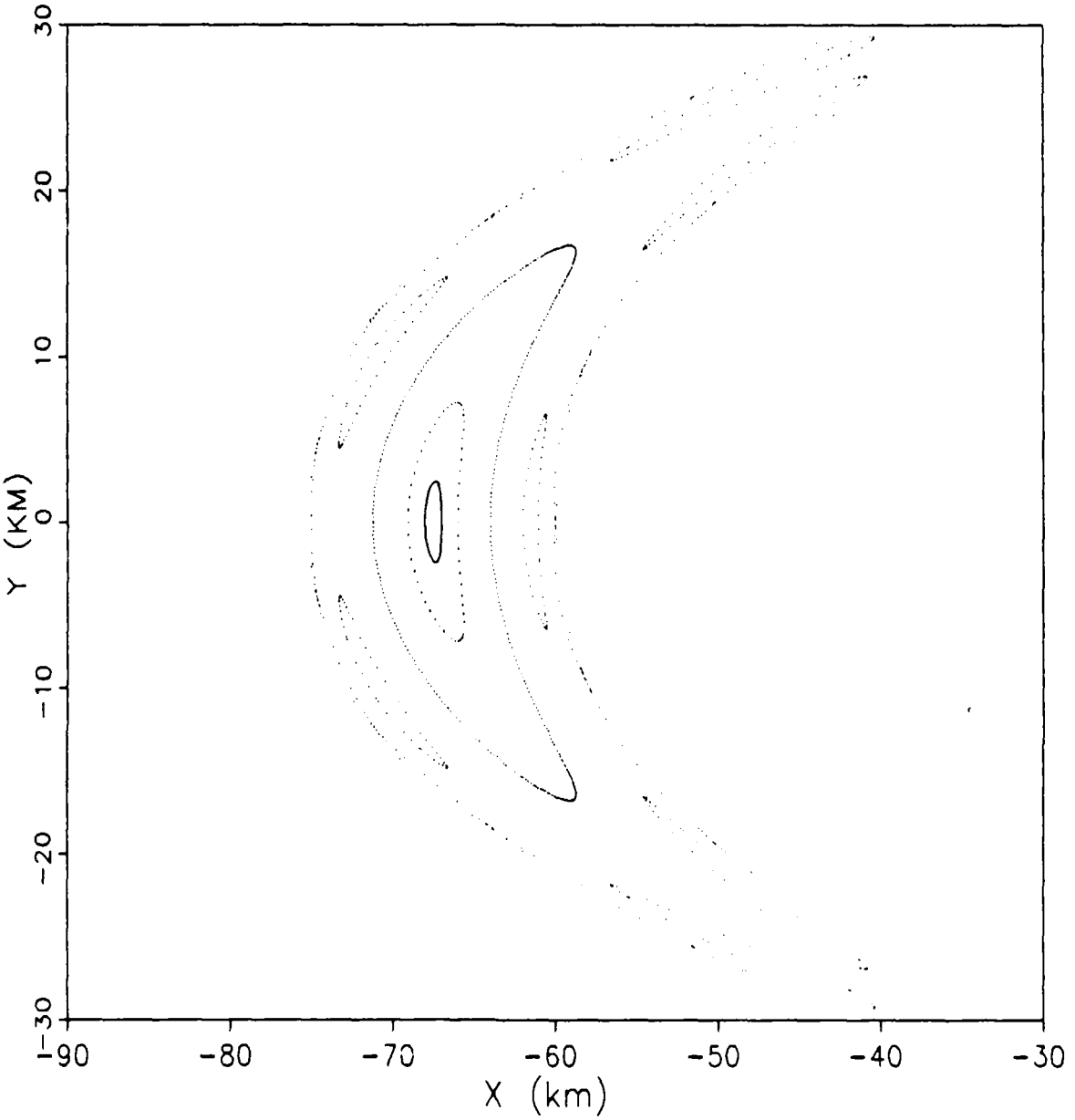

Figure 28. Phobos Surface of Section, H = -6.8527

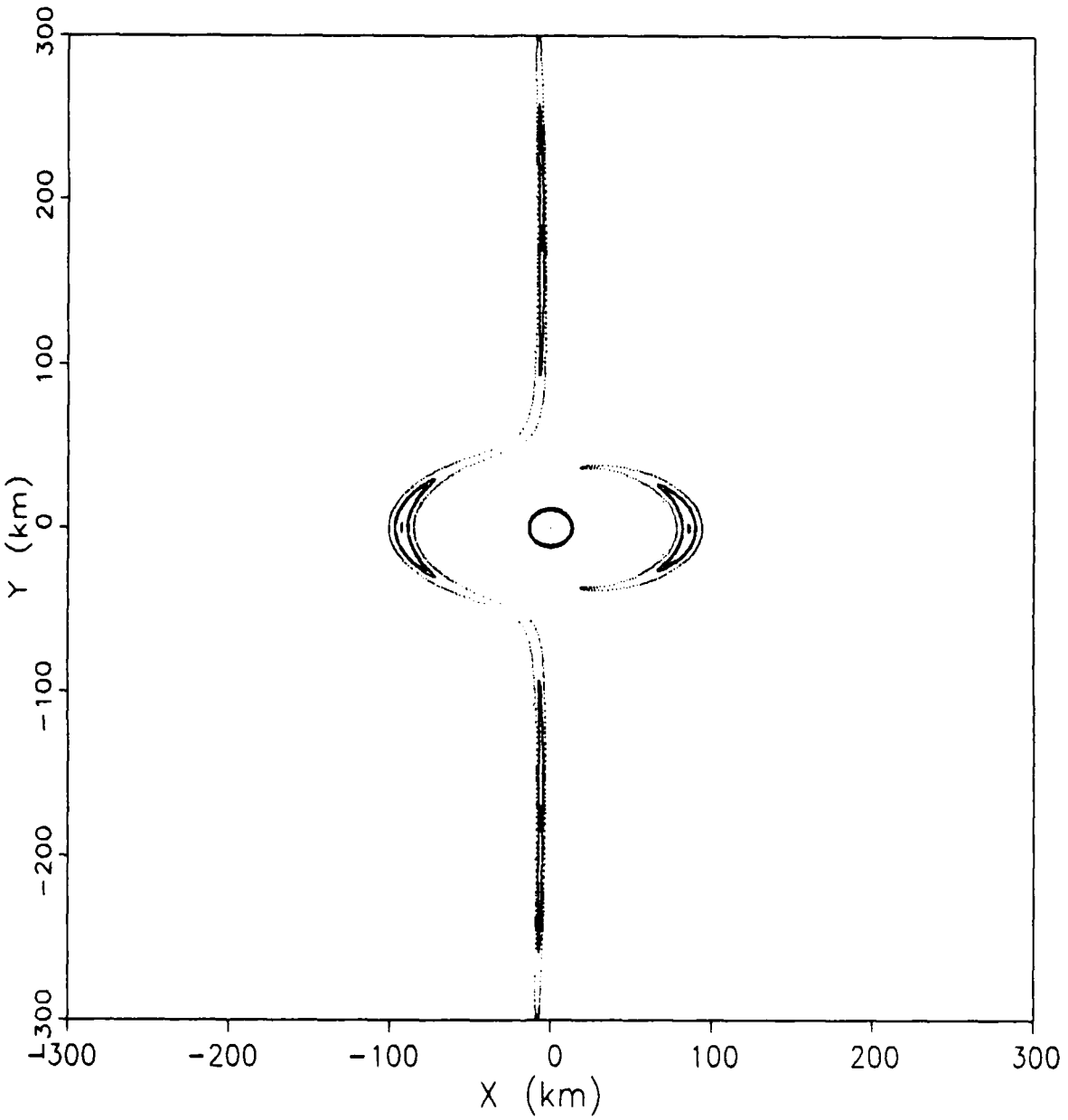

Figure 29. Phobos Surface of Section, H = -6.8526

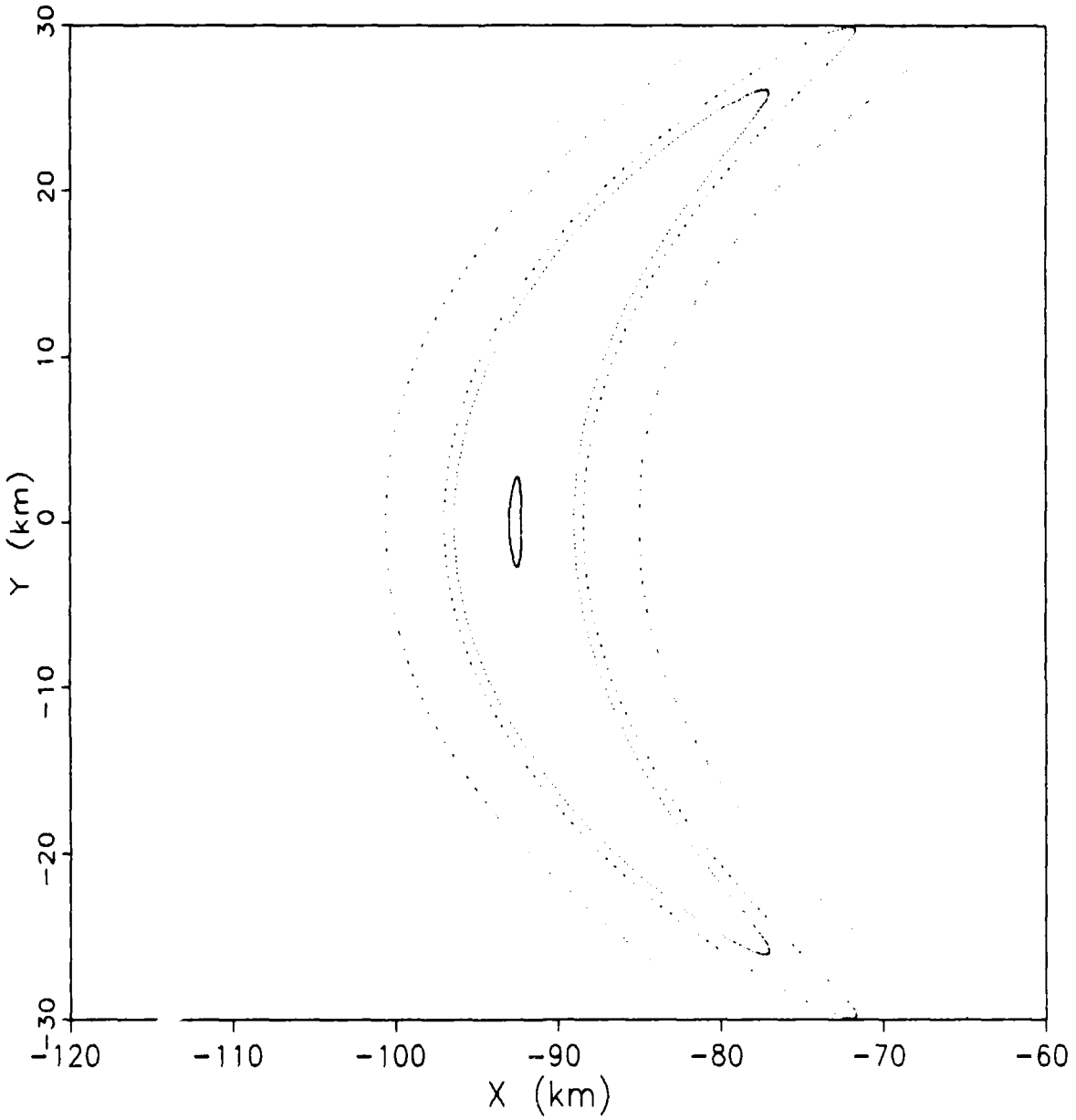

Figure 30. Phobos Surface of Section, H = -6.8526

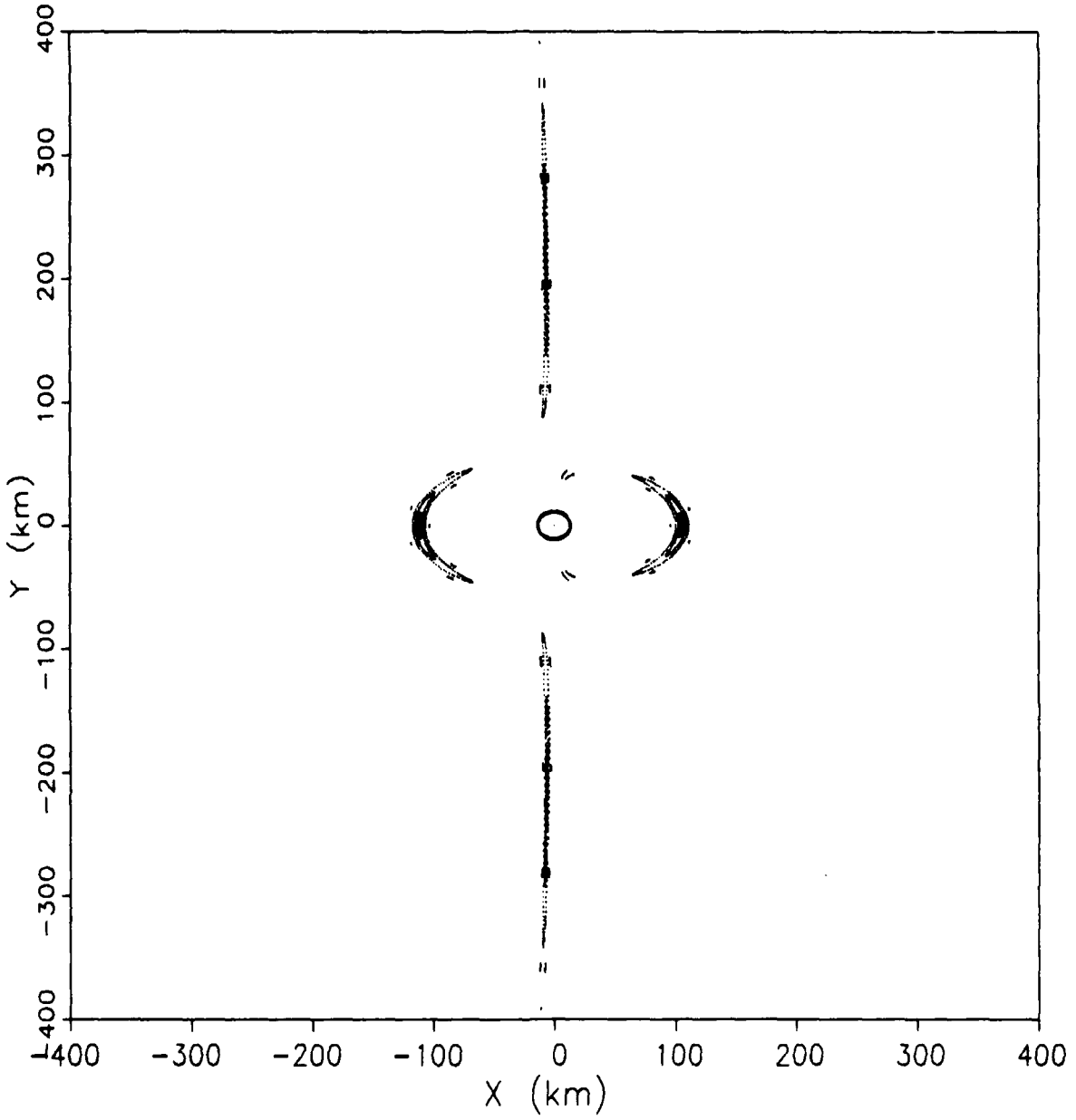

Figure 31. Phobos Surface of Section, H = -6.8525

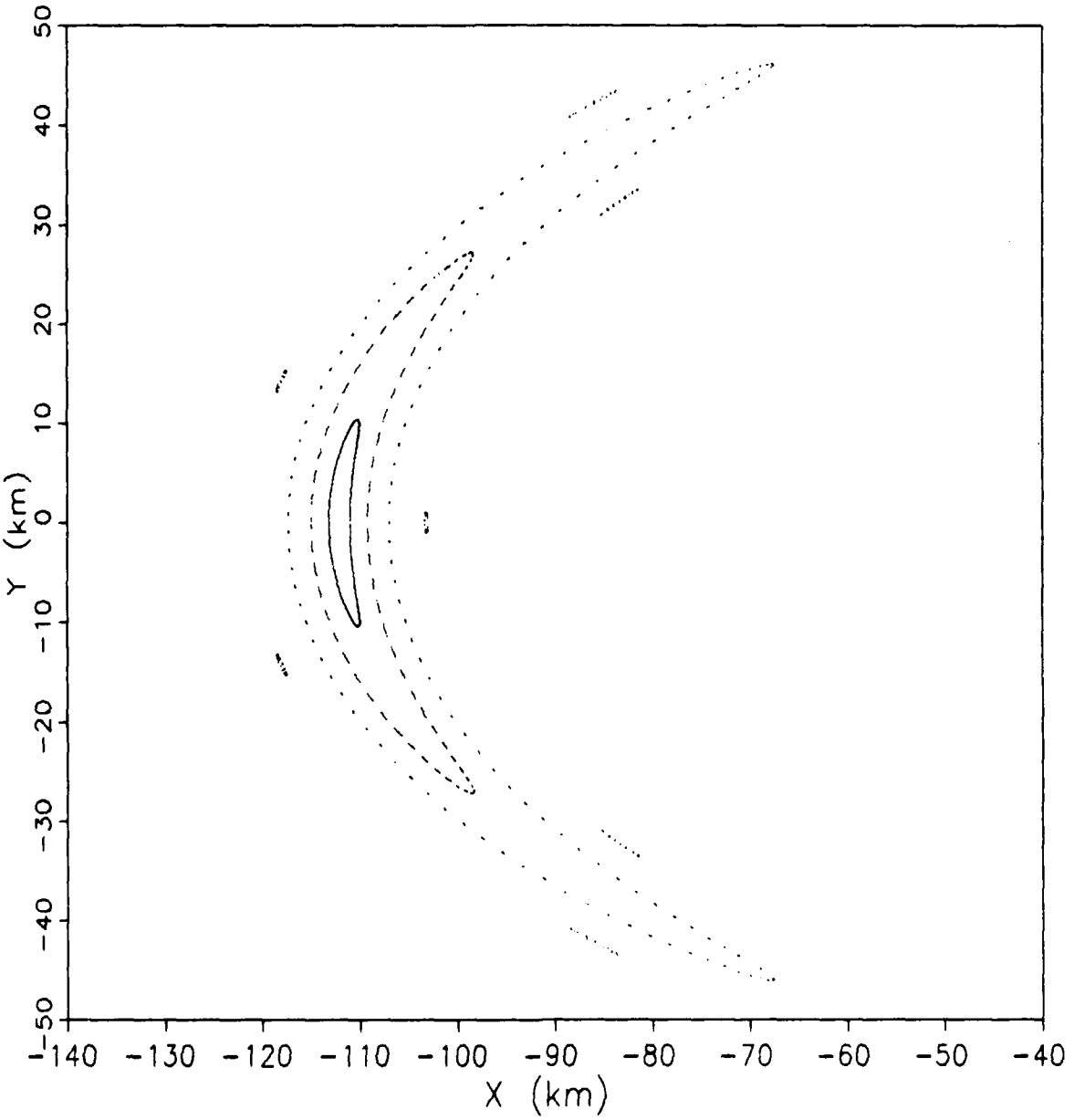

Figure 32. Phobos Surface of Section, H = -6.8525

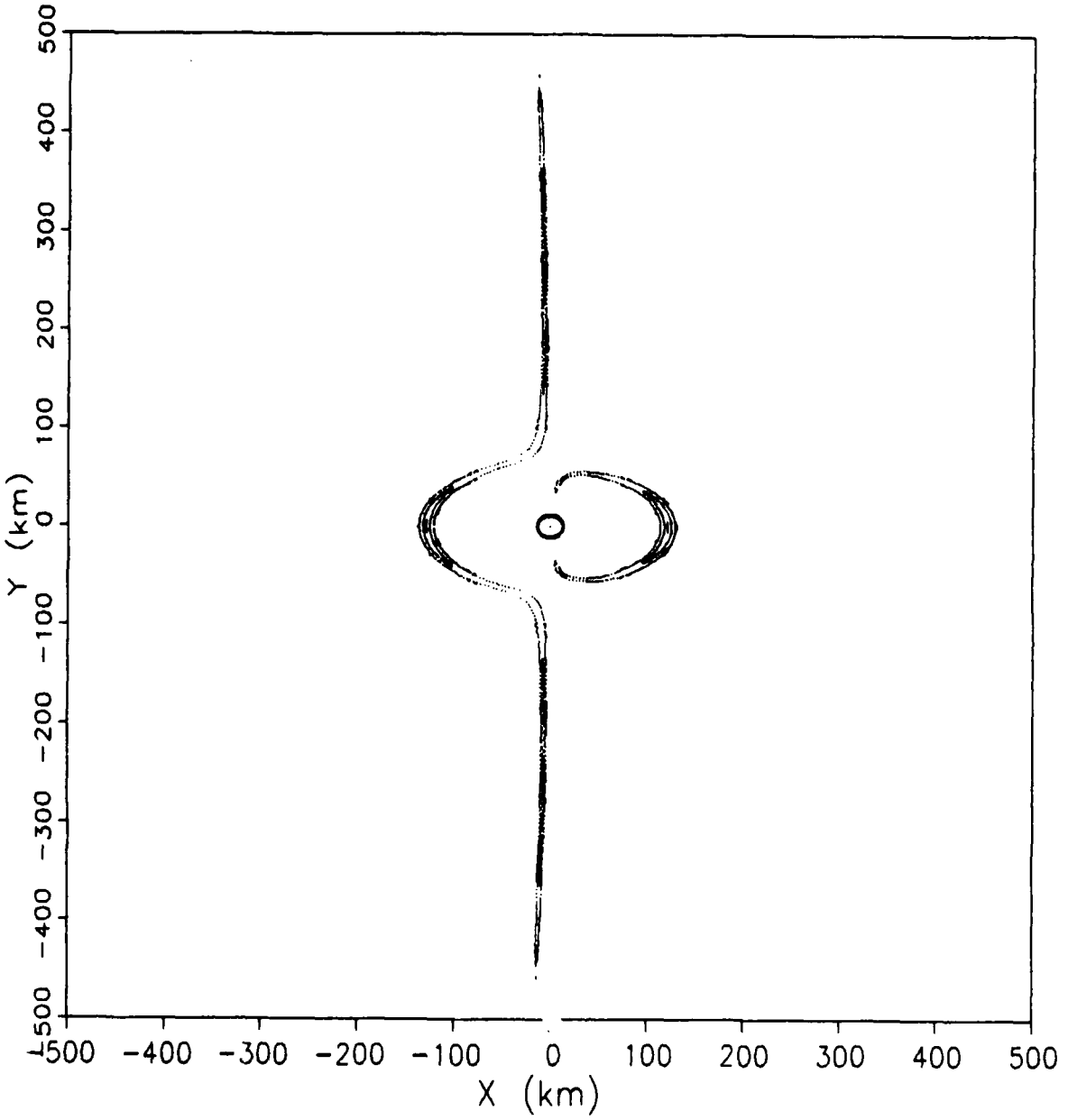

Figure 33. Phobos Surface of Section, H = -6.8524

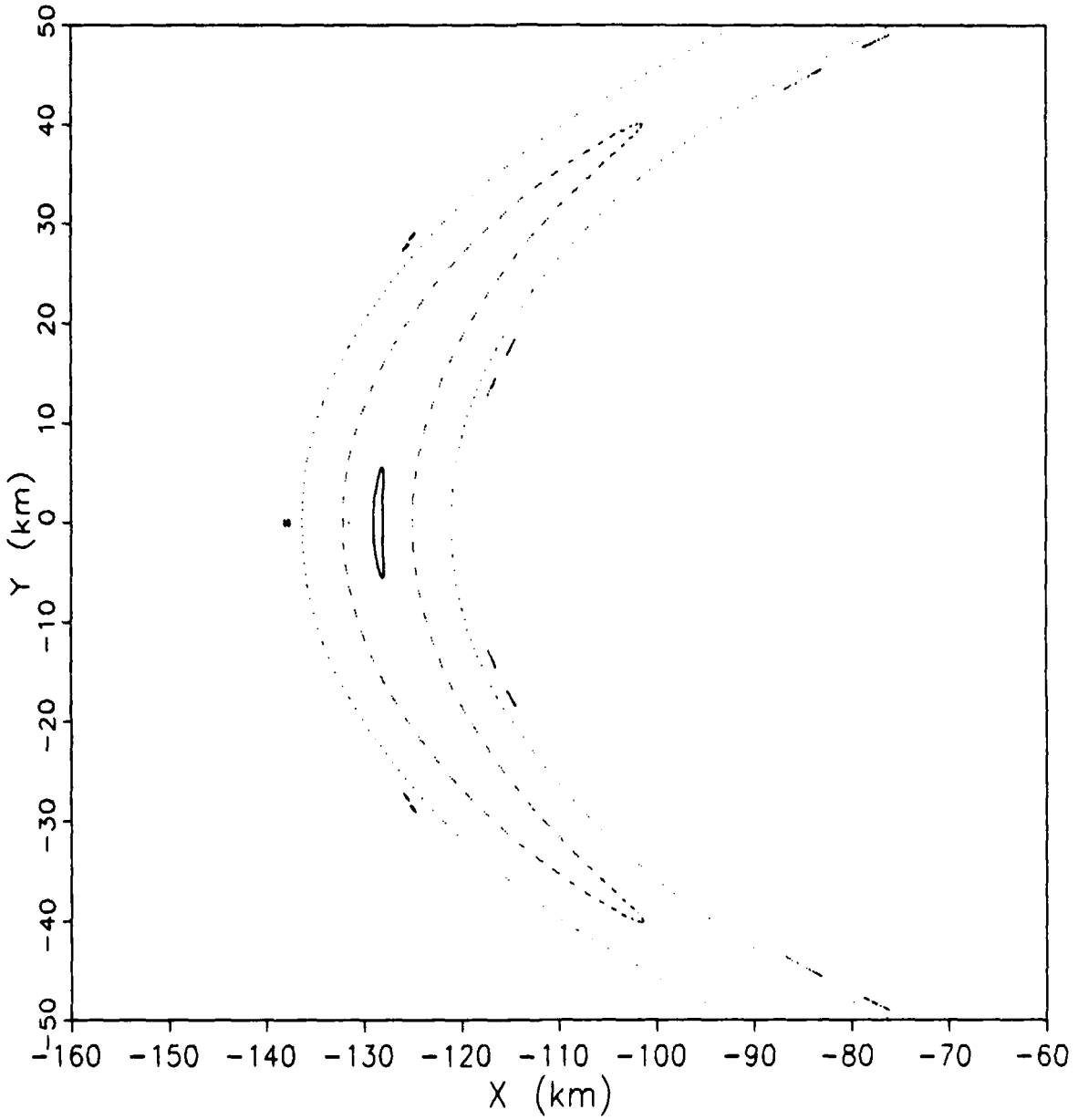

Figure 34. Phobos Surface of Section, H = -6.8524

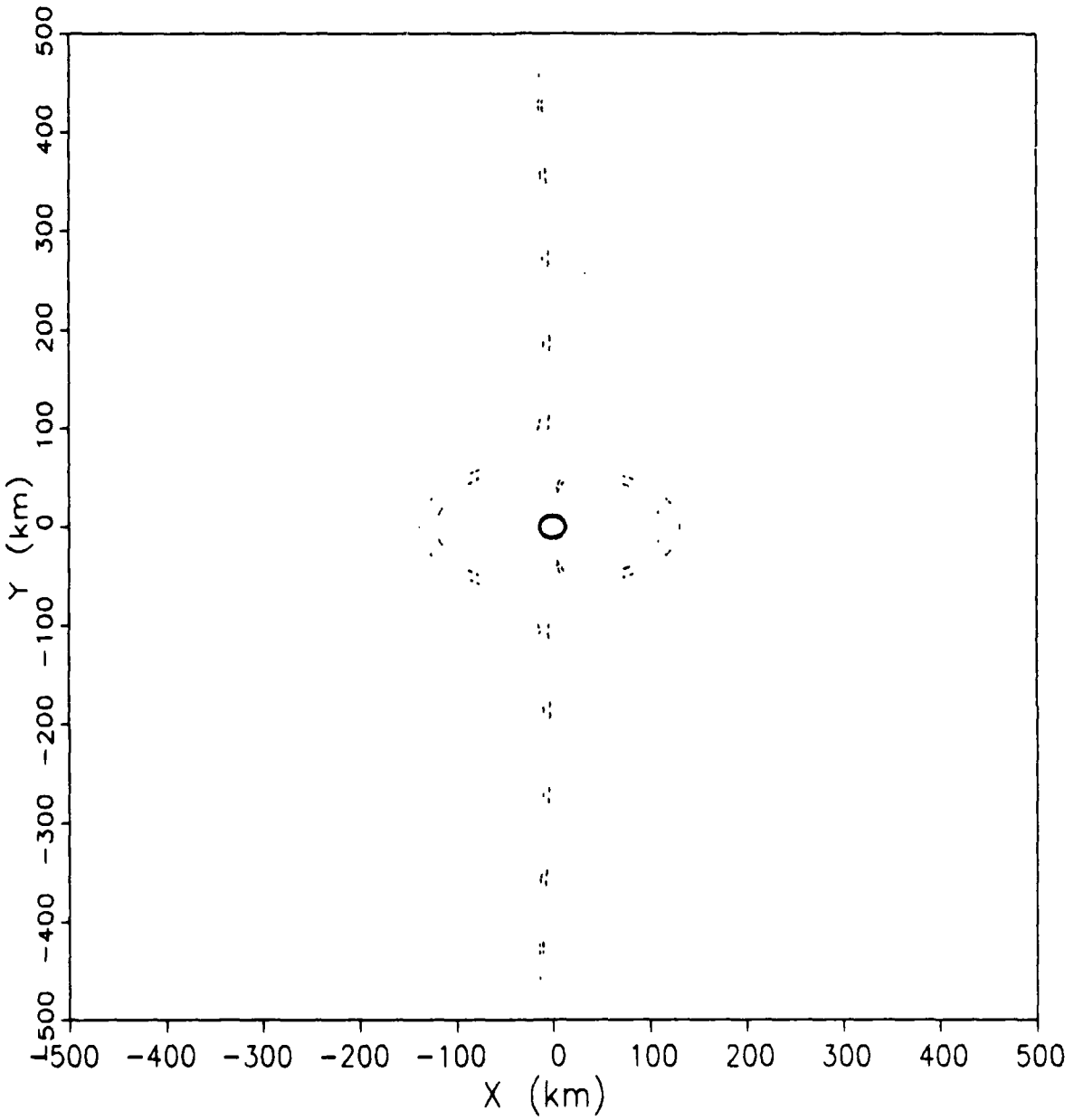

Figure 35. Phobos Surface of Section, H = -6.8524

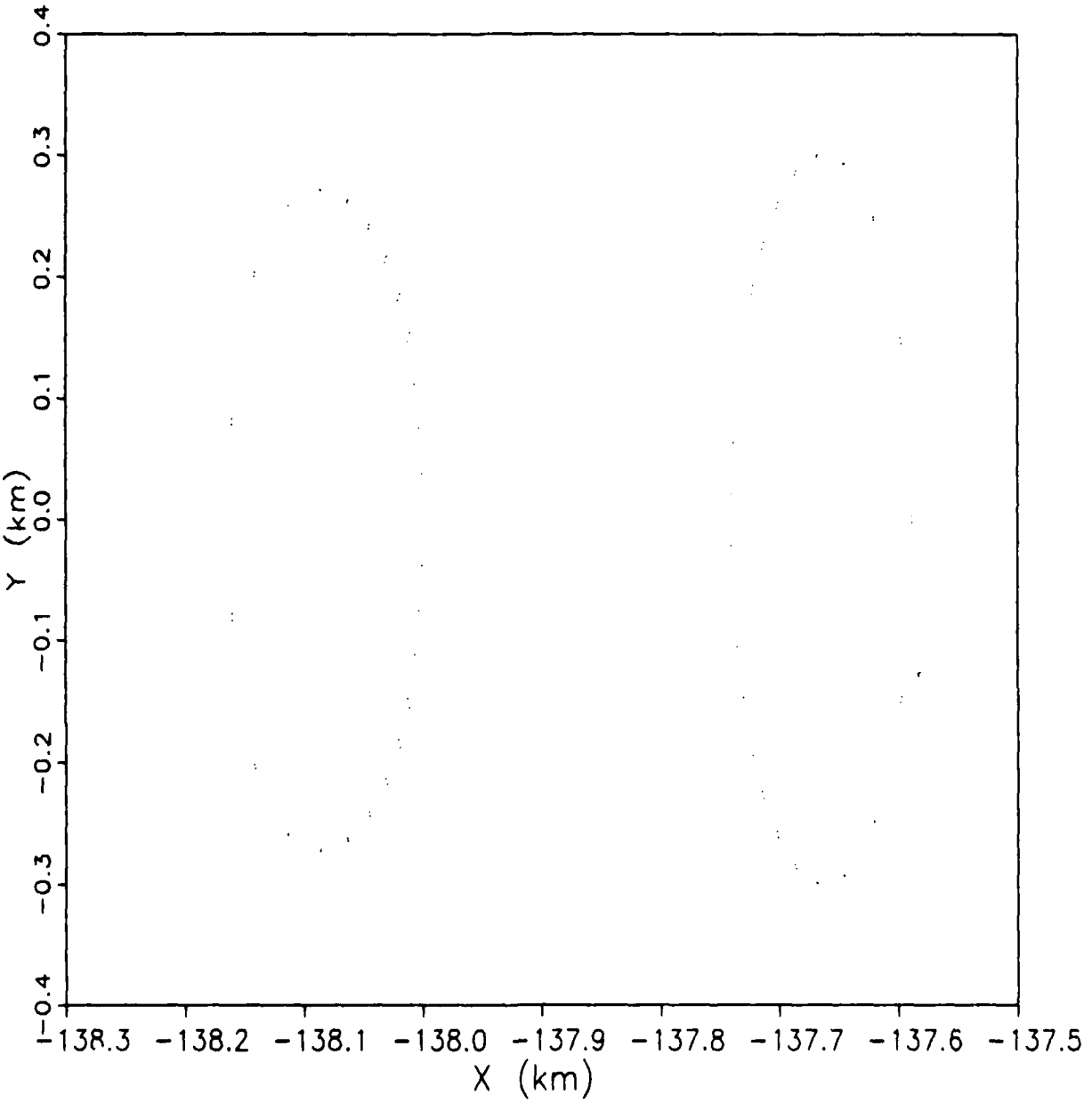

Figure 36. Phobos Surface of Section, H = -6.8524

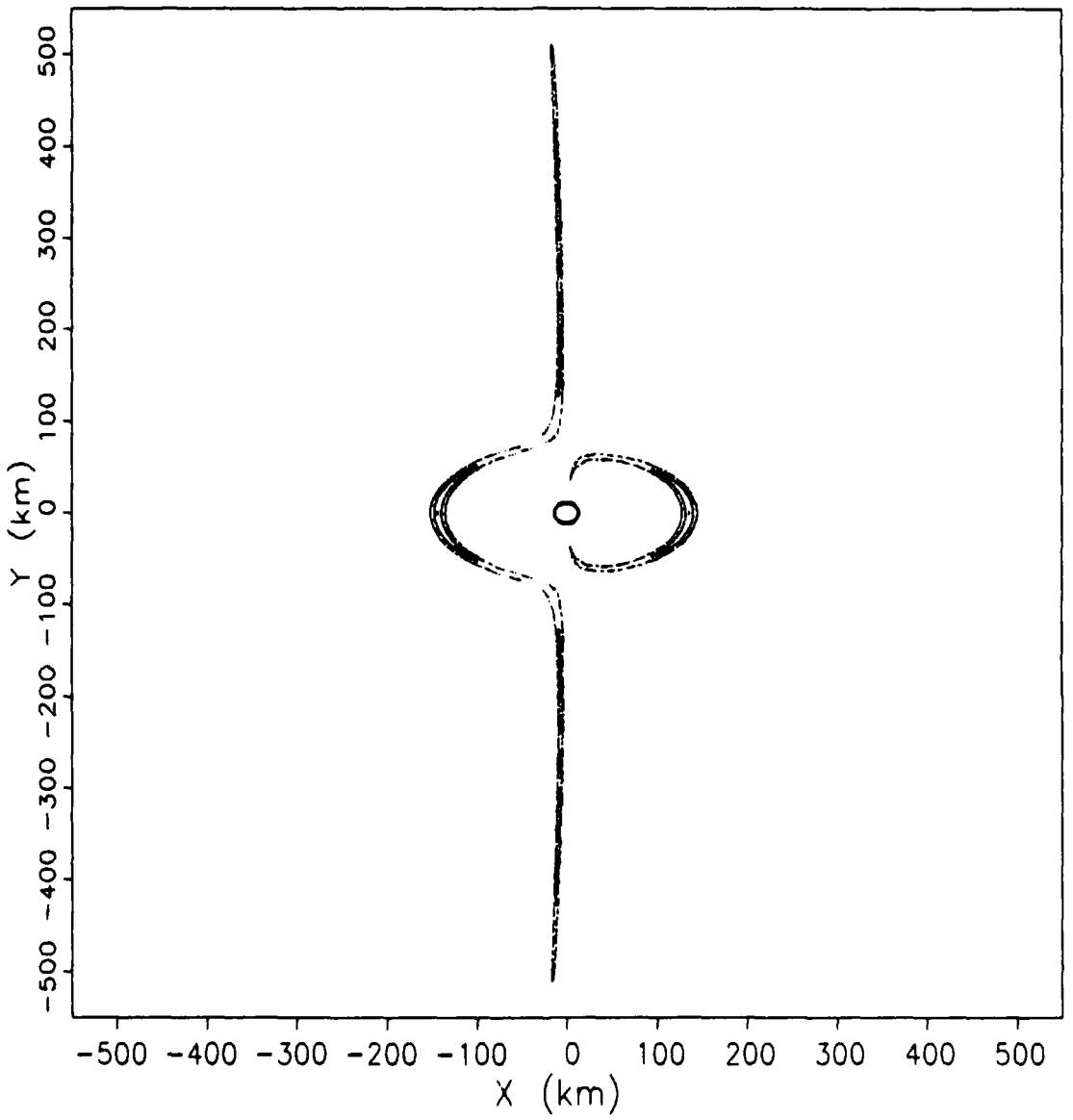

Figure 37. Phobos Surface of Section, H = -6.8523

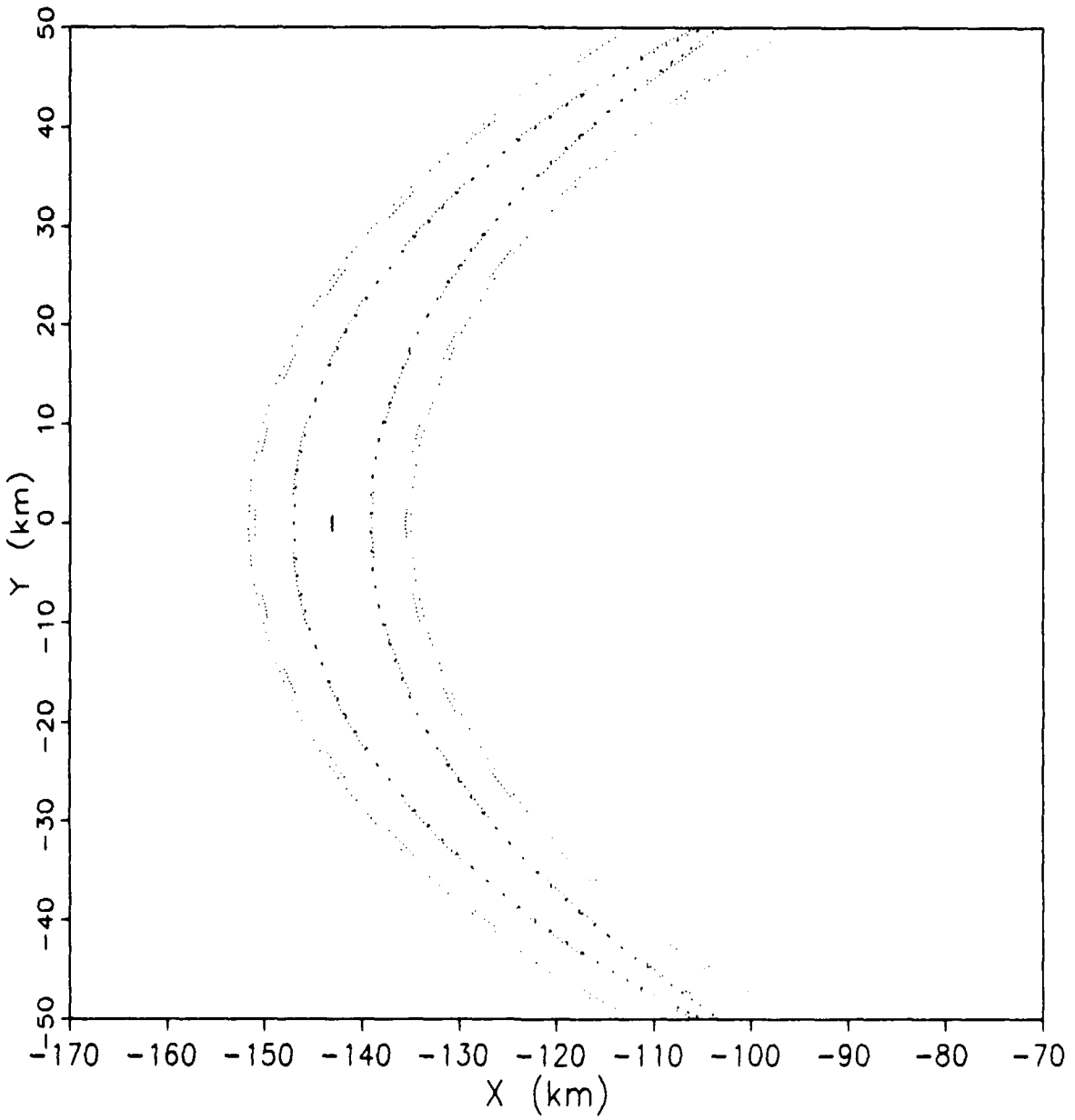

Figure 38. Phobos Surface of Section, H = -6.8523

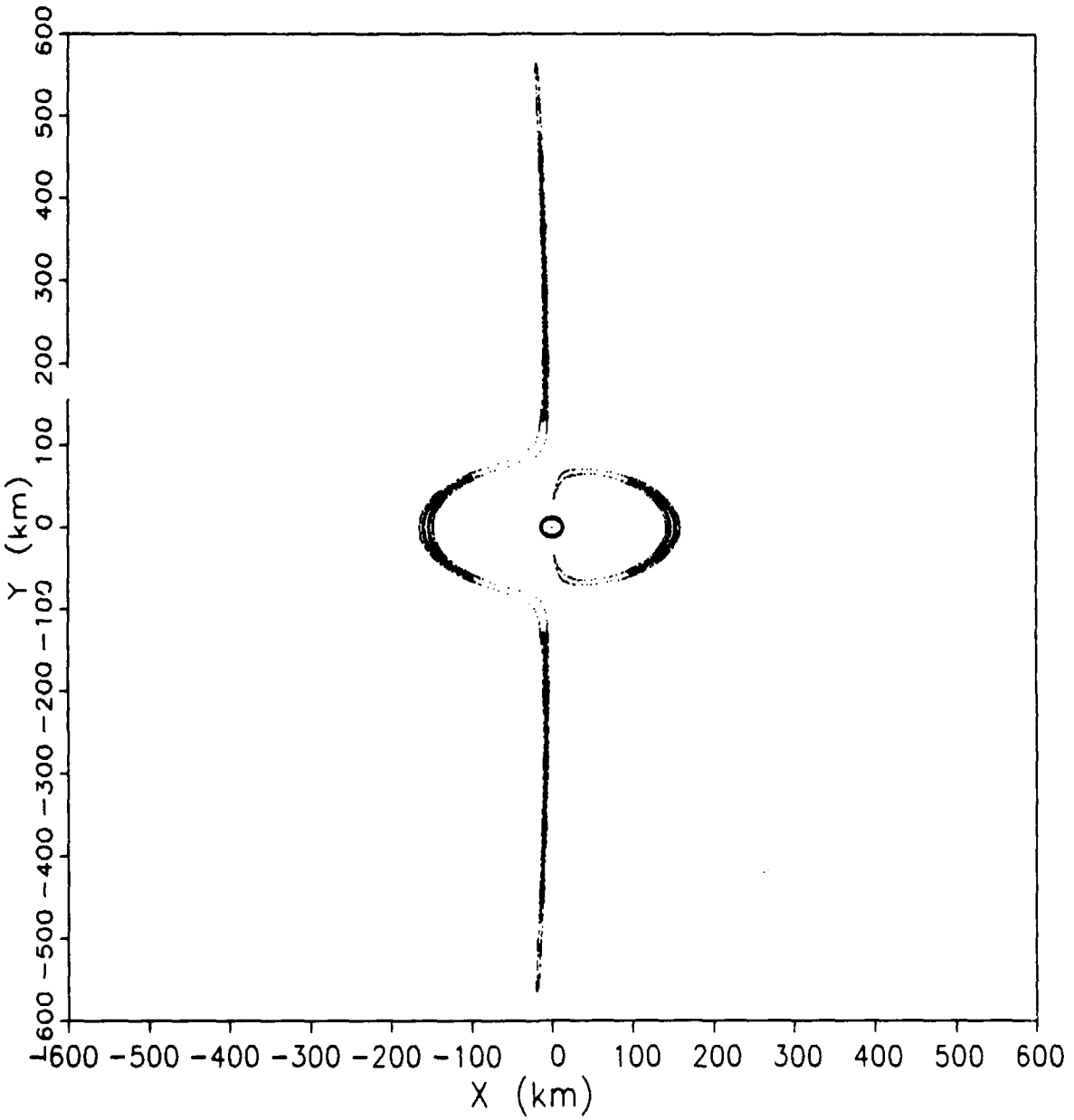

Figure 39. Phobos Surface of Section, H = -6.8522

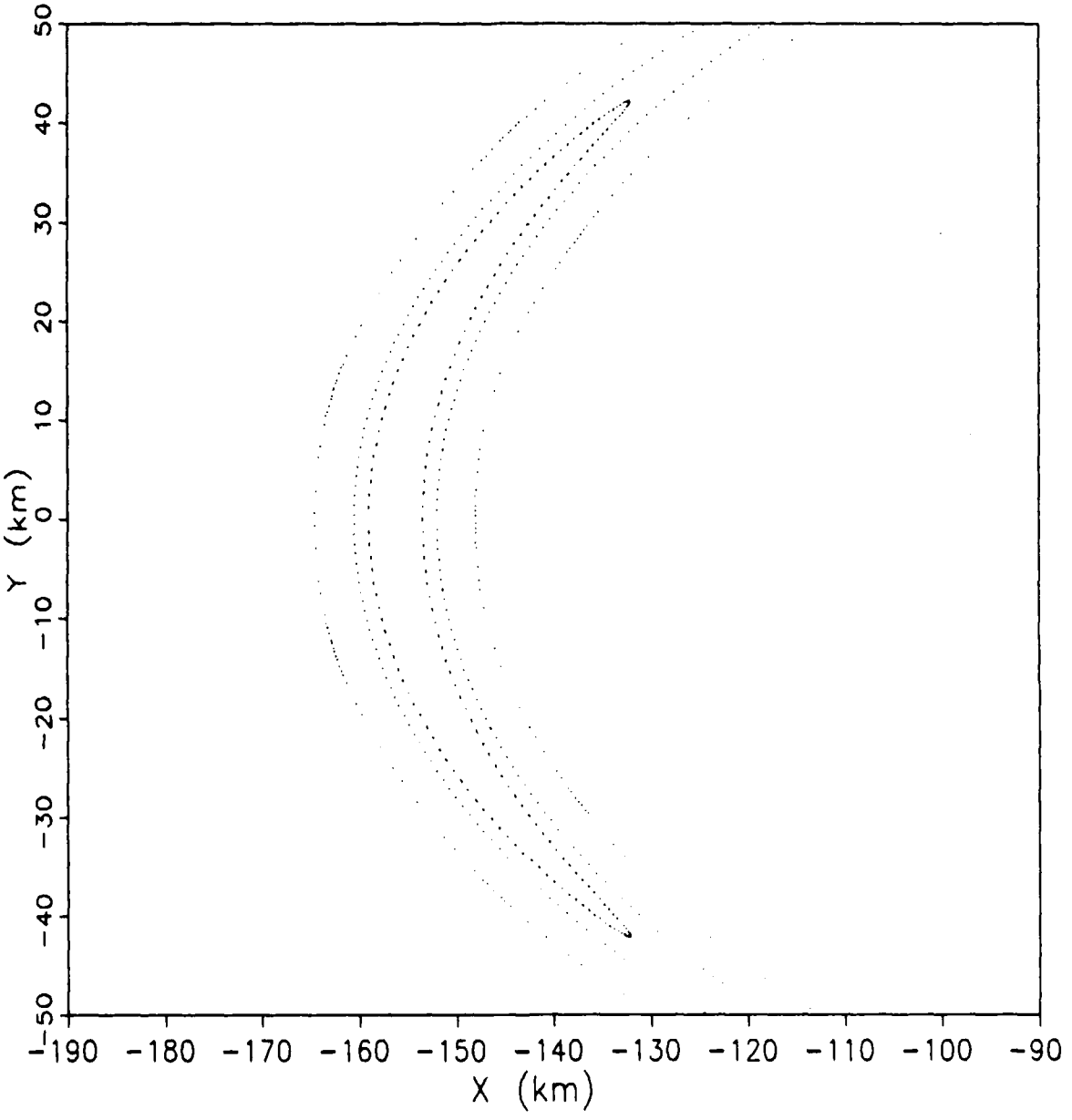

Figure 40. Phobos Surface of Section, H = -6.8522

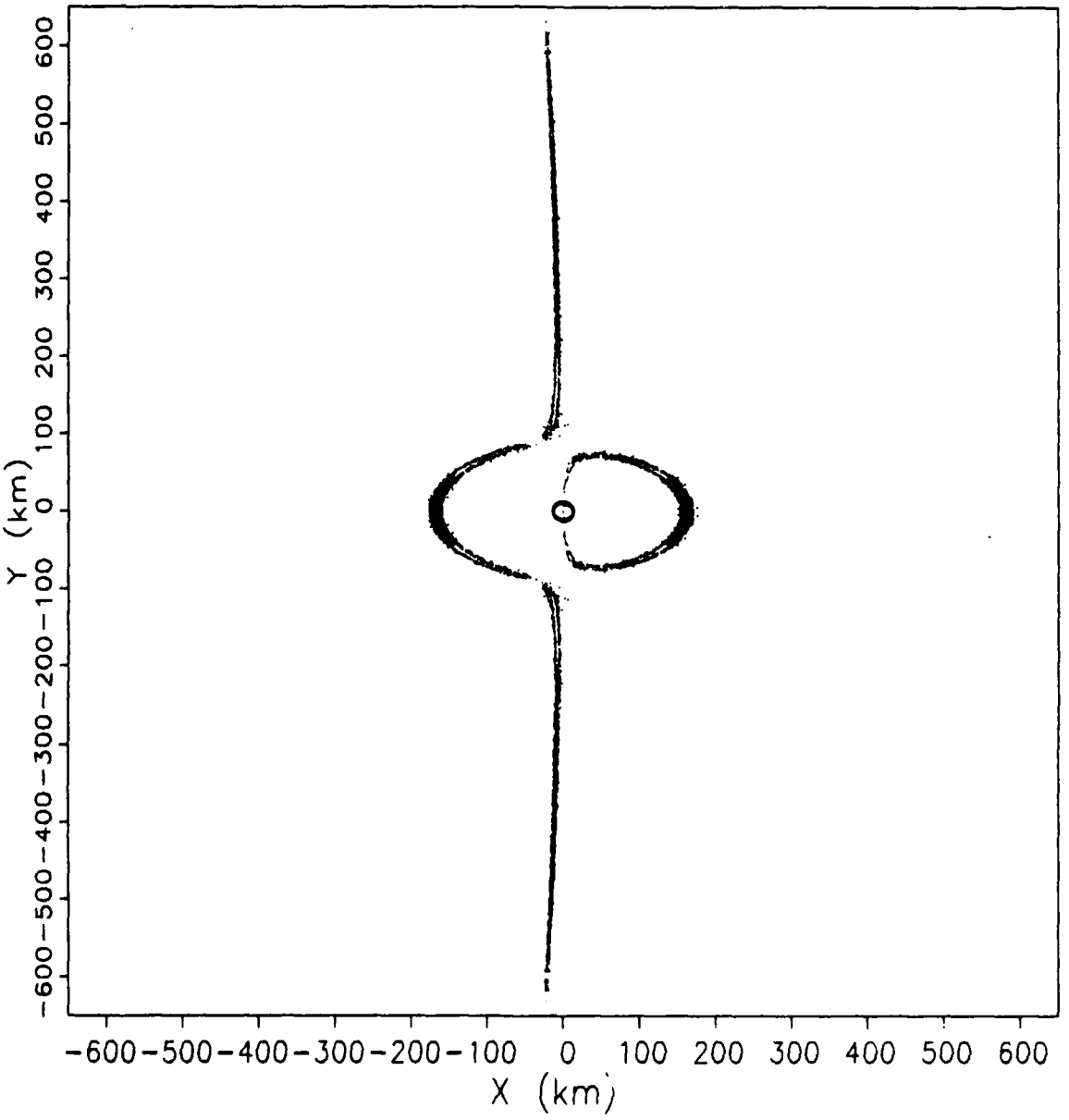

Figure 41. Phobos Surface of Section, H = -6.8521

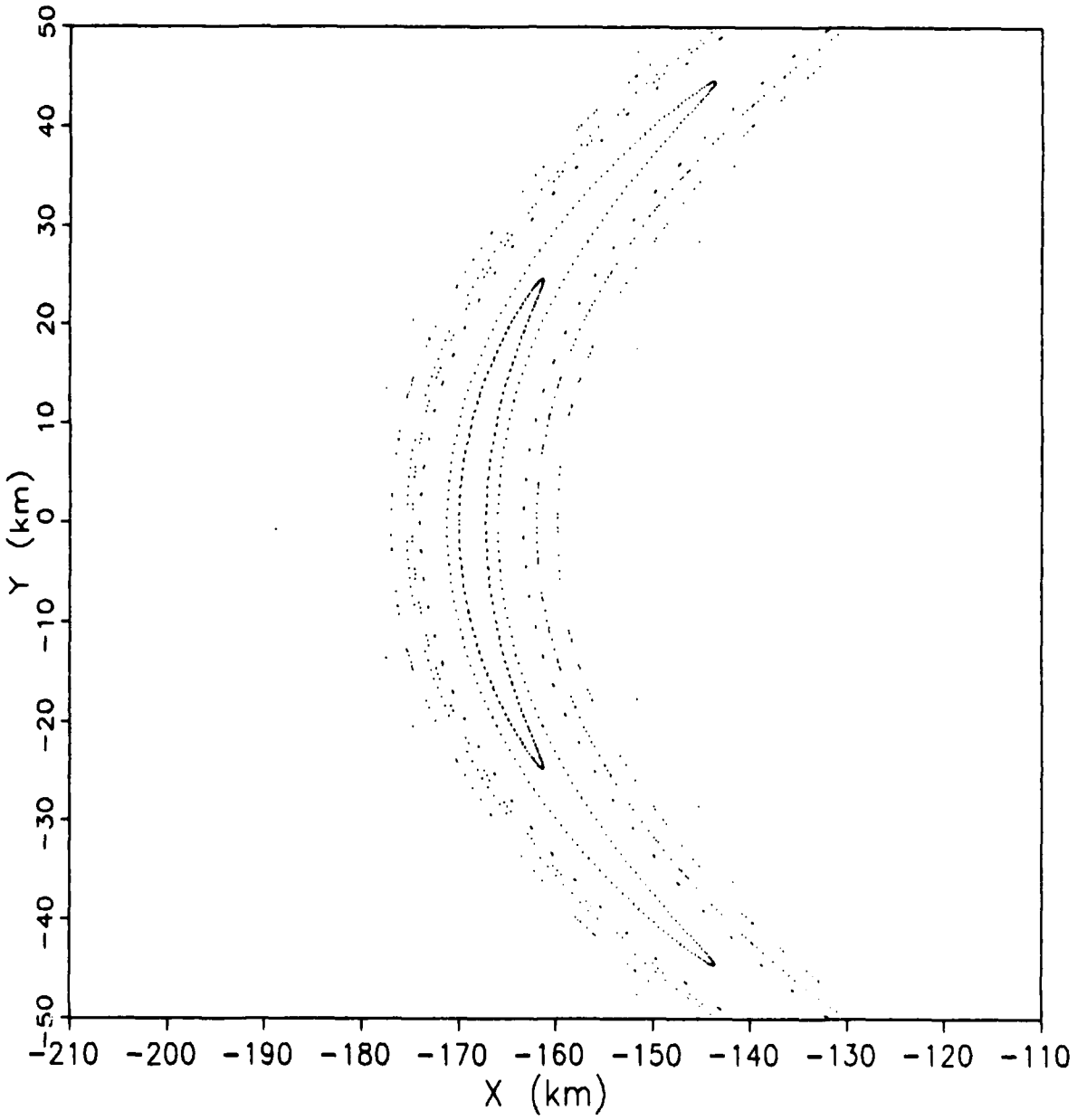

Figure 42. Phobos Surface of Section, H = -6.8521

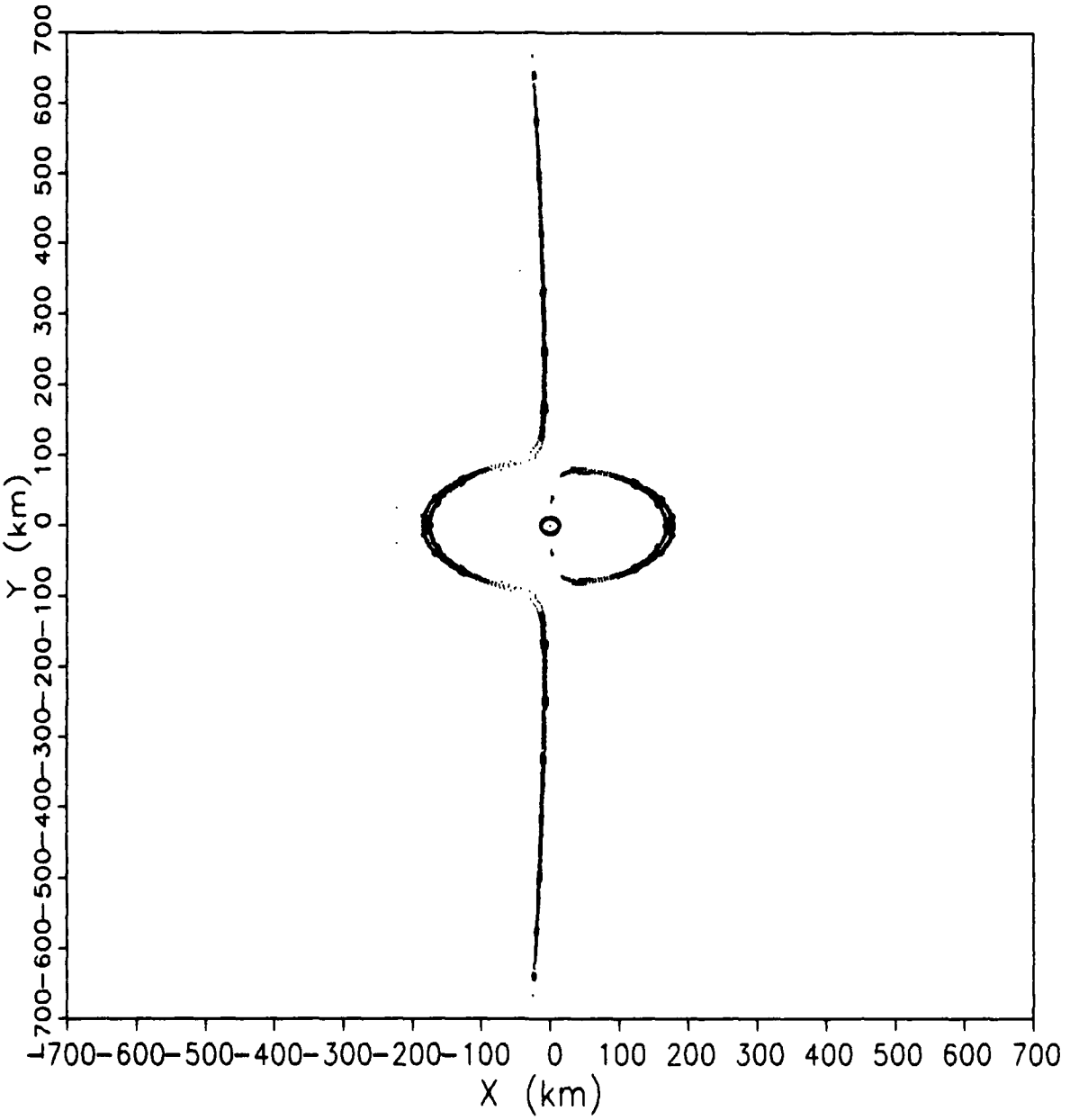

Figure 43. Phobos Surface of Section, H = -6.852

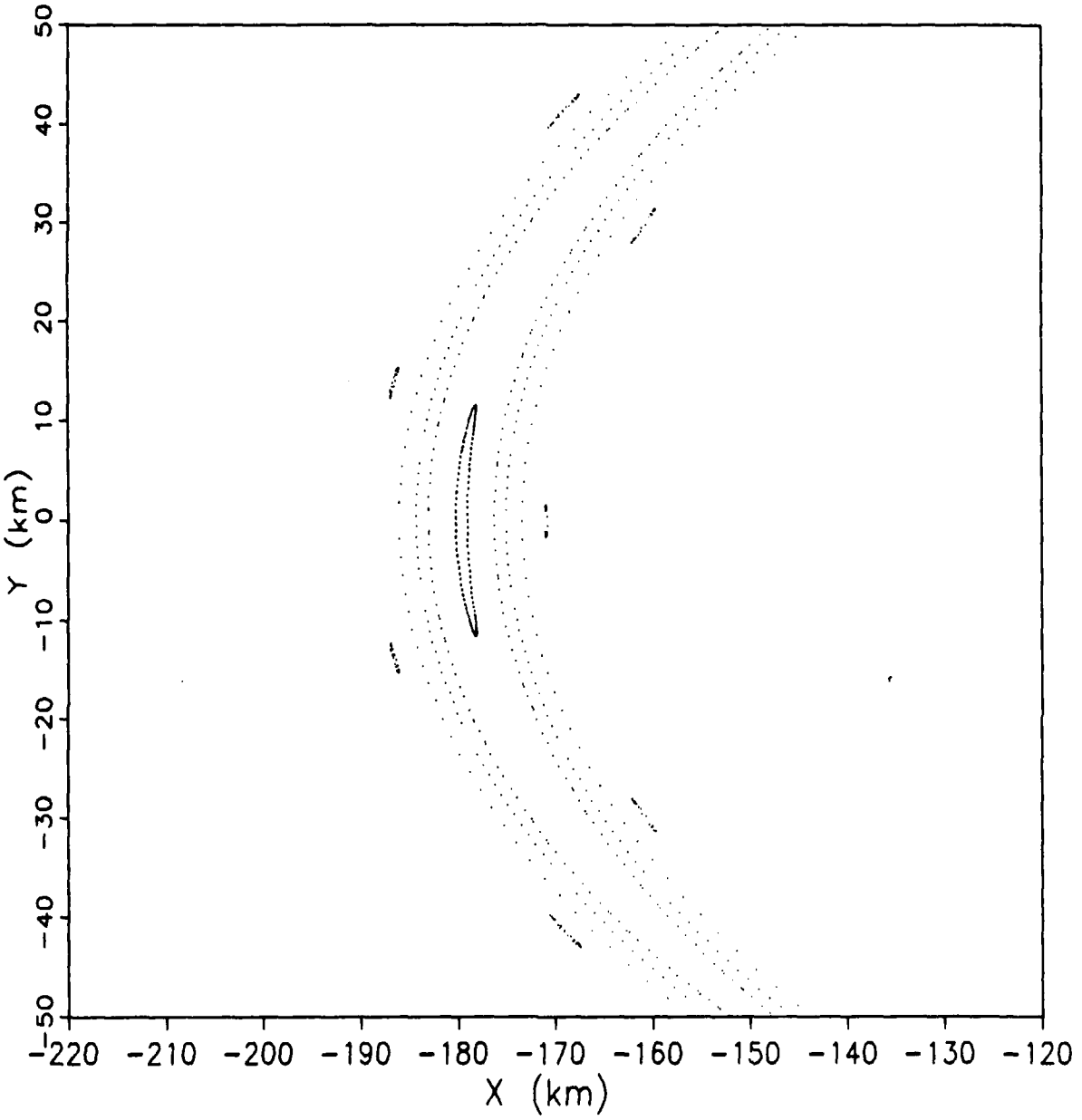

Figure 44. Phobos Surface of Section, H = -6.852

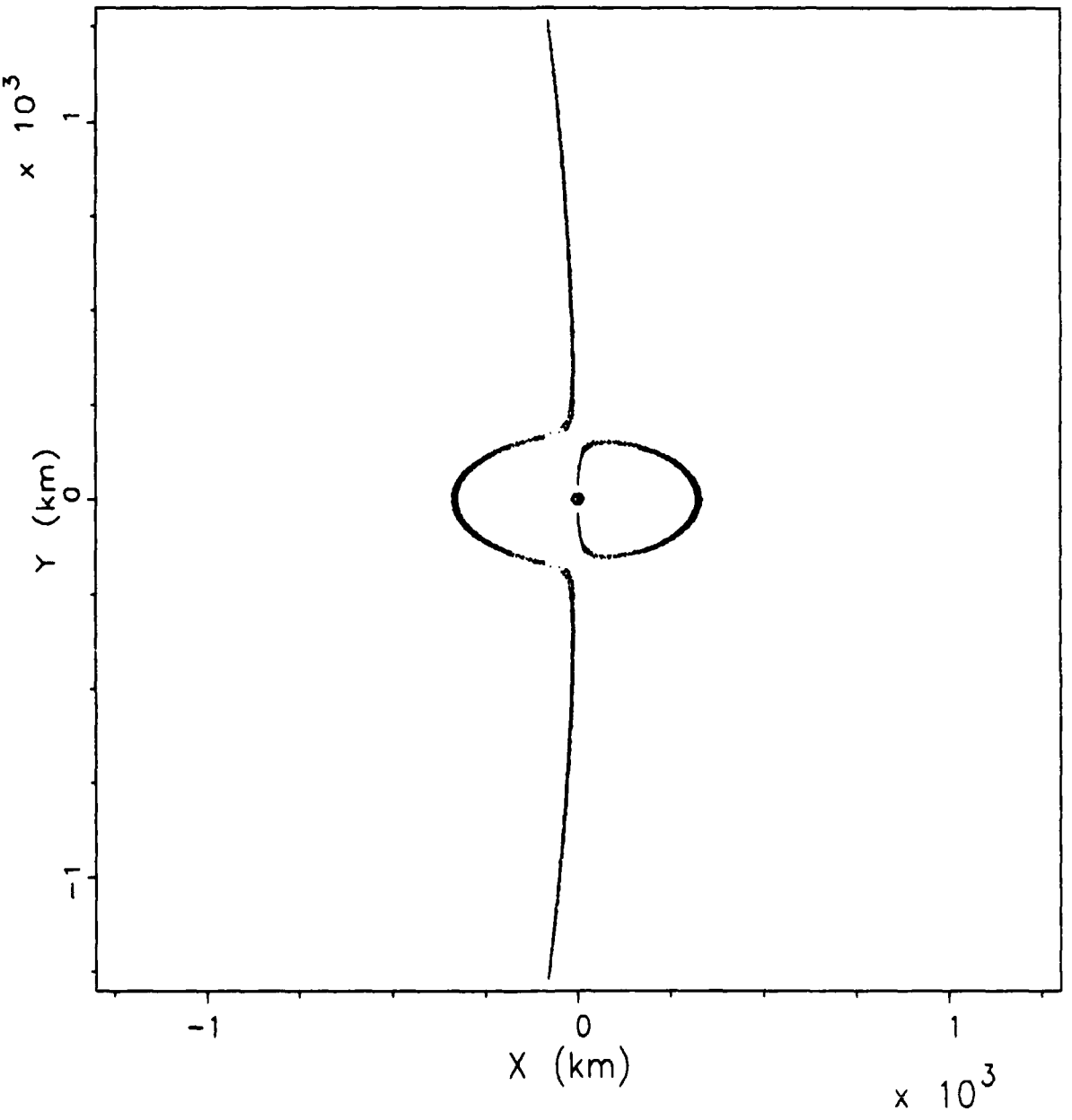

Figure 45. Phobos Surface of Section, H = -6.85

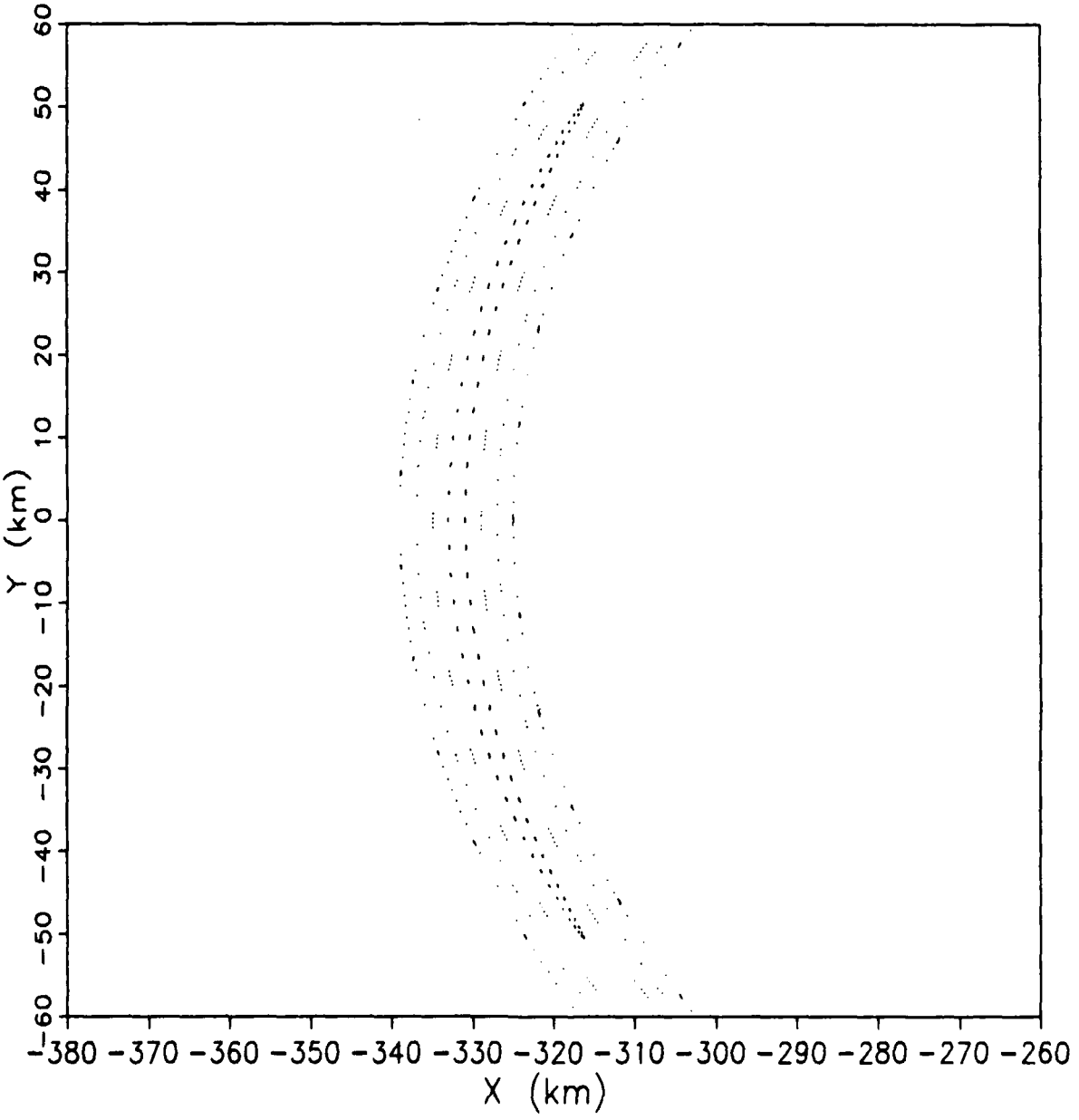

Figure 46. Phobos Surface of Section, H = -6.85

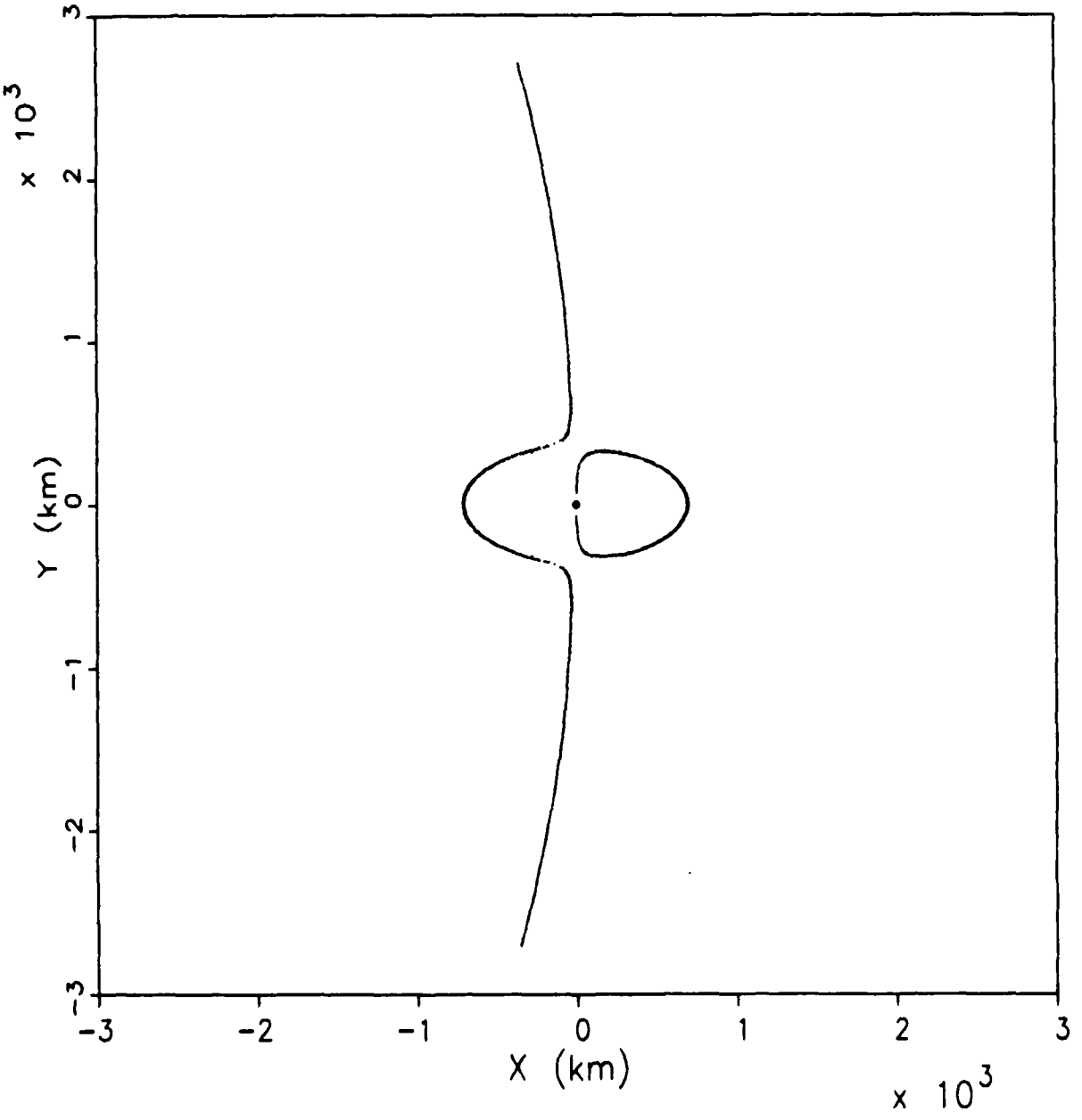

Figure 47. Phobos Surface of Section, H = -6.84

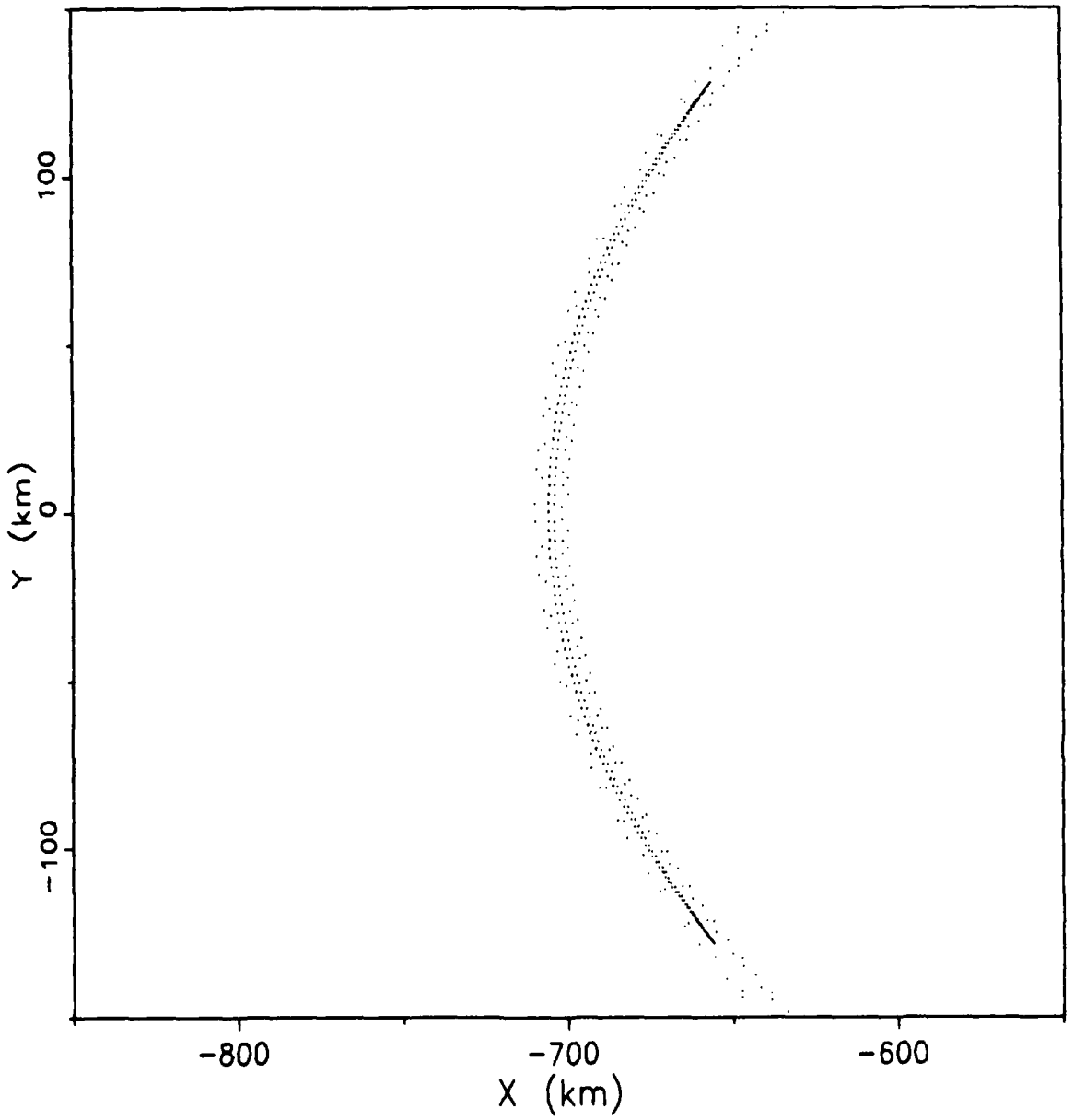

Figure 48. Phobos Surface of Section, H = -6.84

Appendix D: Deimos Surface of Section Plots

Figure Page

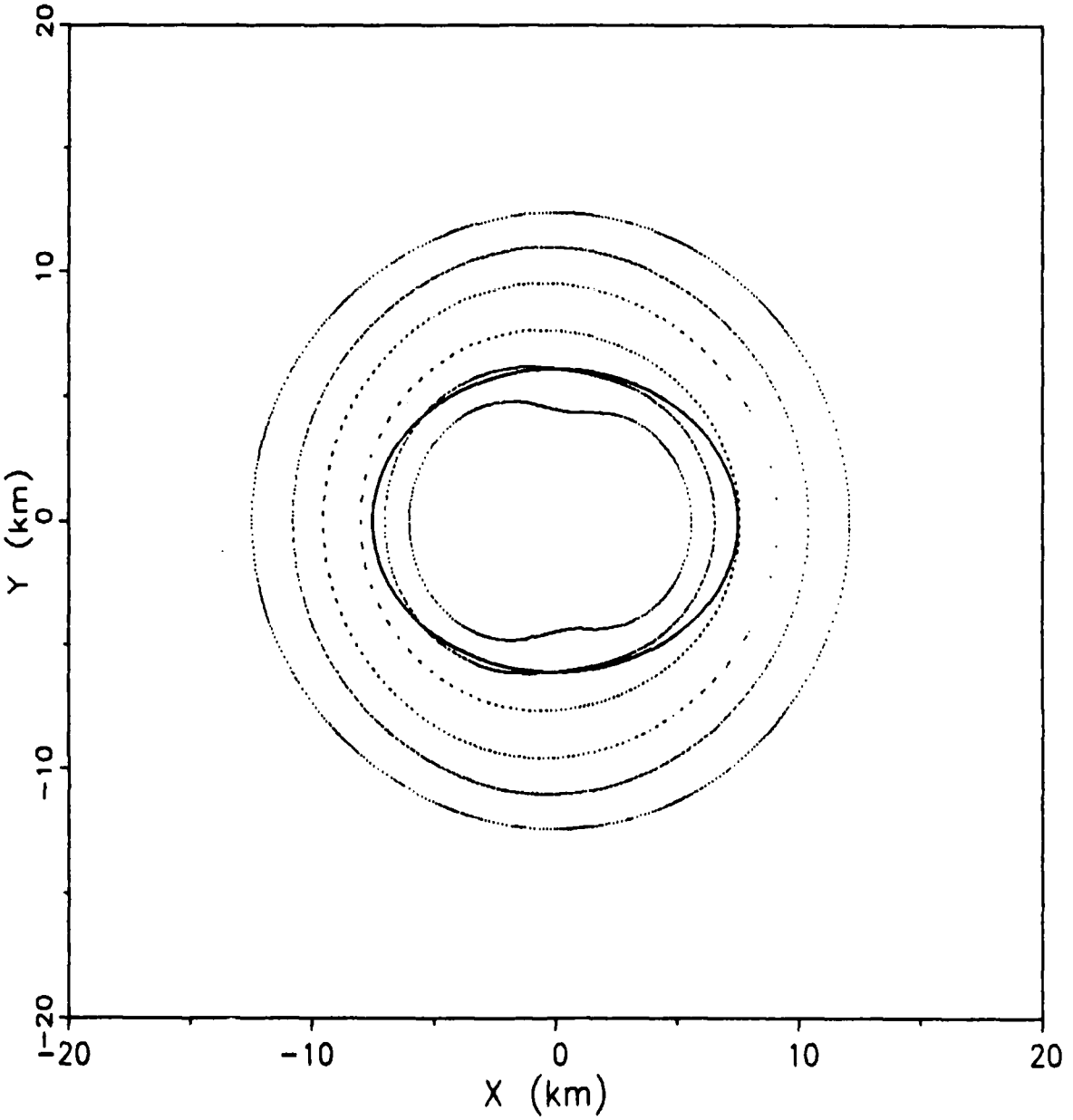

Figure 49. Deimos Surface of Section, H = -2.738593

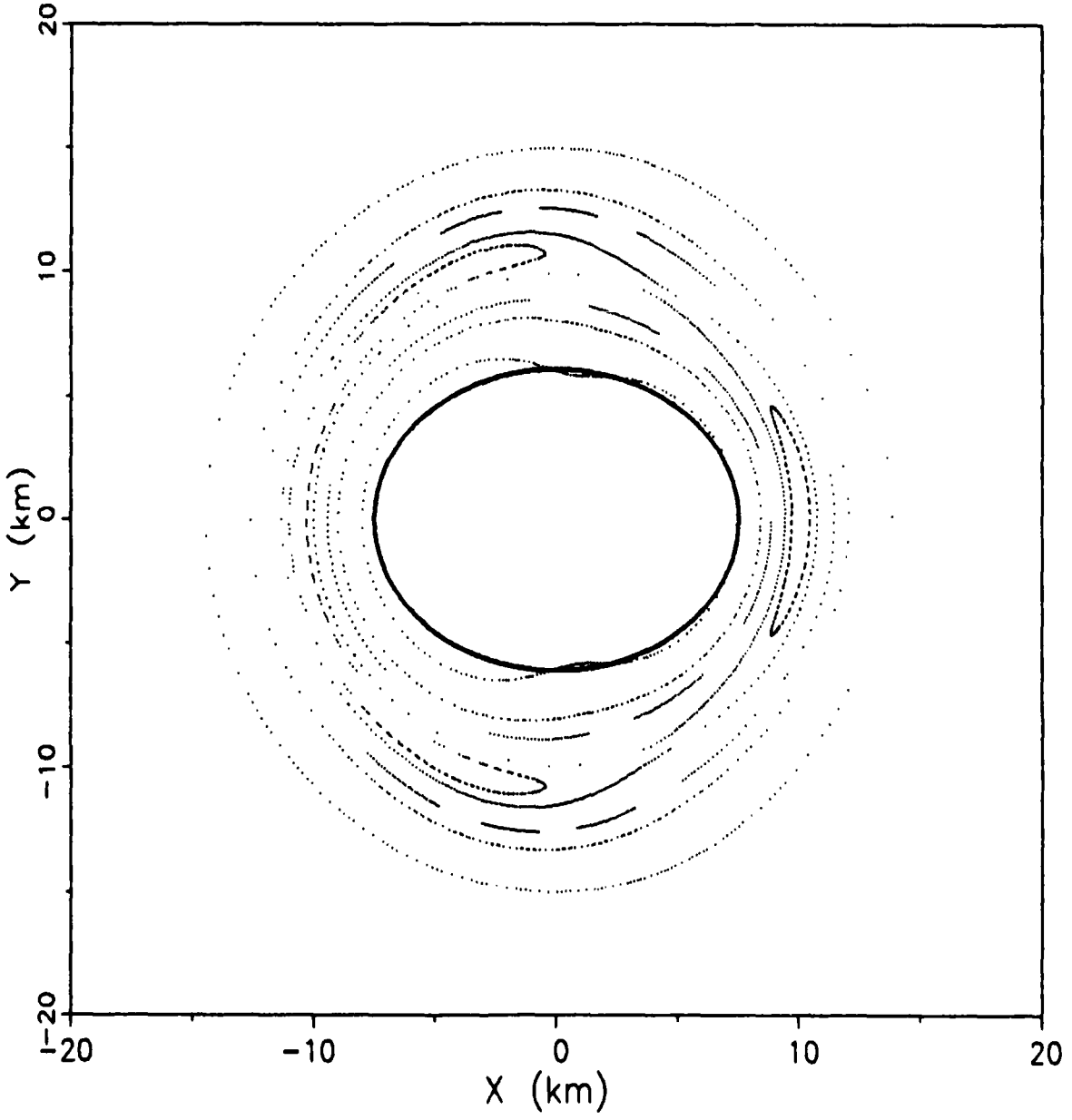

Figure 50. Deimos Surface of Section, H = -2.738592

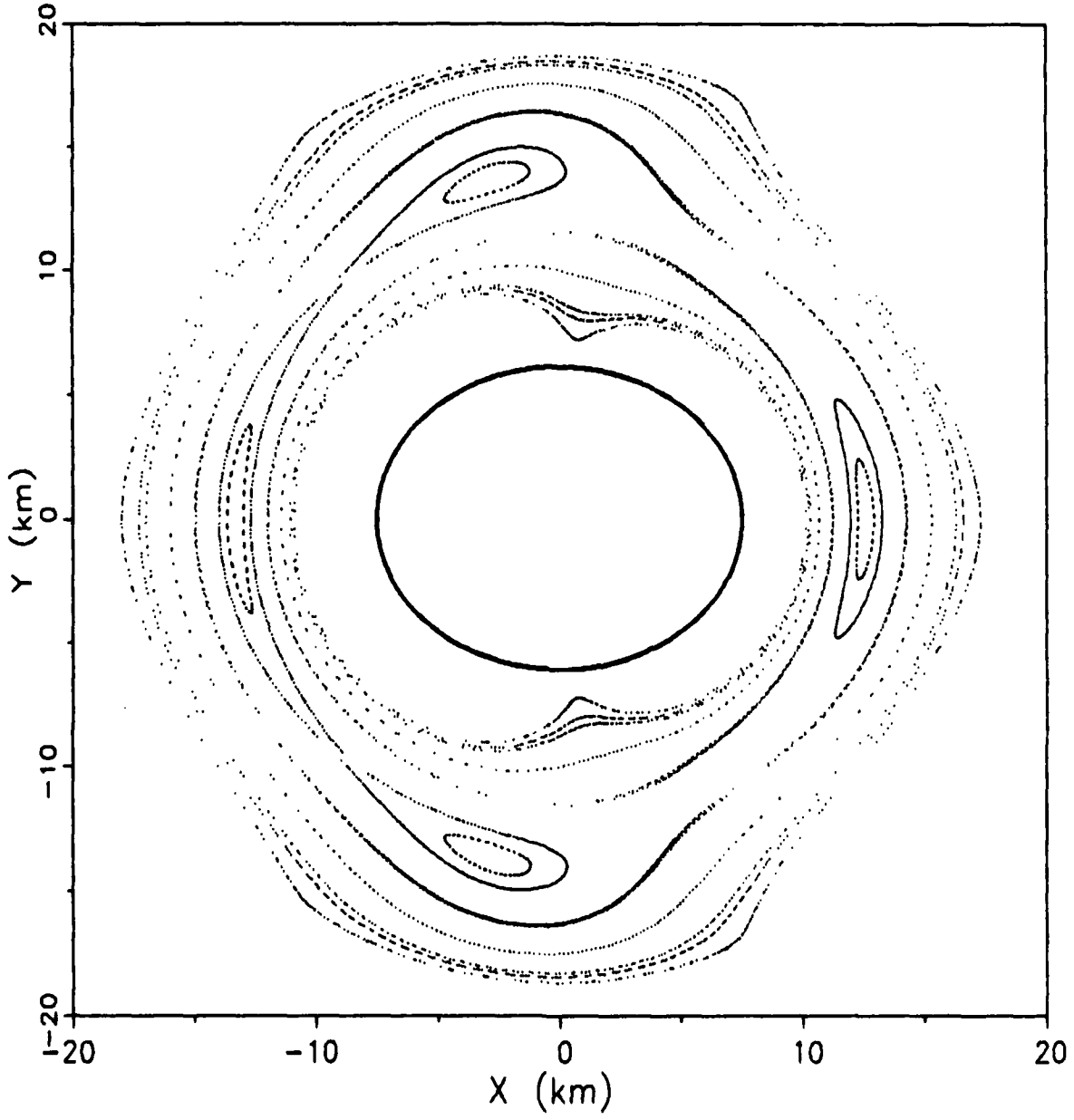

Figure 51. Deimos Surface of Section, H = -2.738591

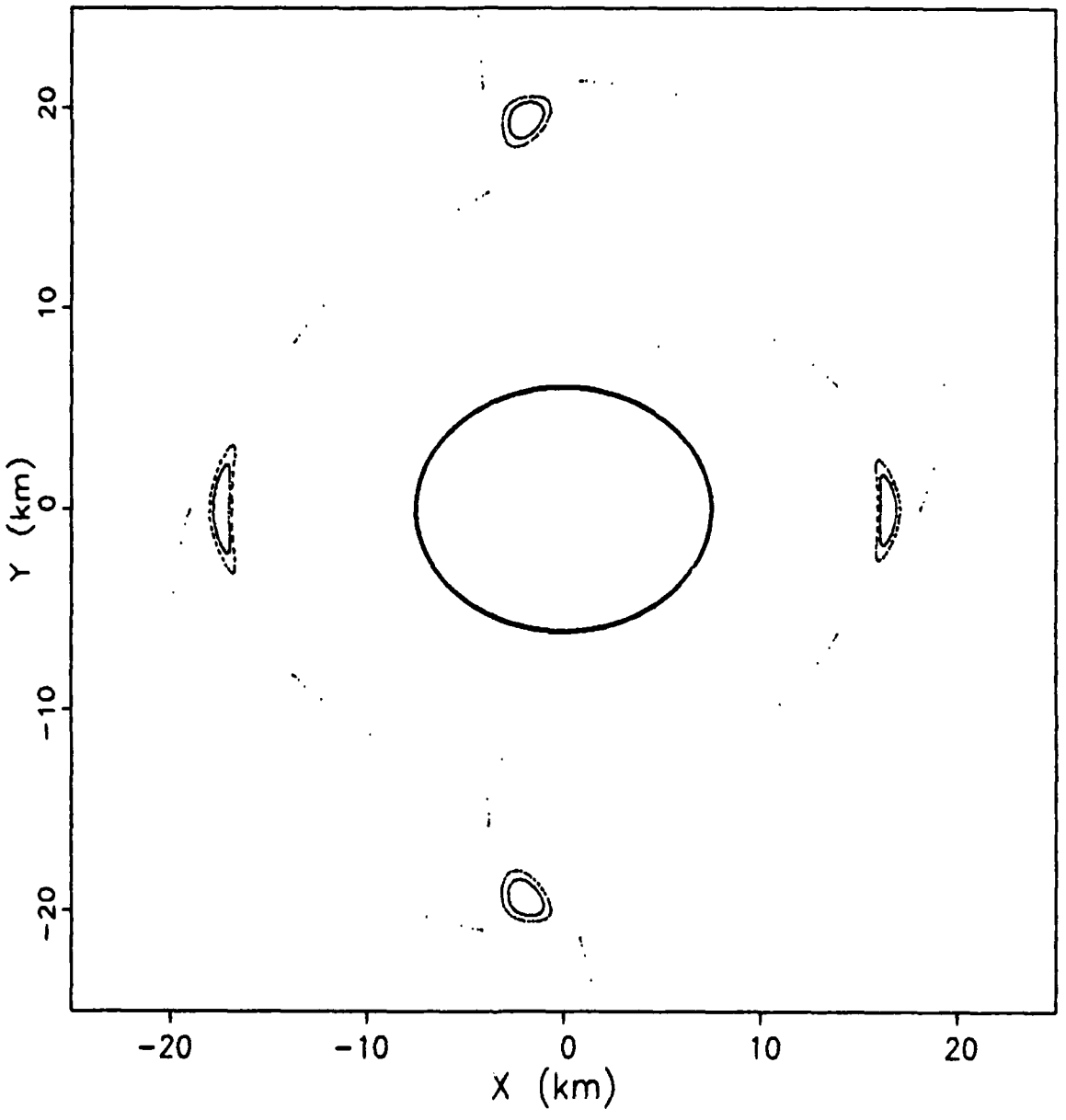

Figure 52. Deimos Surface of Section, H = -2.73859

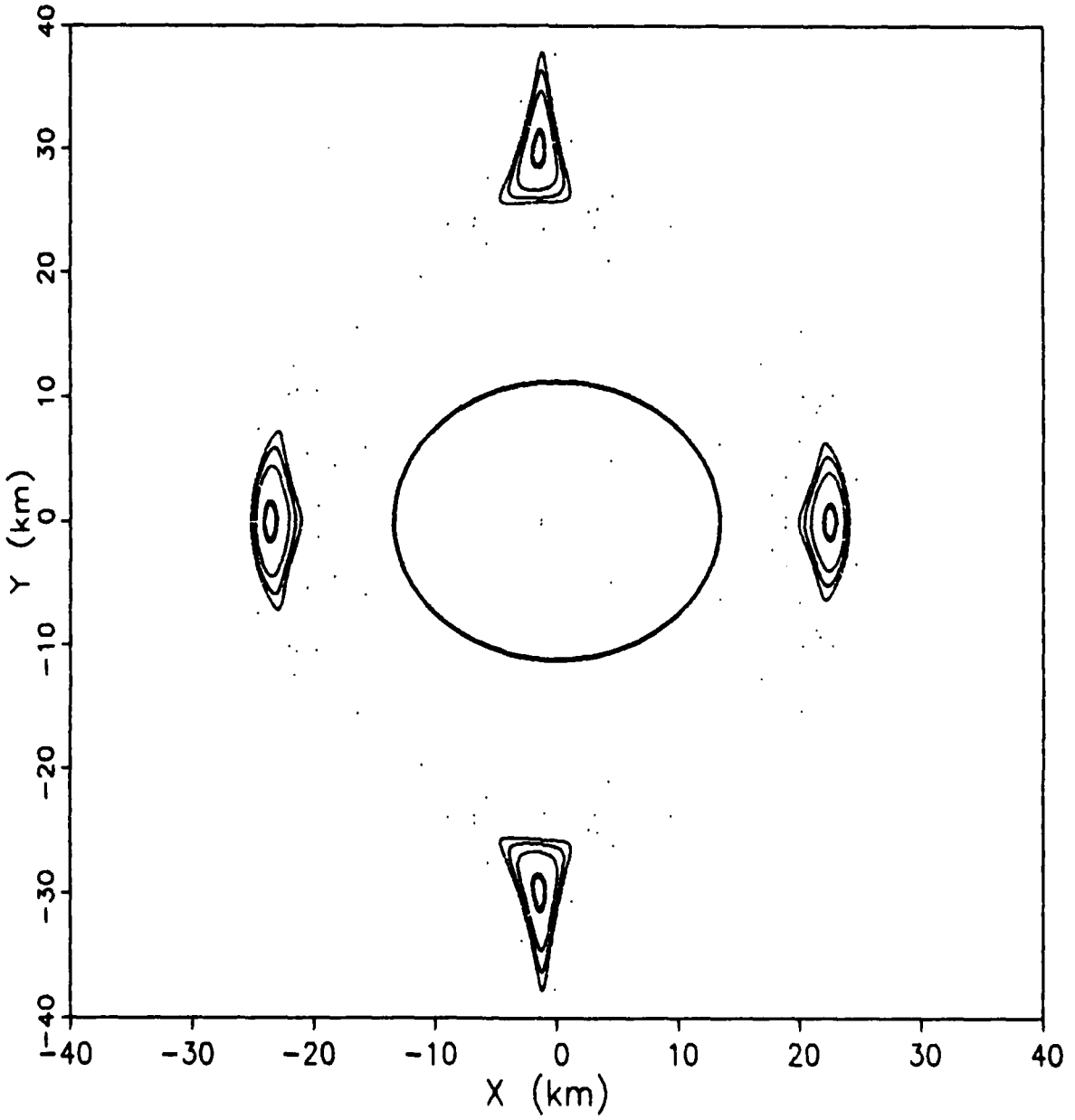

Figure 53. Deimos Surface of Section, H = -2.738589

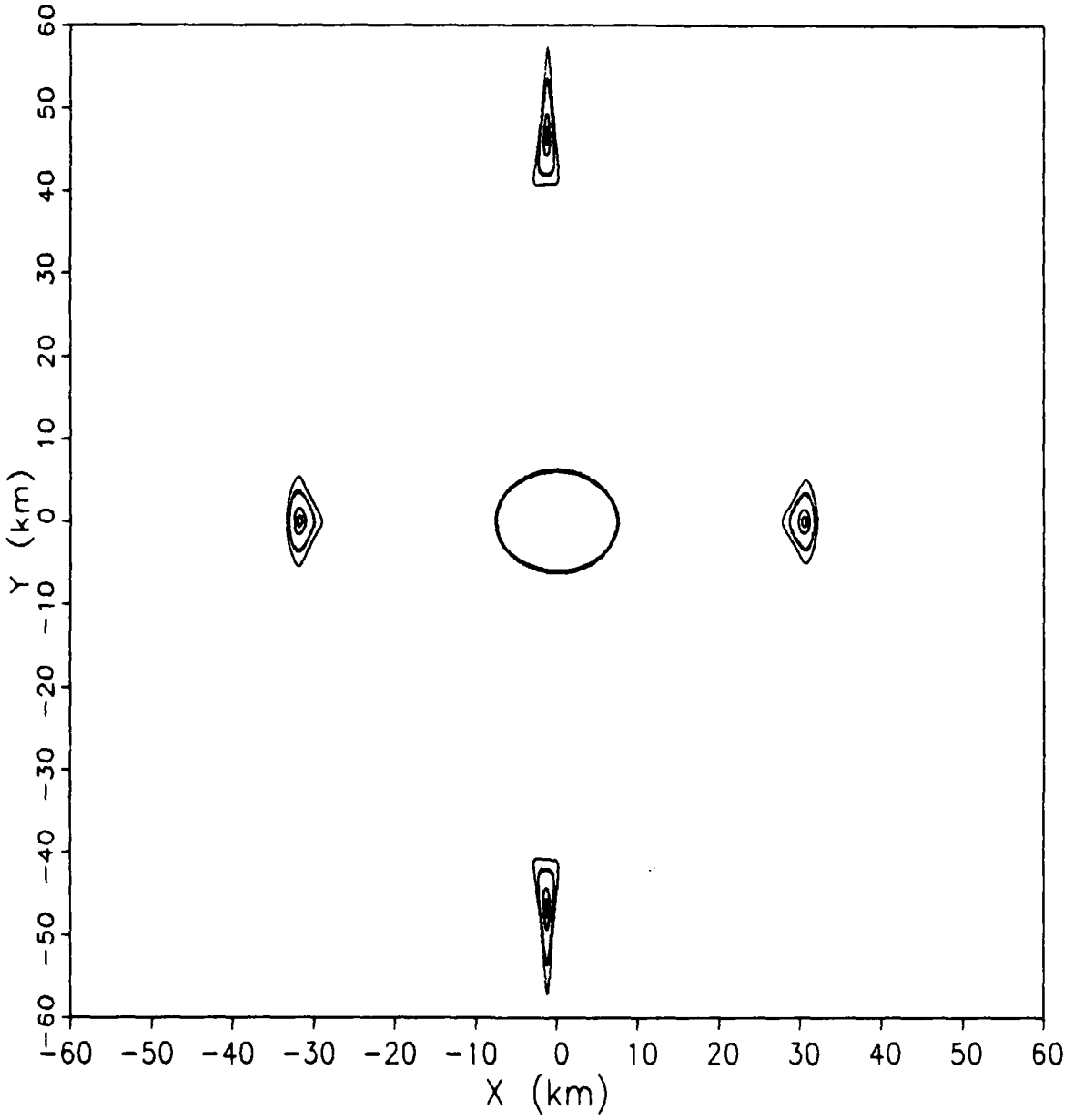

Figure 54. Deimos Surface of Section, H = -2.738588

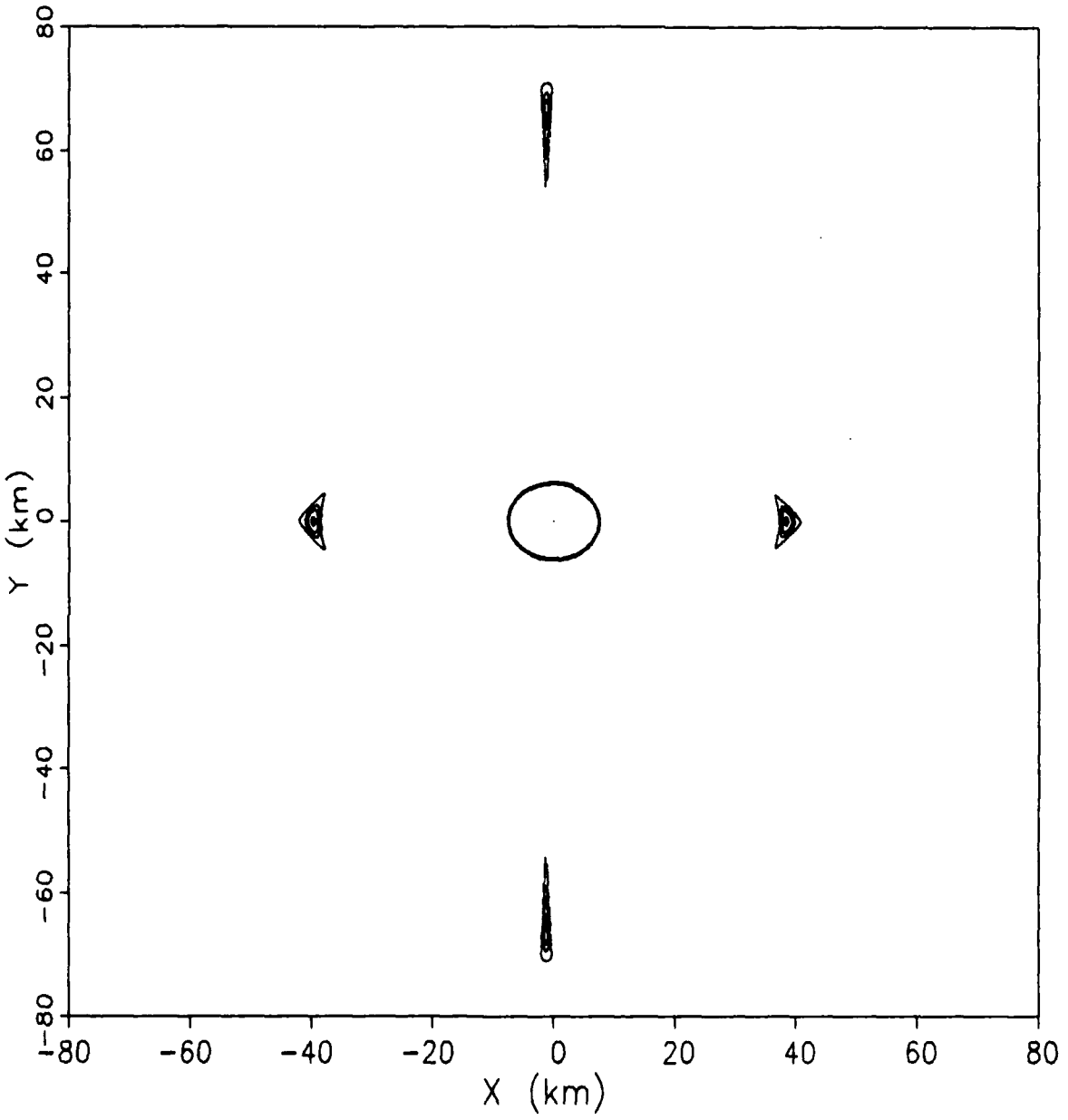

Figure 55. Deimos Surface of Section, H = -2.738587

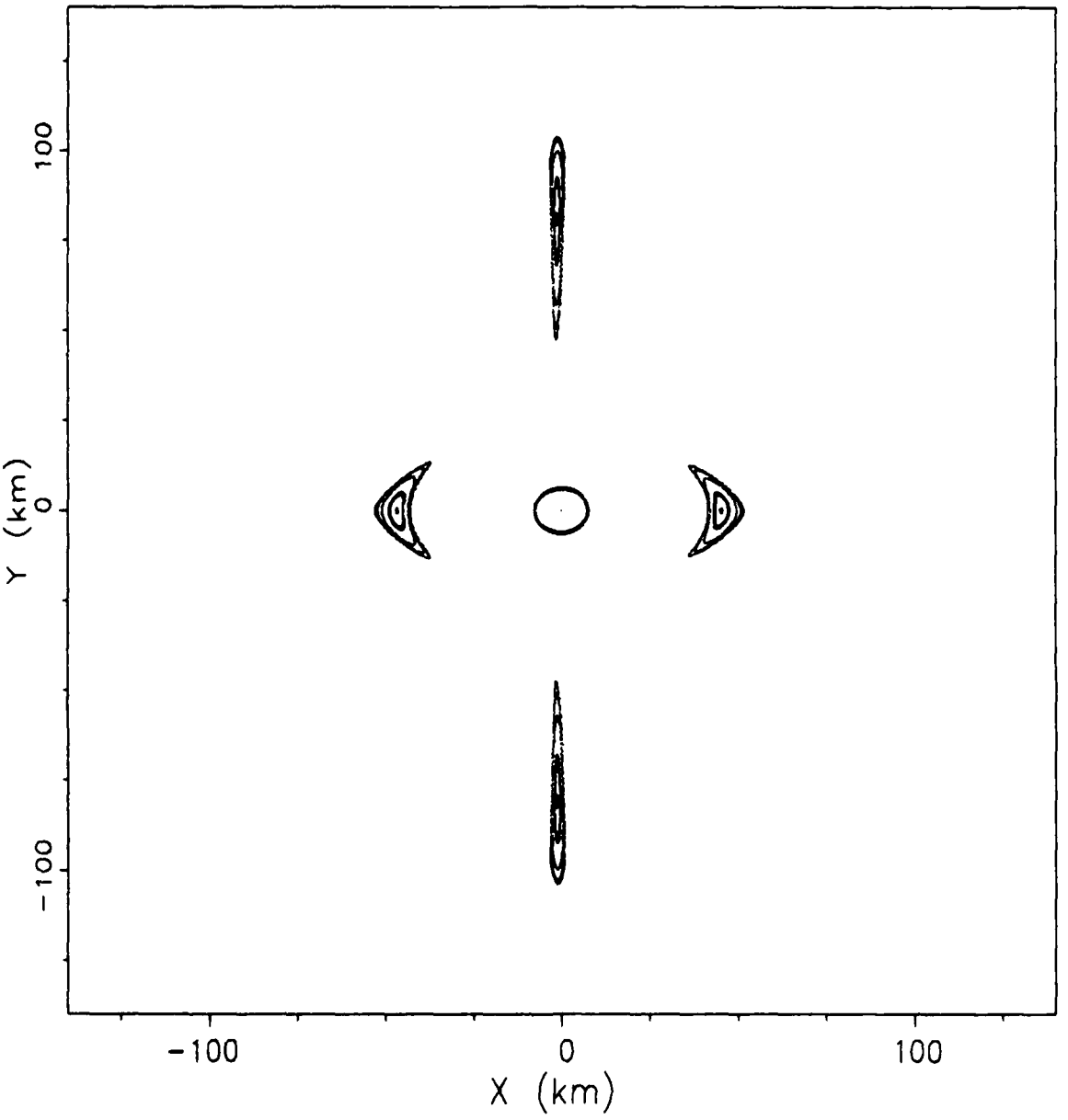

Figure 56. Deimos Surface of Section, H = -2.738586

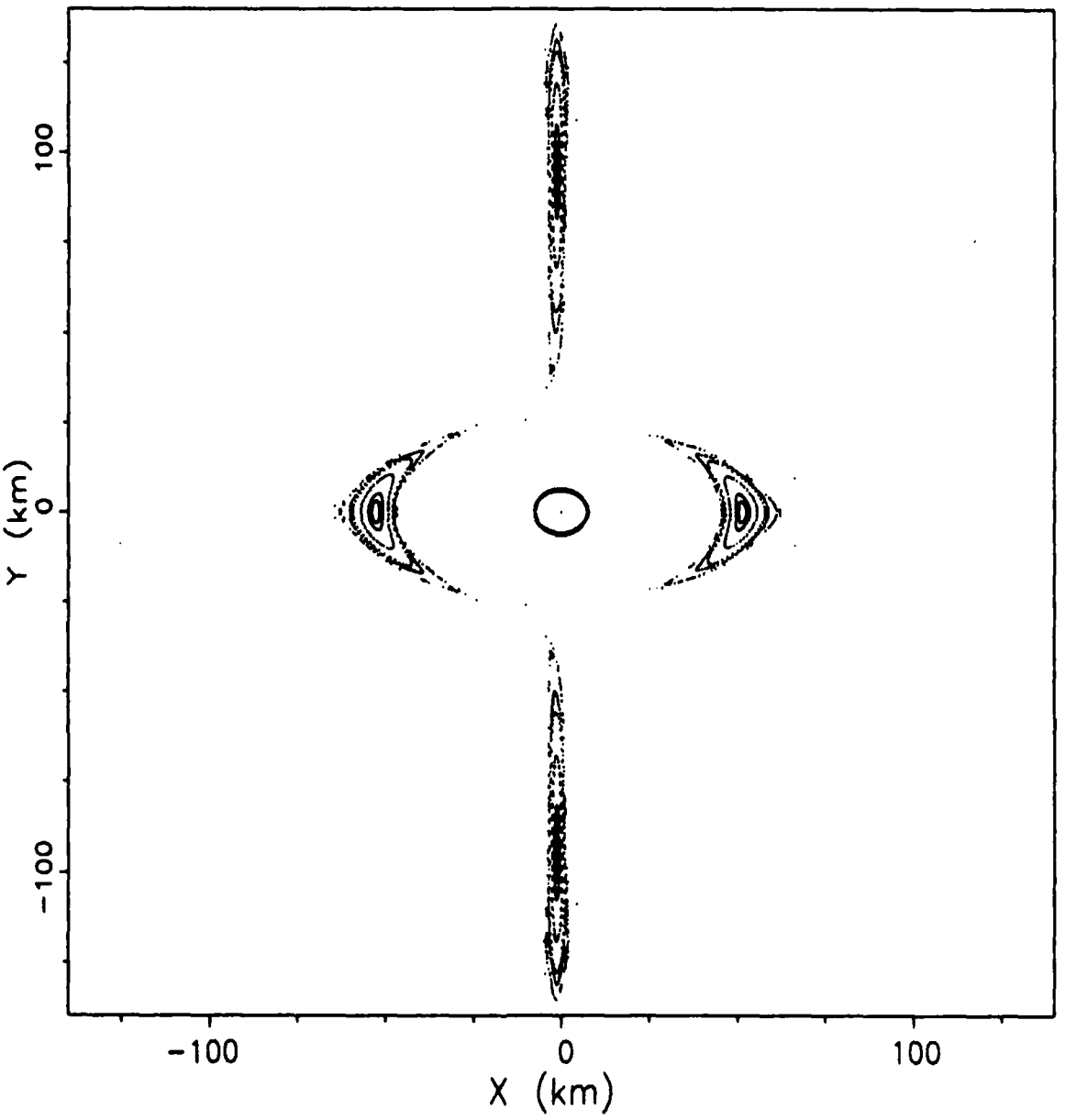

Figure 57. Deimos Surface of Section, H = -2.738585

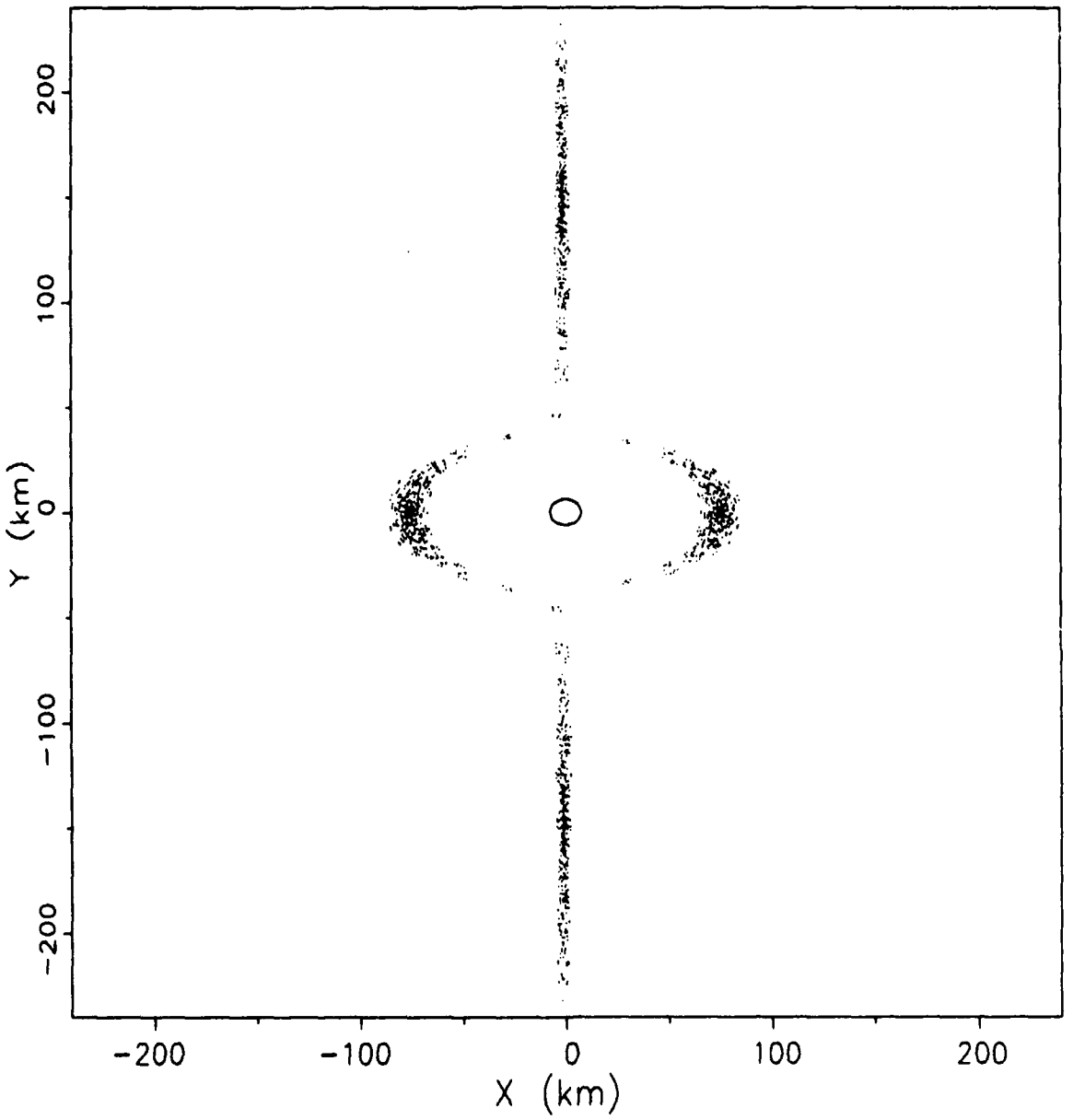

Figure 58. Deimos Surface of Section, H = -2.73858

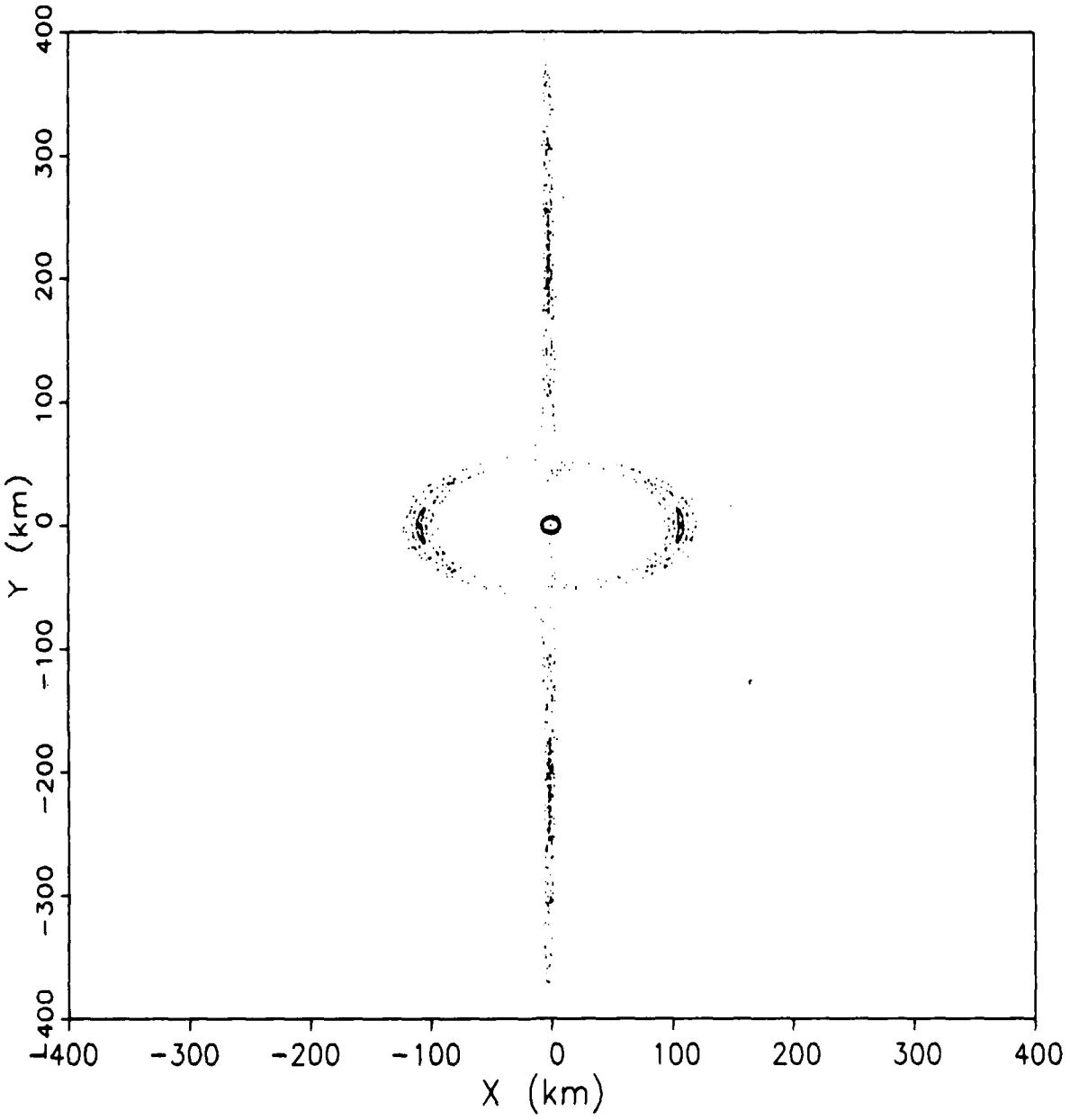

Figure 59. Deimos Surface of Section, H = -2.73857

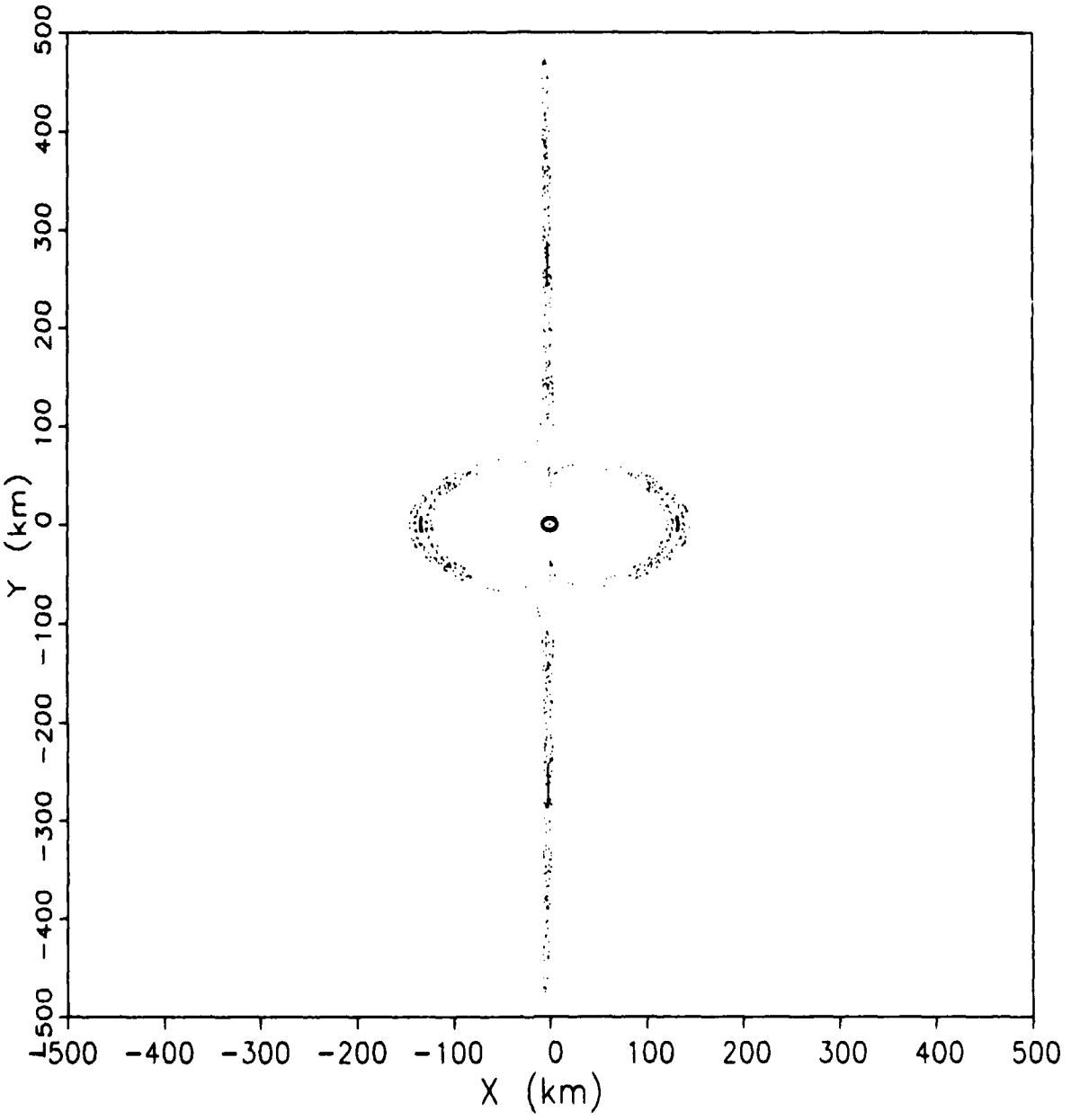

Figure 60. Deimos Surface of Section, H = -2.73856

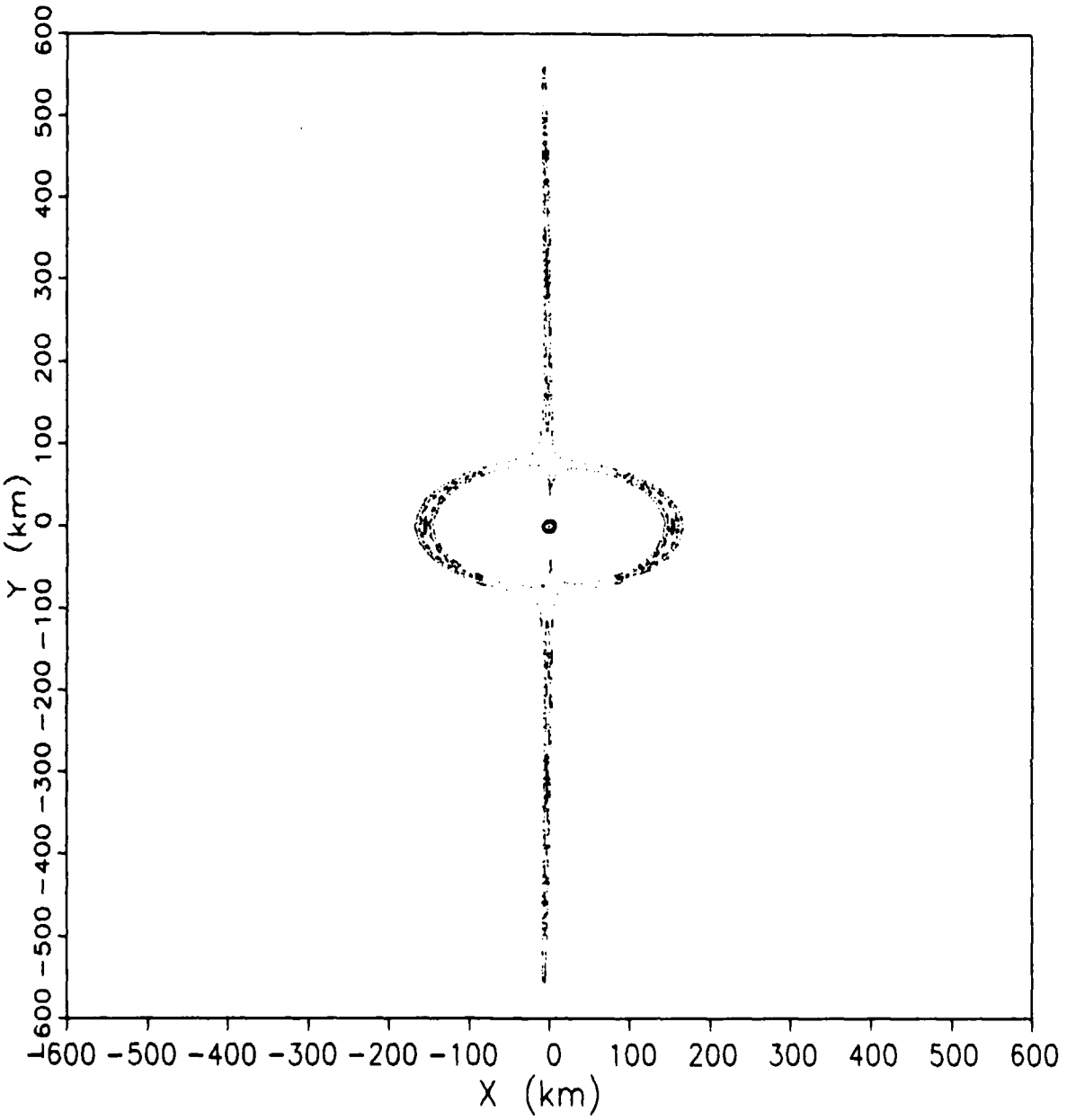

Figure 61. Deimos Surface of Section, H = -2.73855

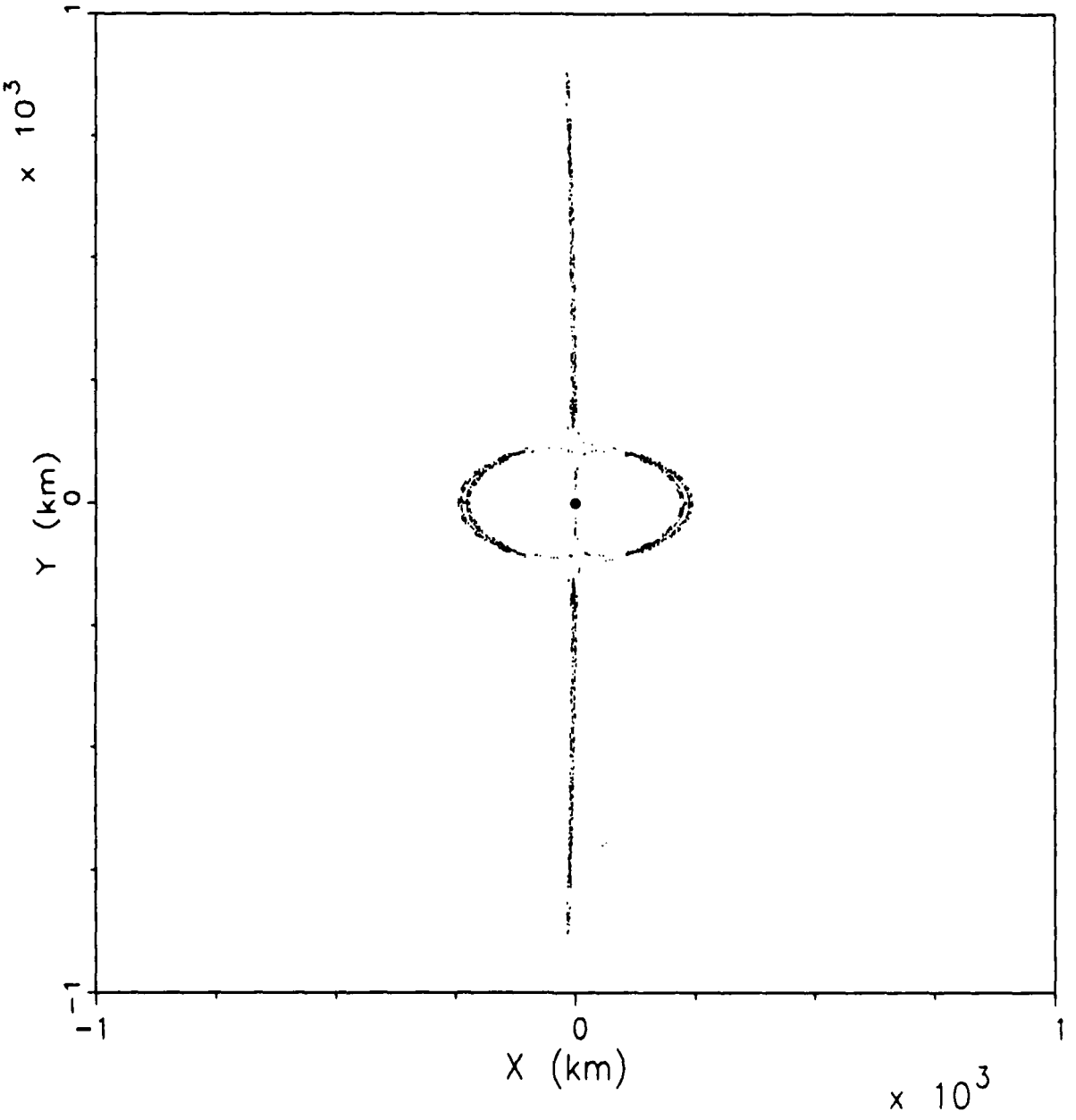

Figure 62. Deimos Surface of Section, H = -2.7385

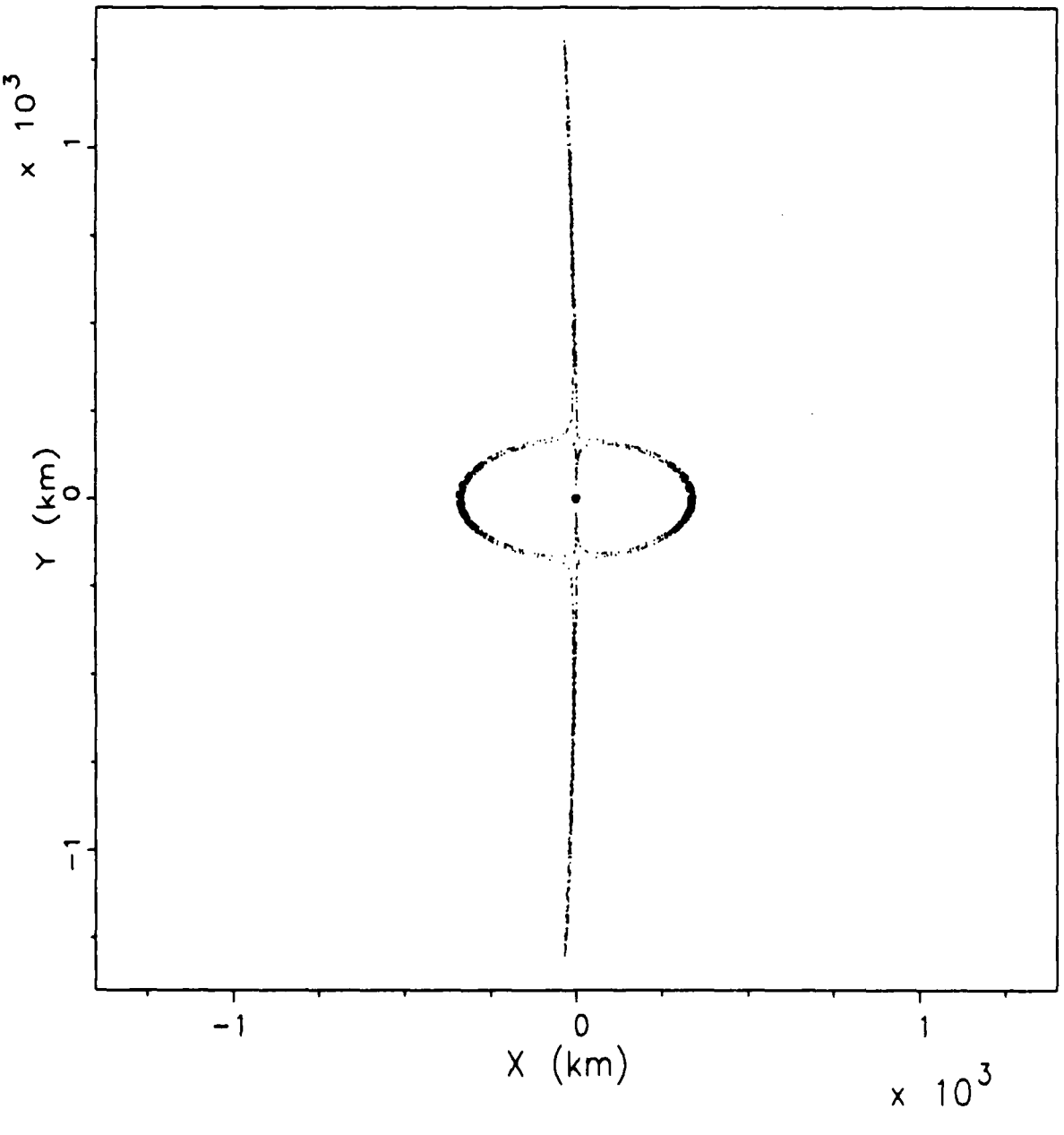

Figure 63. Deimos Surface of Section, H = -2.7384

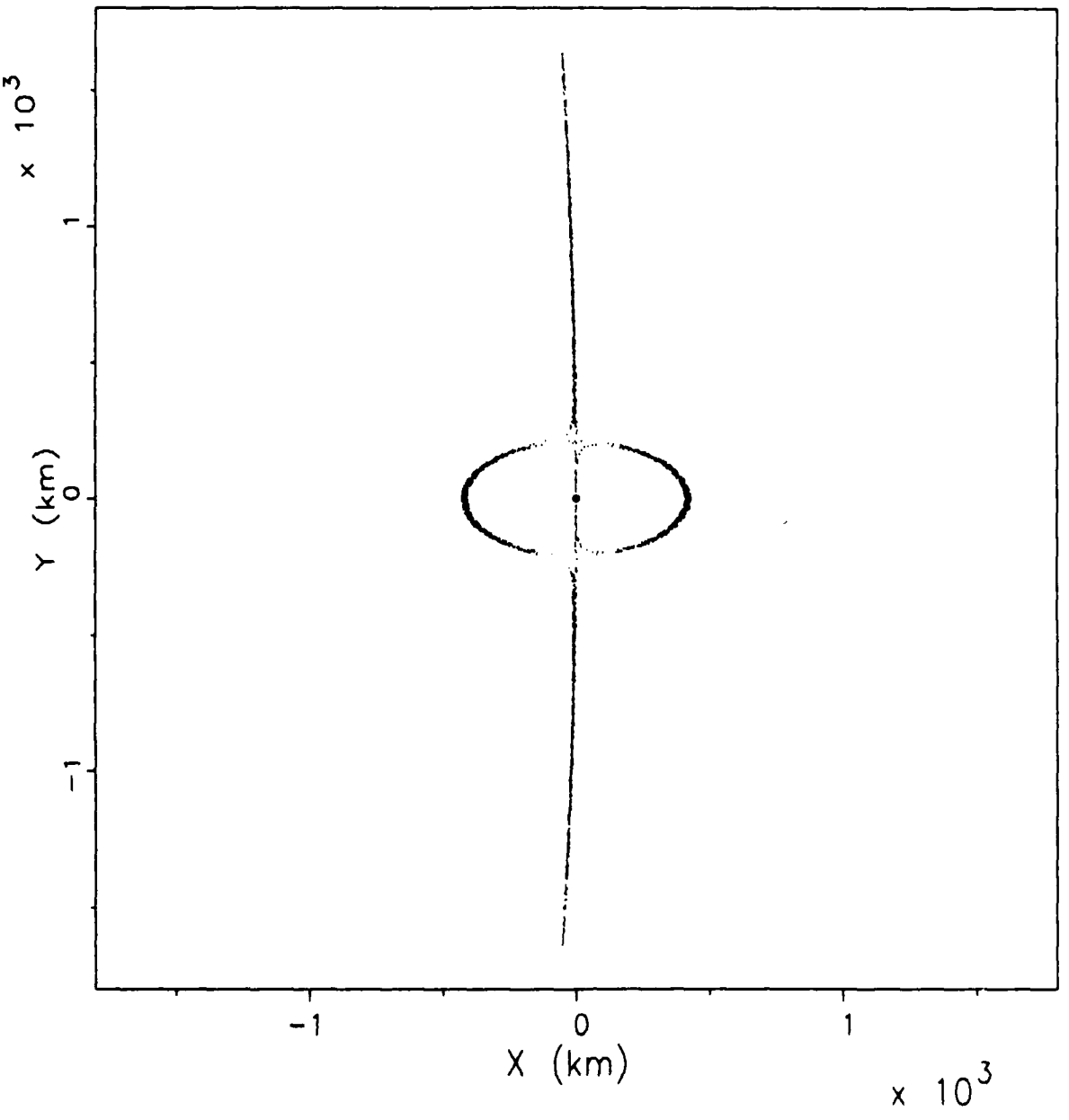

Figure 64. Deimos Surface of Section, H = -2.7383

Bibliography

1. Cheney, Ward and David Kincaid. Numerical Mathematics and Computing (Second Edition). Monterey CA: Brooks/Cole Publishing Company, 1985.

2. Danby, John M.A. Fundamentals of Celestial Mechanics. New York: The MacMillan Company, 1962.

3. Dobrovoloskis, A.R. and Joseph A. Burns. "Life Near the Roche Limit: Behavior of Ejecta from Satellites Close to Planets," Icarus, 42: 422-441 (1980).

4. Duxbury, T.C. and J.D. Callahan. "Phobos and Deimos Cartography," Abstract of a talk given at the 13th Lunar and Planetary Science Conference, Houston Texas, 15 March 1982.

5. Hnon, Michel and Heiles, Carl. "The Applicability of the Third Integral of Motion: Some Numerical Experiments," The Astronomical Journal, 69: 73-79 (February 1964).

6. Hicks, 2Lt Kerry D. Periodic Orbits About Rotating Asteroids in Free Space. MS Thesis, AFIT/GA/AA/86D-7. School of Engineering, Air Force Institute of Technology (AU), Wright Patterson AFB OH, December 1986.

7. Jefferys, William H. An Atlas of Surfaces of Section for the Restricted Problem of Three Bodies. Publications of the Department of Astronomy, The University of Texas at Austin, Series II, Volume 3, Number 6, May 1971.

8. Likens, Peter W. Elements of Engineering Mechanics. New York: McGraw-Hill Book Company, 1973.

9. Meirovitch, Leonard. Methods of Analytical Dynamics. New York: McGraw-Hill Book Company, 1970.

10. NASA. Space and Planetary Environment Criteria Guidelines for Use in Space Vehicle Development. Technical Memorandum 82478, Revision 1, Volume 1, 1982.

11. Smart, W.M. Celestial Mechanics. New York: John Wiley & Sons Inc., 1953.

12. Solomon, Capt Mary K. Control System for Maintaining Stable Orbits Around Phobos. MS Thesis, AFIT/GA/AA/88D-10. School of Engineering, Air Force Institute of Technology (AU), Wright Patterson AFB OH, December 1988.

13. Szebehely, Victor. Theory of Orbits, The Restricted Problem of Three Bodies. New York: Academic Press Inc., 1967.

14. Thomas, Peter C. "The Shape of Small Satellites," Icarus, 77: 248-274 (1989).

15. Werner, Capt Rodney A. Periodic Orbits Around a Satellite Modeled as a Triaxial Ellipsoid. MS Thesis, AFIT/GA/AA/87D-8. School of Engineering, Air Force Institute of Technology (AU), Wright Patterson AFB OH, December 1987.

16. Wiesel, William E. Advanced Astrodynamics. Lecture Notes for MC636, School of Engineering, Air Force Institute of Technology (AU), Wright Patterson AFB OH, November 1987.

Vita

Captain Scott W. Jansson [redacted] He graduated from high school in Averill Park, New York, in 1980. He received the degree of Bachelor of Science in Astronautical Engineering from the U.S. Air Force Academy in 1984. His first assignment was to HQ Space Division, Los Angeles AFB, California, where he served as Chief, GPS Nuclear Detonation Detection Section, in the NAVSTAR Global Positioning System (GPS) Joint Program Office. Captain Jansson entered the Air Force Institute of Technology, School of Engineering, in May of 1988.

[redacted]

REPORT DOCUMENTATION PAGE

Form Approved
OMB No. 0704-0188

1a. REPORT SECURITY CLASSIFICATION UNCLASSIFIED	1b. RESTRICTIVE MARKINGS
2a. SECURITY CLASSIFICATION AUTHORITY	3. DISTRIBUTION/AVAILABILITY OF REPORT Approved for public release; distribution unlimited.
2b. DECLASSIFICATION/DOWNGRADING SCHEDULE	
4. PERFORMING ORGANIZATION REPORT NUMBER(S) AFIT/GA/ENY/89D-3	5. MONITORING ORGANIZATION REPORT NUMBER(S)
6a. NAME OF PERFORMING ORGANIZATION School of Engineering 6b. OFFICE SYMBOL (*If applicable*) AFIT/ENY	7a. NAME OF MONITORING ORGANIZATION
6c. ADDRESS (*City, State, and ZIP Code*) Air Force Institute of Technology (AU) Wright Patterson AFB, Ohio 45433-6583	7b. ADDRESS (*City, State, and ZIP Code*)
8a. NAME OF FUNDING/SPONSORING ORGANIZATION 8b. OFFICE SYMBOL (*If applicable*)	9. PROCUREMENT INSTRUMENT IDENTIFICATION NUMBER
8c. ADDRESS (*City, State, and ZIP Code*)	10. SOURCE OF FUNDING NUMBERS PROGRAM ELEMENT NO. / PROJECT NO. / TASK NO. / WORK UNIT ACCESSION NO.

11. TITLE (*Include Security Classification*)
STABLE ORBITS ABOUT THE MARTIAN MOONS

12. PERSONAL AUTHOR(S)
Scott W. Jansson, Capt, USAF

13a. TYPE OF REPORT	13b. TIME COVERED	14. DATE OF REPORT (*Year, Month, Day*)	15. PAGE COUNT
MS Thesis	FROM _____ TO _____	1989 December	124

16. SUPPLEMENTARY NOTATION

17. COSATI CODES			18. SUBJECT TERMS (*Continue on reverse if necessary and identify by block number*)
FIELD	GROUP	SUB-GROUP	
22	03		Orbits, Phobos, Surface of Section, Mars, Deimos,

19. ABSTRACT (*Continue on reverse if necessary and identify by block number*)

Thesis Chairman: William E. Wiesel, Ph.D.
Professor of Astronautics

20. DISTRIBUTION/AVAILABILITY OF ABSTRACT	21. ABSTRACT SECURITY CLASSIFICATION
☐ UNCLASSIFIED/UNLIMITED ☒ SAME AS RPT. ☐ DTIC USERS	UNCLASSIFIED
22a. NAME OF RESPONSIBLE INDIVIDUAL William E. Wiesel, Ph.D.	22b. TELEPHONE (*Include Area Code*) (513) 255-2362 / 22c. OFFICE SYMBOL AFIT/ENY

Abstract

Orbits about the Martian moons, Phobos and Deimos, were investigated using the Poincare' surface of section technique. Hamilton's canonical equations were derived to describe the dynamics of the modified restricted three-body problem (Mars, moon, artificial satellite). The surface of section technique involved the numerical integration of several test orbits with the same value for the Hamiltonian. Apoapsis and periapsis points of the orbits are plotted in the two-dimensional configuration space. Stable orbits were discovered when the points formed sets of closed curves; chaotic orbits were indicated by the scattering of the points.